



## Early View

Original article

### **Neuropeptide regulation of secretion and inflammation in human airway gland serous cells**

Derek B. McMahon, Ryan M. Carey, Michael A. Kohanski, Charles C.L. Tong, Peter Papagiannopoulos, Nithin D. Adappa, James N. Palmer, Robert J. Lee

Please cite this article as: McMahon DB, Carey RM, Kohanski MA, *et al.* Neuropeptide regulation of secretion and inflammation in human airway gland serous cells. *Eur Respir J* 2020; in press (<https://doi.org/10.1183/13993003.01386-2019>).

This manuscript has recently been accepted for publication in the *European Respiratory Journal*. It is published here in its accepted form prior to copyediting and typesetting by our production team. After these production processes are complete and the authors have approved the resulting proofs, the article will move to the latest issue of the ERJ online.

Copyright ©ERS 2020

## **Neuropeptide regulation of secretion and inflammation in human airway gland serous cells**

Derek B. McMahon,<sup>1</sup> Ryan M. Carey,<sup>1</sup> Michael A. Kohanski,<sup>1</sup> Charles C.L. Tong,<sup>1</sup> Peter Papagiannopoulos,<sup>1</sup> Nithin D. Adappa,<sup>1</sup> James N. Palmer,<sup>1</sup> and Robert J. Lee<sup>1,2</sup>

<sup>1</sup>Department of Otorhinolaryngology and <sup>2</sup>Department of Physiology, University of Pennsylvania Perelman School of Medicine, Philadelphia, PA USA

Correspondence: Robert J. Lee, Department of ORL-HNS, Hospital of the University of Pennsylvania, 3400 Spruce Street, 5<sup>th</sup> floor Ravdin, Suite A, Philadelphia, PA 19104. USA. Phone: 215-573-9766, email: rjl@penncmedicine.upenn.edu

**Summary:** VIP and NPY are neuropeptides up-regulated in allergy and asthma, respectively, which inversely regulate CFTR-dependent secretion and inflammation in airway submucosal gland serous cells, which secrete much of the fluid that lines conducting airways.

## ABSTRACT

Airway submucosal gland serous cells are sites of expression of the cystic fibrosis transmembrane conductance regulator (CFTR) and are important for fluid secretion in conducting airways. To elucidate how neuropeptides regulate serous cells, we tested if human nasal turbinate serous cells secrete bicarbonate ( $\text{HCO}_3^-$ ), important for mucus polymerization and antimicrobial peptide function, during stimulation with cAMP-elevating vasoactive intestinal peptide (VIP) and if this requires CFTR. Serous cells stimulated with VIP exhibited a ~15-20% cAMP-dependent decrease in cell volume and a ~0.15 unit decrease in intracellular pH ( $\text{pH}_i$ ), reflecting activation of  $\text{Cl}^-$  and  $\text{HCO}_3^-$  secretion, respectively.  $\text{HCO}_3^-$  secretion was directly dependent on CFTR and was absent in cells from CF patients. In contrast, neuropeptide Y (NPY) reduced VIP-evoked cAMP increases, CFTR activation, and  $\text{Cl}^-/\text{HCO}_3^-$  secretion. Culture of primary serous cells in a model that maintained a serous phenotype confirmed the activating and inhibiting effects of VIP and NPY, respectively, on fluid and  $\text{HCO}_3^-$  secretion. Moreover, VIP enhanced antimicrobial peptide secretion and antimicrobial efficacy of secretions while NPY reduced antimicrobial efficacy. In contrast, NPY enhanced cytokine release while VIP reduced cytokine release through a mechanism requiring CFTR. As levels of VIP and NPY are up-regulated in diseases like allergy, asthma, and chronic rhinosinusitis, the balance of these two peptides in the airway may control mucus rheology and inflammatory responses in serous cells. Furthermore, the loss of CFTR conductance in serous cells may contribute to CF pathophysiology by increasing serous cells inflammatory responses in addition to directly impairing  $\text{Cl}^-$  and  $\text{HCO}_3^-$  secretion.

## INTRODUCTION

Several obstructive airway diseases share phenotypes of thickened mucus, including chronic rhinosinusitis (CRS), cystic fibrosis (CF), asthma, and COPD [1-3]. From nasal turbinate down to small bronchi, a large percentage of airway surface liquid (ASL) and mucus is generated by submucosal exocrine glands [3]. Gland serous cells are sites of expression of the CF transmembrane conductance regulator (CFTR) [3]. Observations of occluded gland ducts and gland hypertrophy, hyperplasia, and infection in CF [3] suggest that defects in CFTR-dependent serous secretion contribute to CF pathology. Intact CF glands secrete less fluid in response to cAMP-elevating agonists such as vasoactive intestinal peptide (VIP) compared with non-CF glands [3]. Gland hypertrophy, duct plugging, and excess mucus are also observed in COPD and asthma [3], with gland hypertrophy more common in fatal asthma [4].

Bicarbonate ( $\text{HCO}_3^-$ ) secretion by serous cells facilitates polymerization of mucins secreted by more proximal mucous cells [5] (**supplementary figure S1a**).  $\text{HCO}_3^-$  is also critical to efficacy of antimicrobial peptides secreted by serous cells [3]. However, mechanisms by which serous cells secrete  $\text{HCO}_3^-$  are unknown. Identifying these mechanisms may yield insights into pathophysiology of CF and other diseases exhibiting altered mucus secretion or rheology. We previously studied nasal serous cell  $\text{HCO}_3^-$  secretion during cholinergic-induced secretion [6], which is largely intact in CF [3], as it is mediated by the  $\text{Ca}^{2+}$  activated  $\text{Cl}^-$  and  $\text{HCO}_3^-$  channel (CaCC) TMEM16A [7]. Our initial goal was to directly test if serous cells also secrete  $\text{HCO}_3^-$  during VIP stimulation, if this occurs through CFTR, and if TMEM16A could substitute during loss of CFTR.

A further goal was to understand how VIP and neuropeptide Y (NPY), both upregulated in inflammatory airway diseases, interact to control airway secretion. Parasympathetic VIPergic [8, 9] and NPYergic [10, 11] neurons exist in the respiratory tract and may be increased in mucosa from patients with allergic rhinitis [12] or irritative toxic rhinitis [13]. Some nerves co-express VIP and NPY [14], including in the proximity of glands [15, 16]. VIP and NPY are found in the pedicle of nasal polyps, suggesting they may play a role in polyp formation [17]. Activated macrophages ( $\text{M}\phi$ s) [18] or epithelial cells [19] can also make NPY, perhaps because NPY has direct antimicrobial effects [20]. Elevated NPY

in asthma [21] may link psychological stress with allergic asthma exacerbations [22]. Mice lacking NPY or NPY1R have reduced allergic airway inflammation [23]. Other studies outside the airway suggest NPY increases Th2 responses [24, 25]. NPY and NPYR1 expression are elevated in mouse lungs after influenza, and knockout of NPY reduced disease severity and IL-6 levels [18]. Allergic rhinitis patients have nasal secretions with elevated concentrations of VIP compared with control individuals at baseline [26] and during allergen challenge [27].

A recent review highlighted need for elucidation of neuropeptide regulation of submucosal glands in obstructive lung diseases [28]. The role of VIP as a cAMP-dependent activator of secretion is established [3], but the role of NPY is unclear. A cocktail of NPY and norepinephrine inhibited cultured tracheal gland cell glycoprotein secretion [29], and NPY inhibited bulk mucus secretion in ferret trachea [30], but there is little mechanistic data for if/how NPY affects serous cells. NPY receptors are often  $G_i$ -coupled and could reduce cAMP responses to  $G_s$ -coupled VIP receptors [31], reducing secretion by lowering PKA activation of CFTR. Moreover, VIP and NPY are immunomodulators [32] and may regulate gland cytokine secretion.

We examined effects of VIP and NPY in primary serous cells isolated from human nasal glands. Cells were studied acutely as well as in an air-liquid interface (ALI) culture model that retained expression of serous cell markers, facilitating polarized studies and co-culture with human M $\phi$ s. Results below contribute to our understanding of airway serous cells and the role of CFTR in both secretion and inflammation, suggesting therapeutic targets for obstructive airway diseases.

## METHODS

### *Experimental Procedures*

Isolation of primary serous acinar cells, immunofluorescence, and live cell imaging of cell volume,  $\text{pH}_i$ , and  $\text{Cl}^-$  was carried out as described [6, 33]. Culture of gland serous cells was carried out as described [34]. ASL height, ASL pH measurements, ELISAs, and bacterial assays were carried out as reported [27, 35]. More detailed methods and reagents used provided in the **supplementary materials**.

### *Study Approval*

Tissue was acquired in accordance with the University of Pennsylvania guidelines regarding residual clinical material in research (IRB protocol #800614), the US Department of Health and Human Services Title 45 CFR 46.116, and the Declaration of Helsinki. Turbinate samples from 42 non-CF and 9 CF patients (seven  $\Delta\text{F508}/\Delta\text{F508}$ , one  $\Delta\text{F508}/\text{G542X}$ , and one  $\Delta\text{F508}/\text{E585X}$ ) were used (**supplementary table S1**).

### *Statistics*

Data were analyzed in GraphPad Prism. Multiple comparisons used 1-way ANOVA with Bonferroni (preselected pairwise comparisons), Dunnett's (comparisons to a control set), or Tukey-Kramer (comparison of all values) posttests. A  $p$  value  $<0.05$  was considered significant. All data are mean  $\pm$  SEM from independent experiments using cells from  $\geq 4$  patients. Minimal patient-to-patient variability was observed beyond effects of CFTR genotype, as described in the supplementary material. Data points in each figure represent independent experiments, some of which used separate cell cultures that originated from the same patient (common in studies using ALI cultures). In this case, an equal number of independent experiments, typically 2, was performed using cells from each patient to ensure that cells from each patient were equally represented to prevent cells from any one patient skewing results.

## RESULTS

### *VIP stimulates Cl<sup>-</sup> and HCO<sub>3</sub><sup>-</sup> secretion through CFTR*

Submucosal gland acinar cells (**supplementary figure 1b**) were isolated from human middle turbinate [33]. Serous acini exhibited secretory-granule immunofluorescence for lysozyme (**supplementary figure 1c**), basolateral immunofluorescence for VIP receptors (**figure 1d-e**), and apical immunofluorescence for TMEM16A and CFTR (**supplementary figure 1f-g**) as described [6, 7, 33]. Secretion was studied in isolated serous cells using simultaneous differential interference contrast (DIC) measurement of cell volume and quantitative fluorescence microscopy of indicator dyes to measure the concentrations of ions involved in driving secretion (Cl<sup>-</sup>/HCO<sub>3</sub><sup>-</sup>), a technique pioneered in salivary cells adapted for serous cells [6, 7, 33].

Epithelial fluid secretion is driven largely by Cl<sup>-</sup>. Serous cell shrinkage during agonist stimulation reflects efflux of cellular K<sup>+</sup> and Cl<sup>-</sup> upon activation of secretion and movement of osmotically obliged water. Cell swelling upon removal of agonist reflects solute uptake via mechanisms that sustain secretion, such as the Na<sup>+</sup>K<sup>+</sup>2Cl<sup>-</sup> co-transporter NKCC1 [7] (**figure 1a**). Human nasal serous cells shrank by ~20% when stimulated with cAMP-elevating agonists forskolin or VIP (**figure 2b**), as previously reported [33].

Shrinkage was accompanied by transient acidification of intracellular pH (pH<sub>i</sub>) followed by more sustained alkalinization (**figure 1c-d**). Agonist-evoked acidification was absent in HCO<sub>3</sub><sup>-</sup>-free media (**supplementary figure S2a-c**), and the secondary alkalinization was blocked with inhibition of the Na<sup>+</sup>HCO<sub>3</sub><sup>-</sup> co-transporter (NBC; **supplementary figure S2d**). Thus, the transient acidification reflects HCO<sub>3</sub><sup>-</sup> efflux during activation of secretion, while the alkalinization reflects activation of NBC, sustaining HCO<sub>3</sub><sup>-</sup> secretion by keeping intracellular [HCO<sub>3</sub><sup>-</sup>] high. This is similar to cholinergic-evoked serous cell acidification and subsequent alkalinization by Na<sup>+</sup>/H<sup>+</sup> exchangers (NHEs) [6], but reveals an important mechanistic difference between cAMP and Ca<sup>2+</sup> pathways.

Acidification was blocked by eliminating the driving forces for conductive HCO<sub>3</sub><sup>-</sup> efflux using ion substitution (**supplementary figure S2e**), suggesting acidification is mediated by an ion channel.

Forskolin- or VIP-induced shrinkage and acidification were absent in cells from CF patients (**figure 1c-d**), and were inhibited by CFTR inhibitor CFTR<sub>inh</sub>172 or K<sup>+</sup> channel inhibitors clofilium and clotrimazole in non-CF cells (**figure 1e-f**), demonstrating a requirement for both CFTR and counterion K<sup>+</sup> efflux. VIP-evoked responses were not reduced by TMEM16A inhibitors niflumic acid (NFA), T16A<sub>inh</sub>-A01, CaCC<sub>inh</sub>-A01, or 4,4'-diisothiocyanato-2,2'-silbenedisulfonic acid (DIDS) (**figure 1f**). Representative traces are in **supplementary figure S3a and b**.

In contrast, carbachol (CCh), which activates Ca<sup>2+</sup>-driven secretion [7, 33], stimulated shrinkage and acidification blocked by TMEM16A inhibitors NFA, T16A<sub>inh</sub>-A01, CaCC<sub>inh</sub>-A01, or DIDS (**figure 1g**). CCh-induced secretion was intact in CF cells (**figure 1h**). Pharmacological activation of TMEM16A (E<sub>act</sub>) restored secretion responses to VIP in CF cells (**figure 1h**). Representative traces are in **supplementary figure S3c and d**. The concentration of E<sub>act</sub> used here had no acute (2-3 min) effects on intracellular calcium in these cells (**supplementary figure S3e**)

Thus, cAMP elevation activates both Cl<sup>-</sup> and HCO<sub>3</sub><sup>-</sup> secretion directly through CFTR (**figure 1i**), and targeting TMEM16A might restore HCO<sub>3</sub><sup>-</sup> secretion in CF glands. We found no evidence for Cl<sup>-</sup>/HCO<sub>3</sub><sup>-</sup> exchanger-mediated HCO<sub>3</sub><sup>-</sup> efflux (**supplementary figure S4**), agreeing with data showing Calu-3 cells [36], a bronchial line frequently used as a serous cell surrogate, secrete HCO<sub>3</sub><sup>-</sup> mainly through CFTR while Cl<sup>-</sup>/HCO<sub>3</sub><sup>-</sup> exchanger pendrin (SLC26A4) is more important in surface epithelial cells. These data show a fundamental defect in HCO<sub>3</sub><sup>-</sup> secretion in CF cells caused directly by loss of CFTR conductance, which may be restored directly by pharmacological CFTR correction.

### ***NPY reduces CFTR-mediated fluid and HCO<sub>3</sub><sup>-</sup> secretion during VIP stimulation***

Calu-3s express high amounts of NPY1R relative to other airway lines (**supplementary tables S2 and S3**). We thus tested for NPYRs in primary serous cells. We observed no secretory responses to NPY, but the magnitudes of VIP-evoked acidification and shrinkage were reduced with NPY (**figure 2a-b**). We hypothesized that G<sub>i</sub>-coupled NPYRs might blunt the magnitude of VIP-evoked cAMP increases, reducing CFTR activation. We measured Cl<sup>-</sup> permeability using 6-methoxy-N-(3-sulfopropyl)quinolinium (SPQ), a dye quenched by Cl<sup>-</sup> but not by NO<sub>3</sub><sup>-</sup>. Substitution of extracellular Cl<sup>-</sup> for NO<sub>3</sub><sup>-</sup> results in

decreased intracellular  $[Cl^-]$  and the resulting rate of SPQ fluorescence increase is roughly equivalent to anion permeability [7, 33, 35]. In the presence of VIP, fluorescence rapidly increased upon  $NO_3^-$  substitution. This was reduced by ~50% by NPY (**figure 2c-d**). In the presence of CFTR<sub>inh</sub>172, anion permeability was almost completely reduced and NPY had no effect (**figure 2d**). Even after 24 hours stimulation with NPY, isolated serous cells exhibited reduced VIP-activated  $Cl^-$  permeability during acute VIP stimulation (**supplementary figure S5**).

CFTR is activated by PKA downstream of cAMP. We imaged real time cAMP changes using an mNeonGreen cAMP biosensor (cADDis [37]). VIP induced a rapid, reversible increase in cAMP blocked by VIPR antagonist VIP<sub>(6-28)</sub> (**figure 3a-b**). The cAMP increase was independent of  $Ca^{2+}$  (**figure 3c**). There was no difference in cAMP increases in non-CF or CF cells (**supplementary figure S6**), in contrast to previous hypotheses of defective cAMP signaling in CF [38]. However, NPY reduced VIP-evoked cAMP responses (**figure 3d-e**); the NPY effects were eliminated with NPY1R antagonist BIBO 3304 or pertussis toxin (PTX), which inactivates  $G_i$  proteins (**figure 3d-e**). Thus, NPY blunts CFTR-mediated  $Cl^-$ ,  $HCO_3^-$ , and fluid secretion by reducing cAMP signaling.

### ***NPY and VIP have opposing effects on $Cl^-$ and $HCO_3^-$ secretion in primary cultures of serous cells***

To facilitate polarized studies, we used culture methods that preserved a serous phenotype [34]. Serous cells cultured at air liquid interface (ALI) expressed markers Muc7, VIPR1, VIPR2, lysozyme, NKCC1, and alpha-1-antitrypsin, as well as both NPY1R and NPY4R (**figure 4a-c**). Lysozyme, Muc7, VIPR1, and VIPR2 were detected by immunofluorescence in serous cells (**figure 4d-e**) and Calu-3 cells (**supplementary figure S7-S8**). ELISA and qPCR confirmed that serous cultures expressed Muc7 but not Muc5AC or Muc5B (**supplementary figure S9**). Serous ALIs also expressed functional CFTR. Apical substitution of  $Cl^-$  for  $NO_3^-$  led to a decrease in  $[Cl^-]_i$  that was enhanced by VIP, blocked by CFTR<sub>inh</sub>172, and blunted by NPY (**figure 5a**). Similar to freshly isolated cells above, TMEM16A inhibitors did not affect VIP-activated  $Cl^-$  permeability (**figure 5a**). ALIs were resistant to viral expression of cADDis, but steady-state cAMP levels were measured 5 min after stimulation with VIP  $\pm$  NPY. NPY reduced cAMP increases, and this was abrogated by PTX (**figure 5b**).

Airway surface liquid (ASL) was labeled with Texas red dextran to track fluid secretion. VIP increased ASL height; this was inhibited by NKCC1 inhibitor bumetanide, PKA inhibitor H89, or VIP<sub>(6-28)</sub> (**figure 5c-d**), supporting that this reflected fluid secretion. NPY inhibited VIP-induced secretion (**figure 5c-d**) and isoproterenol-induced secretion (**figure 5d**), but not Ca<sup>2+</sup>-activated CCh-induced secretion (**figure 5d**), showing effects of NPY were specific for cAMP. To test if phagocyte-produced NPY could produce these effects, we used primary human monocyte-derived macrophages (Mφs) primed with phorbol myristate acetate (PMA), which produce NPY (**supplementary figure S10**). Serous ALIs transwells were transferred into plates above the Mφs with 24 hour Mφ-conditioned media on the basolateral side. Addition of VIP increased ASL height, but this was reduced in the presence of PMA-primed Mφs, and this effect was reversed by BIBO 3304 (**figure 5e**).

To track HCO<sub>3</sub><sup>-</sup> secretion, ASL was labeled with SNARF-1-dextran sonicated in perfluorocarbon, allowing measurement of pH in physiological ASL with no addition of aqueous fluid [39]. Steady-state unstimulated ASL pH (pH<sub>ASL</sub>) was 7.2 ± 0.04, equivalent to ~15 mM HCO<sub>3</sub><sup>-</sup> at 5% CO<sub>2</sub> ([HCO<sub>3</sub>]<sub>i</sub> = 1.2 mM × 10<sup>pH-6.1</sup>); pH<sub>ASL</sub> was reduced by NBC inhibitor DNDS (6.9 ± 0.06; 7.6 mM HCO<sub>3</sub><sup>-</sup>) but not with NPY alone (**figure 5f**). VIP increased pH<sub>ASL</sub> (7.6 ± 0.04; 38 mM HCO<sub>3</sub><sup>-</sup>), suggesting VIP stimulated HCO<sub>3</sub><sup>-</sup> secretion; increased pH<sub>ASL</sub> was reduced by NPY (7.3 ± 0.05) or DNDS (7.1 ± 0.03). Effects of NPY were blocked by PTX. NPY similarly inhibited forskolin and isoproterenol (**figure 5f**). Note that with increased ASL volume (**figure 5c**) and buffering capacity, actual secreted HCO<sub>3</sub><sup>-</sup> would be larger than changes in [HCO<sub>3</sub>].

Serous ALIs were incubated with unstimulated or PMA-stimulated Mφs as above and steady-state pH<sub>ASL</sub> was measured 2 hours later; pH<sub>ASL</sub> was unchanged by unstimulated Mφs, but PMA-stimulated Mφs reduced pH<sub>ASL</sub> (**figure 5g**). This was inhibited by BIBO 3304. Addition of VIP increased pH<sub>ASL</sub> (**figure 5g**). Effects observed were verified using a real-time HCO<sub>3</sub><sup>-</sup> secretion assay, which also confirmed secretion was dependent on apical CFTR (**supplementary figure S11**).

Type 2 inflammation was suggested to upregulate Cl<sup>-</sup>/HCO<sub>3</sub><sup>-</sup> exchanger pendrin in airway surface epithelial cells [40, 41]. We examined if NPY or IL-13 induced altered expression of pendrin or Cl<sup>-</sup>

channels in primary serous cells, perhaps shifting serous cells away from CFTR toward a more TMEM16A- and/or pendrin-dominated secretory phenotype. However, there was no change in *SLC26A4* (encoding pendrin), *ANO1* (encoding TMEM16A) or *CFTR* expression in primary serous ALIs after 24 hours IL-13 or NPY (**supplementary figure S12**). Up-regulation of pendrin was observed in surface epithelial cells (**supplementary figure S12**), fitting a lack of a role for pendrin in serous cells [36].

***VIP acutely increases antimicrobial secretions and bactericidal activity while NPY reduces it***

Carbonate and/or  $\text{HCO}_3^-$  have been reported to enhance antimicrobial activity of airway secretions [42]. We observed a small effect of  $\text{HCO}_3^-$  on antimicrobial activity of secretions produced by Calu-3 cells (**supplementary figure S13**). However, we hypothesized that NPY might have more profound effects through inhibition of both  $\text{HCO}_3^-$  secretion via CFTR and reduction of serous cell antimicrobial peptide secretion, likely mediated by a combination of constitutive and regulated vesicular release driven by both  $\text{Ca}^{2+}$  and cAMP, as in salivary and pancreatic exocrine acinar cells [43, 44]. Reductions of cAMP by NPY may lower antimicrobial secretion independent of effects on CFTR function.

Forskolin and VIP both increased secretion of serous cell antimicrobials lysozyme, Muc7, and  $\beta$ -defensin 1 ( $\text{h}\beta\text{D1}$ ) over 2 hours as measured by ELISA; this was reduced by NPY (**figure 6a**). There was no effect of inhibition of CFTR or TMEM16A on secretion of these antimicrobials (**supplementary figure S14a**). Neither lysozyme nor  $\text{h}\beta\text{D1}$  secretion was reduced in cultures derived from CF patients (**supplementary figure S14b**). NPY had no effect on CCh-activated secretion of lysozyme or  $\text{h}\beta\text{D1}$  over 2 hours (**supplementary figure S14c**), supporting a specific effect of NPY on cAMP. Fitting with increased antimicrobial peptide secretion, VIP acutely increased the antibacterial effects of serous ASL washings against clinical isolates of *Pseudomonas aeruginosa* and methicillin-resistant *Staphylococcus aureus* (MRSA; **figure 6b-c**). NPY blunted the effects of VIP (**figure 6b-c**). A fluorescent live-dead staining of *P. aeruginosa* confirmed reduced bactericidal efficacy of NPY+VIP-stimulated ASL (**supplementary figure S15**).

Neither VIP nor NPY alone had longer-term (24-48 hrs) effects on expression of h $\beta$ D1 by qPCR (**supplementary figure S16a**) despite increased secretion over 48 hours (**supplementary figure s16b**). LPS treatment up-regulated h $\beta$ D2 expression and secretion (**supplementary figure S16a-c**), but this was not significantly affected by NPY or VIP. Lysozyme expression was significantly increased by VIP at 24 hours (**supplementary figure S16d**), with lysozyme and Muc7 secretion also increased at 24 hours (**supplementary figure S16e**). VIP-treated cultures exhibited more bactericidal ASL even at 48 hours, reduced by NPY even in the presence of LPS (**supplementary figure S16f**). Thus more chronic VIP and NPY stimulation can have longer term effects on serous cell antimicrobials.

### ***NPY is pro-inflammatory***

We hypothesized that airway gland cytokine secretion may be modulated by VIP and/or NPY. We first focused on epithelial cell-derived cytokines involved in asthma and allergy, where alterations of VIP and/or NPY have been reported. In serous ALLs, IL-6, TNF $\alpha$ , IL-1 $\beta$ , and GM-CSF release were increased after 48 hours treatment with toll-like receptor 4 (TLR4) activator lipopolysaccharide (LPS), TLR3 activator poly(I:C), TLR2 activator lipoteichoic acid (LTA), TNF $\alpha$ , or type 2 cytokines (IL-4 + IL-13; **supplementary figure S17a-d**). While NPY or VIP had no effect alone on IL-6, TNF $\alpha$ , or GM-CSF release, NPY increased IL-1 $\beta$  release ~2-fold at baseline. NPY also increased IL-1 $\beta$  mRNA at 4 hours (**supplementary figure S17e**)

NPY also potentiated release of these cytokines in combination with LPS, LTA, IL-4+IL-13, and TNF- $\alpha$  (**supplementary figure S17a-d**). NPY also enhanced LPS-induced IL-6 and IL-8 mRNA as well as IL-13- or TNF- $\alpha$ -induced GM-CSF mRNA at 4 hours (**supplementary figure S17f-g**). NPY effects were blocked by PTX, implicating G<sub>i</sub> signaling (**supplementary figure S17a-d**). In contrast, VIP reduced cytokine secretion 25-50%; these reductions were eliminated by NPY (**supplementary figure S17a-d**). Co-stimulation with IL-4+IL-13 increased cytokines in response to either poly(I:C) or LPS, and this was enhanced further by NPY (**supplementary figure S18a**), suggesting that NPY is pro-inflammatory even within the context of Th2 inflammation observed in airway diseases like asthma.

NPY also enhanced cytokine release in response to heat-killed clinical isolates of *P. aeruginosa* and MRSA (**figure 7a-c**), which likely activate TLRs as above. To validate results from cultured ALLs, we incubated freshly dissociated serous cells with  $\text{TNF}\alpha$  or poly(I:C)  $\pm$  NPY; NPY enhanced cytokine secretion (**supplementary figure S18b**), confirming NPY is pro-inflammatory and may contribute to increased inflammation in airway diseases like asthma.

***Anti-inflammatory effects of VIP require functional CFTR conductance; TMEM16A can substitute.***

In airway cells,  $\text{Cl}^-$  conductance may be anti-inflammatory [45, 46], with increased  $[\text{Cl}^-]_i$  promoting inflammation [47]. This may have implications for CF; in serous cells stimulated with VIP,  $[\text{Cl}^-]_i$  may be higher in CF cells due to lack of CFTR-mediated efflux. We tested if CFTR contributes to anti-inflammatory effects of VIP using NPY to increase release of IL-1 $\beta$ , a cytokine upregulated in the lungs of some children with CF [48, 49]. NPY-induced IL-1 $\beta$  was not altered by CFTR<sub>inh</sub>172 or TMEM16A activator  $E_{\text{act}}$  (**figure 7d**). However, VIP reduced IL-1 $\beta$  by >50% (**figure 7d**). CFTR<sub>inh</sub>172 reversed the effect of VIP, while  $E_{\text{act}}$  restored effects of VIP, and the effect of  $E_{\text{act}}$  was further reversed with CaCC<sub>inh</sub>-A01 (**figure 7d**). We saw similar results when serous cells were stimulated with heat-killed *P. aeruginosa*. VIP reduced release of GM-CSF and IL-6, another cytokine involved in early CF inflammation [48]; this was blocked by CFTR<sub>inh</sub>172 but subsequently restored by  $E_{\text{act}}$  (**figure 7e**).

Thus, CFTR is required for anti-inflammatory effects of VIP, but TMEM16A can substitute. However, activation of  $\text{Cl}^-$  conductance by  $E_{\text{act}}$  was not sufficient for anti-inflammatory effects in the absence of VIP (**figure 7e**), likely because a reduction in  $[\text{Cl}^-]_i$  requires counter-ion ( $\text{K}^+$ ) flux activated downstream of secretagogues [33] but not activated by  $E_{\text{act}}$  alone. Supporting this,  $\text{K}^+$  channel activator 1-ethyl-2-benzimidazolinone (1-EBIO [7]) in combination with  $E_{\text{act}}$  was anti-inflammatory in serous cells (**figure 7e**). VIP also reduced *P. aeruginosa*-induced release of IL-8 (**figure 7f**), another cytokine upregulated in CF [48, 49].

## DISCUSSION

This study suggests serous cells secrete  $\text{HCO}_3^-$  in addition to  $\text{Cl}^-$  during VIPergic stimulation directly through CFTR (**figure 8a**). NPY impairs both VIPergic fluid and antimicrobial peptide secretion by reducing cAMP signaling (**figure 8b**). The novel inverse relationship between NPY and VIP in the regulation of secretion suggests that the balance of these neuropeptides affects mucus rheology by promoting or inhibiting  $\text{Cl}^-$  and  $\text{HCO}_3^-$  secretion from serous cells, which control the hydration of mucins secreted by more proximal gland mucous cells.

This study reveals several insights relevant to CF pathogenesis (**figure 8c**). We found no evidence of  $\text{Cl}^-/\text{HCO}_3^-$  exchange (e.g., pendrin) activity in serous cells, suggesting loss of CFTR function directly contributes to impaired  $\text{HCO}_3^-$  secretion. Targeting CFTR via correctors and/or potentiators would restore serous cell  $\text{HCO}_3^-$  and  $\text{Cl}^-$  secretion independent of other proteins. Moreover, cAMP signaling was intact in CF cells, suggesting that appropriate pharmacological correction of mutant CFTR could restore secretion in response to the appropriate endogenous physiological stimuli (e.g., VIP). In CF patients that cannot benefit from CFTR correction (e.g., premature stop codon mutations), activation of TMEM16A could also restore  $\text{Cl}^-/\text{HCO}_3^-$  efflux. As CFTR may regulate other channels and transporters like the epithelial  $\text{Na}^+$  channel or pendrin in surface epithelial cells [36, 40, 41], TMEM16A activation may not fully replace CFTR. However, this study and previous work [6] suggest TMEM16A can support levels of  $\text{Cl}^-$  and  $\text{HCO}_3^-$  efflux from serous cells equivalent to CFTR.

These results also reveal potential pathophysiological mechanisms in obstructive airway diseases like asthma (**figure 8d**). Elevated VIP in allergic rhinitis may promote watery serous secretions through elevated fluid and  $\text{HCO}_3^-$  secretion to thin mucus. However, under conditions of increased NPY (e.g., in asthma), the ability of VIP to stimulate fluid and  $\text{HCO}_3^-$  secretion through CFTR and antimicrobial peptide secretion is impaired due to a blunting of cAMP signaling. NPY also decreases airway ciliary beat frequency [50], which may further impair mucociliary clearance and innate defense. Increased inflammation via elevated NPY may exacerbate these effects. In summary, our data suggest that in

some asthma, COPD, or CRS patients, NPYR1 antagonists may be useful to thin secreted mucus, enhance antimicrobial secretion, and/or reduce inflammation.

While elevated NPY has not been reported in CF lungs, one study did suggest elevated NPY in olfactory epithelium of CFTR knockout mice [51]. It may be possible that NPY plays a role in a subset of CF patients; skewing toward a Th17 or Th2 profile may be a risk factor for *P. aeruginosa* infection in CF lungs [52]. NPY might be elevated in these patients. NPY would not be expected to substantially affect ion transport in CF serous cells as the entire pathway is already absent due to loss of CFTR function; however, NPY could still reduce antimicrobial secretion or promote inflammation. A role for NPY in CF lungs and potential therapeutic value of NPYR inhibition requires further investigation. Regardless of NPY's relevance to CF pathophysiology, increased mucus viscosity in CF and asthma may share, at least in part, common mechanisms of reduced CFTR function. In CF this is via direct CFTR mutation. In asthma, reduced CFTR-mediated secretion due to elevated NPY and blunted cAMP signaling may contribute to poorly hydrated gland mucus independent of direct CFTR defects.

The important contribution of exocrine cells to inflammation is established in parotid and pancreatic acini within the context of Sjögren's syndrome and pancreatitis, respectively [53]. However, this is less studied in the airway. Bronchial gland volume may be  $\geq 50$ -fold the volume of goblet cells [3]. Gland acini are likely significant contributors of cytokines [54], particularly when gland hypertrophy and hyperplasia occur during COPD and asthma [3]. Our data support previous observations [45, 46] that the  $\text{Cl}^-$  channel activity of CFTR is anti-inflammatory during VIP stimulation, and may contribute to hyperinflammatory phenotypes reported in CF [45, 46]. Exocrine acinar cells accumulate  $\text{Cl}^-$  above electrochemical equilibrium ( $\geq 65 \text{ mM } [\text{Cl}^-]_i$ ; [7]) to support their dedicated fluid-secreting role. VIP stimulation lowers  $[\text{Cl}^-]_i$  ( $\sim 30 \text{ mM}$ ) in serous cells via  $\text{KCl}$  efflux through CFTR and  $\text{K}^+$  channels. Changes in serous cell intracellular  $[\text{Cl}^-]$  during stimulation are likely greater than the changes in surface epithelial cells, where resting intracellular  $[\text{Cl}^-]_i$  is lower ( $\leq 40 \text{ mM}$ ). Thus, the pro-inflammatory effects of elevated  $[\text{Cl}^-]_i$  may be more pronounced in serous cells, increasing inflammation in the absence of CFTR function. Similar to  $\text{Cl}^-$  and  $\text{HCO}_3^-$  secretion, our data suggest that activation of TMEM16A could compensate for

loss of CFTR, suggesting possible anti-inflammatory benefit to targeting TMEM16A in glands of patients who cannot utilize CFTR potentiator/corrector therapies.

Interestingly, NPY increased cytokine production during co-stimulation with TLR agonists, but it had less effect on  $\beta$ -defensin 2, which is also regulated by TLR-stimulated NF $\kappa$ B. This may suggest that NPY potentiates TLR-induced cytokine secretion via a non-NF $\kappa$ B mechanism, supported by the observation that NPY alone did not induce IL-6 or IL-8. Future work is needed to more fully dissect out the molecular details of NPYR signaling pathway in airway cells, including activated transcription factors.

**Acknowledgements:** We thank N. Cohen (Philadelphia VA Medical Center) for bacteria isolates, J. Riley (University of Pennsylvania Human Immunology Core) for access to human monocytes, M. Victoria (University of Pennsylvania) for assistance with macrophage differentiation and molecular biology, B. Chen (University of Pennsylvania) for assistance growing initial serous cultures, and J.K. Foskett (University of Pennsylvania) for initial training in many techniques used.

**Author Contributions:** D.B.M., R.M.C., M.A.K., and R.J.L. performed experiments and analyzed data. R.M.C., M.A.K., C.C.L.T., P.P., N.D.A., and J.N.P. aided with tissue procurement, primary cell acquisition and culture, maintenance of clinical records, and intellectually contributed. D.B.M., R.M.C., and R.J.L. drafted the manuscript with critical input and approval from all authors.

**Conflict of interest:** R.J.L. reports grants from the Cystic Fibrosis Foundation and National Institutes of Health that supported the conduct of the study. The other authors have nothing to disclose.

**Support statement:** Work was funded by grants from the Cystic Fibrosis Foundation (LEER16G0, LEE19G0) and National Institutes of Health (R21AI137484, R01DC016309). Primary human monocytes were obtained from the University of Pennsylvania Human Immunology Core, supported by National Institutes of Health P30CA016520 and P30AI045008.

## FIGURE LEGENDS

**FIGURE 1** cAMP stimulation of human nasal serous cells results in CFTR-dependent  $\text{Cl}^-$  and  $\text{HCO}_3^-$  secretion. **a)** Diagram showing use of cell volume measurements to track fluid secretion, primarily driven by  $\text{Cl}^-$ , which was combined with simultaneous measurement of  $\text{pH}_i$  to track  $\text{HCO}_3^-$  secretion. **b)** Non-CF serous cells stimulated with adenylyl cyclase-activating forskolin (top) or  $G_s$ -coupled receptor agonist VIP (bottom) exhibited ~15% shrinkage reflecting the activation of fluid secretion. **c-d)** In cells from non-CF patients, forskolin (c) or VIP (d) induced shrinkage (~15%; green) accompanied by a transient decrease in  $\text{pH}_i$  (~0.1-0.15 unit; gray) followed by a sustained secondary alkalinization. CF cells exhibited markedly reduced shrinkage and acidification; subsequent alkalinization was intact. **e-h)** Bar graphs showing peak shrinkage (green) and acidification (gray) in non-CF (e-g) and CF (h) cells. Forskolin-induced shrinkage and acidification was inhibited by  $\text{CFTR}_{\text{inh}}172$  (10  $\mu\text{M}$ ; e). VIP-induced shrinkage and acidification was inhibited by  $\text{CFTR}_{\text{inh}}172$  and  $\text{K}^+$  channel inhibitors clofilium and clotrimazole (30  $\mu\text{M}$  each; f).  $\text{Ca}^{2+}$ -activated  $\text{Cl}^-$  channel inhibitors NFA (100  $\mu\text{M}$ ), T16A<sub>inh</sub>-A01 (10  $\mu\text{M}$ ), CaCC<sub>inh</sub>-A01 (10  $\mu\text{M}$ ) or 4,4'-diisothiocyanostilbene-2,2"-disulfonic acid (DIDS; 1 mM) had no effect on VIP-induced responses (f) but blocked carbachol (CCh; 100  $\mu\text{M}$ ) responses. CF cells exhibited minimal responses to VIP but intact responses to CCh. VIP responses were restored by TMEM16A-activator  $E_{\text{act}}$  (25  $\mu\text{M}$ ). All experiments done at 37°C with 5%  $\text{CO}_2/25$  mM  $\text{HCO}_3^-$ . Data in e-h are mean  $\pm$  SEM of 5-8 individual experiments from  $\geq 4$  individual patients (1-2 experiments per patient). Significances determined by one-way ANOVA, Bonferroni posttest. **i)** Diagram showing activation of serous cell secretion by VIP, with  $\text{Cl}^-$  and  $\text{HCO}_3^-$  efflux through CFTR (apically localized in intact glands) causing a decrease in cell volume and  $\text{pH}_i$ . Influx of  $\text{Cl}^-$  through NKCC1 and influx of  $\text{HCO}_3^-$  through NBC (both basolaterally localized in intact glands) maintains the driving force for  $\text{Cl}^-$  and  $\text{HCO}_3^-$  efflux during sustained secretion.

**FIGURE 2** NPY reduces secretory responses to VIP by reducing anion efflux through CFTR in primary nasal gland serous cells. **a)** Representative traces showing cell volume (green) and  $\text{pH}_i$  (gray) in cells stimulated with VIP in the presence of scrambled NPY (scNPY; left) or NPY (right). **b)** Bar graph

showing peak responses. Cells stimulated with VIP in the presence of NPY exhibited reduced shrinkage ( $\text{Cl}^-$  secretion) and initial acidification ( $\text{HCO}_3^-$  secretion). Significance determined by 1-way ANOVA with Dunnett's posttest (VIP only as control group);  $**p < 0.01$  vs control. **c)** Representative  $\text{NO}_3^-$  substitution experiments showing changes in SPQ fluorescence with substitution of extracellular  $\text{Cl}^-$  for  $\text{NO}_3^-$ , which causes a decrease in  $[\text{Cl}^-]_i$ , and change in SPQ fluorescence. The rate of fluorescence change reflects the relative plasma membrane anion permeability. A downward deflection equals a decrease in  $[\text{Cl}^-]_i$ . **d)** Left is bar graph of initial rate of SPQ fluorescence change after VIP stimulation, which was inhibited by NPY but not scNPY. In the presence of CFTR<sub>inh</sub>172 (10  $\mu\text{M}$ ), rates of SPQ fluorescence change were reduced  $\sim 10$ -fold and there was no effect of NPY. Right shows rates of SPQ fluorescence change over a range of VIP and NPY concentrations, showing dose dependency of VIP activation of anion permeability and NPY inhibition of anion permeability. Significance determined by 1-way ANOVA with Bonferroni posttest; *a* and *c* show representative traces, while *b* and *d* show mean  $\pm$  SEM from  $\geq 6$  experiments using cells from  $\geq 3$  patients ( $\geq 2$  experiments per patient), with  $**p < 0.01$  vs VIP only.

**FIGURE 3** NPY inhibits VIP-induced cAMP increases in primary nasal gland serous cells. **a)** Representative traces of cADDis fluorescence (upward deflection of trace = increase in cAMP) showing reversible VIP-activated cAMP increases blocked by VIP receptor antagonist VIP<sub>6-28</sub>. **b)** Dose response showing peak cADDis fluorescence changes with VIP. Each data point is a separate experiment; graph shows data from at  $\geq 3$  serous cells from  $\geq 3$  patients (1 experiment per patient) for each [VIP]. **c)** Representative traces and bar graph showing intact cADDis responses with calcium chelation by 10  $\mu\text{M}$  BAPTA-AM loading (30 min) and stimulation in solution containing no added calcium + 1 mM EGTA. Bar graph shows mean  $\pm$  SEM of 5 experiments using cells from 5 different patients (1 experiment per patient). No significant difference by Student's *t* test. **d)** Peak cAMP responses to 0.5  $\mu\text{M}$  and 5  $\mu\text{M}$  VIP (top left) were inhibited by NPY (top right); NPY reduction of cAMP responses were abolished by NPY1R antagonist BIBO 3304 (5  $\mu\text{M}$ ; bottom left) or pertussis toxin (PTX; 6 hrs. pretreatment). **e)** Bar graphs showing peak responses (mean  $\pm$  SEM) from experiments as in *D* at two different [VIP]; data points from

≥6 experiments using cells from at least 3 patients (≥2 experiments per patient). Significance determined by 1-way ANOVA with Dunnett's posttest (VIP only as control); \*\* $p < 0.01$  vs VIP only.

**FIGURE 4** Expression of serous cell markers by primary nasal serous ALI cultures. **a)** Acinar cells isolated from middle turbinate were cultured and subject to Western blot for serous cell markers Muc7, VIP receptors VIPR1 and VIPR2, NKCC1 and alpha-1-antitrypsin (A1AT). Results from cultures from 2-3 patients are shown, representative of results observed from at least 3 independent experiments. **b)** Western blot for NPY1R and NPY4R (running at the molecular weight of a dimer due to unboiled samples; see supplementary methods) in cultures from 3 patients (representative blot from 3 independent experiments). **c)** Representative rtPCR showing expression of mRNA for NPY1R in serous ALI; results representative of 3 independent experiments from 3 patients. **d)** Fixed cultures were immunostained for serous markers lysozyme and Muc7, which showed punctate cytoplasmic staining similar to serous-like secretory granules. **e)** Immunocytochemistry for VIPR and VIPR2 revealed lateral membrane staining similar to GLUT1 and NKCC1. All images in *d-e* are representative of cultures from ≥3 separate patients. Scale bars are 20  $\mu\text{m}$ .

**FIGURE 5** Modulation of fluid and  $\text{HCO}_3^-$  secretion by VIP and NPY in serous ALI cultures. **a)** Apical  $\text{NO}_3^-$  substitution experiments (representative traces, left) and rates of SPQ change (bar graph, right) during stimulation with VIP (1  $\mu\text{M}$ )  $\pm$  NPY (100 nM) in the presence or absence of indicated inhibitors. **b)** ELISA results from steady-state cAMP measurements during stimulation with VIP or isoproterenol  $\pm$  NPY or scrambled NPY (scNPY). Concentrations shown are  $\mu\text{M}$ . **c)** Representative orthogonal slices of Texas red dextran-labeled airway surface liquid (ASL) in primary serous ALIs; scale bar is 10  $\mu\text{m}$  in both *x* and *z*. **d)** ASL height after 15 min basolateral stimulation as indicated. **e)** Primary human M $\phi$ s were incubated for 24 hrs with or without PMA, followed by washing to remove PMA and further 24 hour incubation in phenol red-free media alone. ASL height was measured in ALIs incubated in the presence of the M $\phi$ s and M $\phi$ -conditioned media with basolateral compounds added as indicated. **f)** ASL pH ( $\text{pH}_{\text{ASL}}$ ) measured using SNARF-1-dextran in cultures stimulated as indicated for 2 hours. As SNARF-1

is ratiometric, it is insensitive to changes in volume. Concentrations shown are  $\mu\text{M}$ . **g)**  $\text{pH}_{\text{ASL}}$  in ALIs incubated in the presence of  $\text{M}\phi\text{s}$  and  $\text{M}\phi$ -conditioned media as in **e** with basolateral compounds added as indicated. All bar graphs show mean  $\pm$  SEM of  $\geq 6$  independent experiments using ALI cultures from  $\geq 3$  patients ( $\geq 2$  cultures per patient). Significance in each bar graph determined by 1-way ANOVA with Bonferroni posttest; \* $p < 0.05$  and \*\* $p < 0.01$  vs bracketed groups and ## and # in  $F$  represent  $p < 0.05$  and  $p < 0.01$ , respectively vs unstimulated conditions.

**FIGURE 6** Antimicrobial peptide secretion and antibacterial efficacy of serous cells secretions are acutely enhanced by VIP but reduced by NPY. **a)** ALIs were stimulated basolaterally (2 hrs) with forskolin (10  $\mu\text{M}$ ) or VIP (1  $\mu\text{M}$ )  $\pm$  NPY (100 nM) or scrambled NPY (scNPY; 100 nM) as indicated. ASL was collected by washing the apical surface with 25% saline and assayed for lysozyme, Muc7, and  $\text{h}\beta\text{D1}$  by ELISA. Results are mean  $\pm$  SEM from  $\geq 3$  ALIs from  $\geq 3$  individual patients (1 ALI per patient). **b-c)** ASL from similar experiments was mixed with *P. aeruginosa* (**b**) or MRSA (**c**) isolated from CRS patients followed by incubation (2 hrs; 37°C; 5%  $\text{CO}_2$ ), dilution, and plating for CFU counting. Bar graphs show mean  $\pm$  SEM of  $\geq 5$  experiments using ALIs from  $\geq 3$  different patients; \*\* $p < 0.01$  and \* $p < 0.05$  between bracketed groups. Significance determined by 1-way ANOVA with Bonferroni posttest.

**FIGURE 7** Serous cell cytokine secretion in response to bacteria is increased by NPY and decreased by VIP in a CFTR-dependent manner. **a-c)** Primary serous cell ALIs were treated apically with heat-killed bacteria, followed by 24 hr incubation  $\pm$  basolateral NPY (100 nM) or scrambled NPY (scNPY; 100 nM). Basolateral media was collected for quantification of IL-6 (**a**), GM-CSF (**b**), and  $\text{TNF}\alpha$  (**c**). Bar graphs shown mean  $\pm$  SEM of  $\geq 5$  experiments using cells grown from  $\geq 3$  different patients. **d)** Primary serous ALIs were treated basolaterally with VIP (100  $\mu\text{M}$ ) and/or NPY (100 nM) and treated apically with CFTR inhibitor  $\text{CFTR}_{\text{inh}}172$  (15  $\mu\text{M}$ ), TMEM16A activator  $E_{\text{act}}$  (15  $\mu\text{M}$ ), and/or TMEM16A inhibitor  $\text{CaCC}_{\text{inh}}\text{-A01}$  (15  $\mu\text{M}$ ). Basolateral media was collected after 24 hrs. and assayed for IL-1 $\beta$ . **e-f)** Primary serous ALIs were treated apically with heat-killed *P. aeruginosa*, followed by 24 hrs incubation  $\pm$  basolateral NPY

and/or VIP as well as  $\pm$  apical CFTR<sub>inh</sub>172 and/or E<sub>act</sub> and/or 1-EBIO (150  $\mu$ M). Basolateral media was collected and assayed for GM-CSF (e), IL-6 (e), or IL-8 (f) by ELISA. Significance by 1-way ANOVA with Bonferroni posttest comparing the three bars for each separate strain in a-c and comparing bracketed bars in d-e; \*\* p<0.01 and \* p<0.05.

**FIGURE 8** Model of VIPergic and NPYergic regulation of serous cell function and implications for airway diseases. **a)** Activation of VIP receptors on serous cells allows G $\alpha$ <sub>s</sub> (Gs) activation of adenylyl cyclase (AC), elevation of cAMP, and Cl<sup>-</sup> and HCO<sub>3</sub><sup>-</sup> efflux through PKA-activated CFTR. In contrast, activation of muscarinic receptors by acetylcholine (ACh) stimulates G $\alpha$ <sub>q</sub> (Gq)-dependent calcium (Ca<sup>2+</sup>) elevation and Cl<sup>-</sup>/HCO<sub>3</sub><sup>-</sup> secretion through TMEM16A (based on data here and [3, 7]). While regulated by two independent pathways, our data suggest CFTR and TMEM16A are functionally equivalent anion efflux pathways. A result of Cl<sup>-</sup> efflux (and parallel K<sup>+</sup> efflux, not shown [7]) is a reduction intracellular Cl<sup>-</sup> concentration ([Cl<sup>-</sup>]<sub>i</sub>) **b)** NPY receptors, in contrast, activate G $\alpha$ <sub>i</sub> (Gi) proteins to inhibit AC and reduce VIP-activated cAMP responses. This blunts both the CFTR-mediated anion secretion as well as VIP-activated antimicrobial peptide (AMP) secretion, likely vesicular secretion. NPY has no effects on cholinergic anion or AMP secretion because it is driven by Ca<sup>2+</sup> rather than cAMP. **c)** We hypothesize that, in CF, VIP cannot elicit anion and fluid secretion via CFTR. Also, since [Cl<sup>-</sup>]<sub>i</sub> remains elevated, inflammatory responses may be increased. **d)** In asthma, elevated NPY may increase Gi activity to blunt cAMP responses downstream of VIP, reducing CFTR activity and fluid secretion as well as vesicular AMP secretion. NPY also has pro-inflammatory effects.

## References

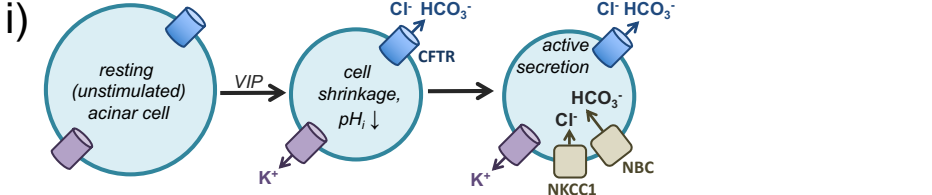
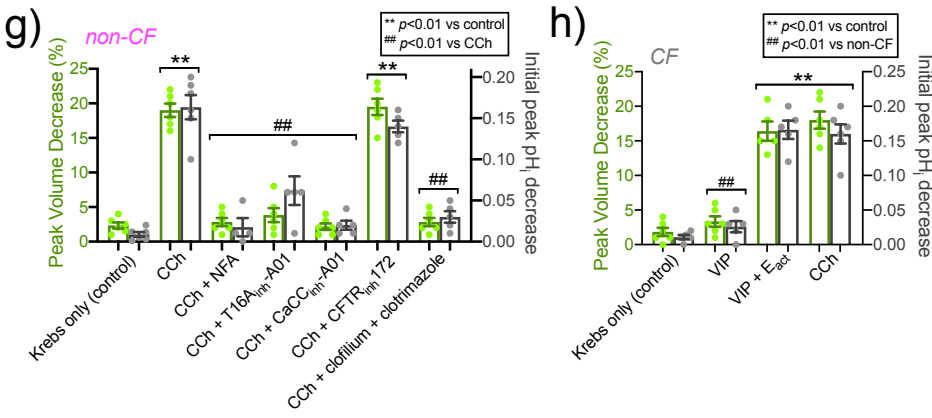
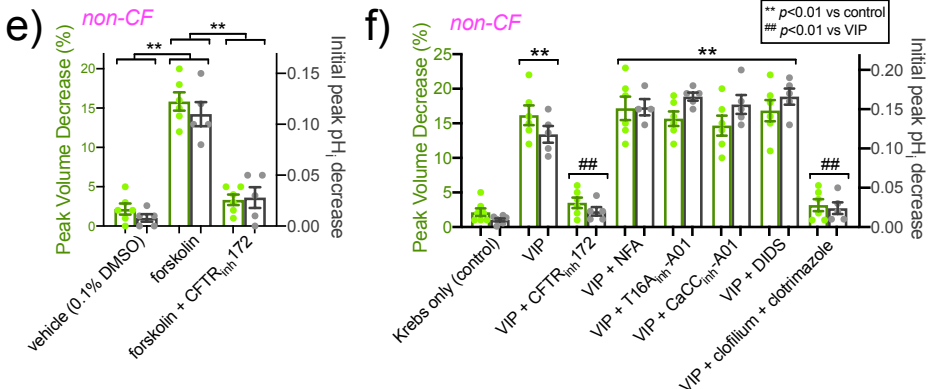
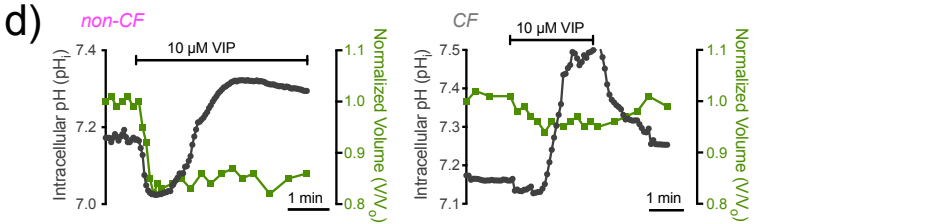
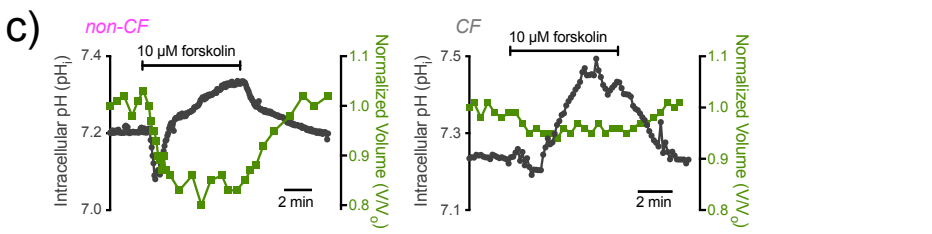
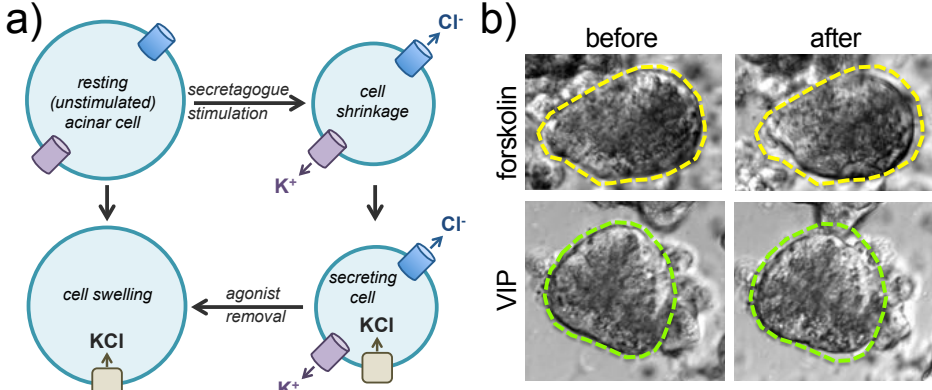
1. Rogers DF. Physiology of airway mucus secretion and pathophysiology of hypersecretion. *Respir Care* 2007; 52(9): 1134-1146; discussion 1146-1139.
2. Kato K, Song BH, Howe CL, Chang EH. A Comprehensive Systematic Review of the Association Between Airway Mucins and Chronic Rhinosinusitis. *Am J Rhinol Allergy* 2019: 1945892419837042.
3. Widdicombe JH, Wine JJ. Airway Gland Structure and Function. *Physiol Rev* 2015; 95(4): 1241-1319.
4. Chen FH, Samson KT, Miura K, Ueno K, Odajima Y, Shougo T, Yoshitsugu Y, Shioda S. Airway remodeling: a comparison between fatal and nonfatal asthma. *J Asthma* 2004; 41(6): 631-638.
5. Kunzelmann K, Schreiber R, Hadorn HB. Bicarbonate in cystic fibrosis. *J Cyst Fibros* 2017; 16(6): 653-662.
6. Lee RJ, Harlow JM, Limberis MP, Wilson JM, Foskett JK. HCO<sub>3</sub><sup>-</sup> secretion by murine nasal submucosal gland serous acinar cells during Ca<sup>2+</sup>-stimulated fluid secretion. *J Gen Physiol* 2008; 132(1): 161-183.
7. Lee RJ, Foskett JK. Ca<sup>2+</sup> signaling and fluid secretion by secretory cells of the airway epithelium. *Cell Calcium* 2014; 55(6): 325-336.
8. Baraniuk JN, Kaliner MA. Neuropeptides and nasal secretion. *J Allergy Clin Immunol* 1990; 86(4 Pt 2): 620-627.
9. Baraniuk JN, Lundgren JD, Okayama M, Mullol J, Merida M, Shelhamer JH, Kaliner MA. Vasoactive intestinal peptide in human nasal mucosa. *J Clin Invest* 1990; 86(3): 825-831.
10. Chanez P, Springall D, Vignola AM, Moradoghi-Hattvani A, Polak JM, Godard P, Bousquet J. Bronchial mucosal immunoreactivity of sensory neuropeptides in severe airway diseases. *Am J Respir Crit Care Med* 1998; 158(3): 985-990.
11. Tanaka Y, Yoshida Y, Hirano M. Precise localization of VIP-, NPY-, and TH-immunoreactivities of cat laryngeal glands. *Brain Res Bull* 1995; 36(3): 219-224.
12. Heppt W, Dinh QT, Cryer A, Zweng M, Noga O, Peiser C, Melvan M, Witt C, Fischer A, Groneberg DA. Phenotypic alteration of neuropeptide-containing nerve fibres in seasonal intermittent allergic rhinitis. *Clin Exp Allergy* 2004; 34(7): 1105-1110.

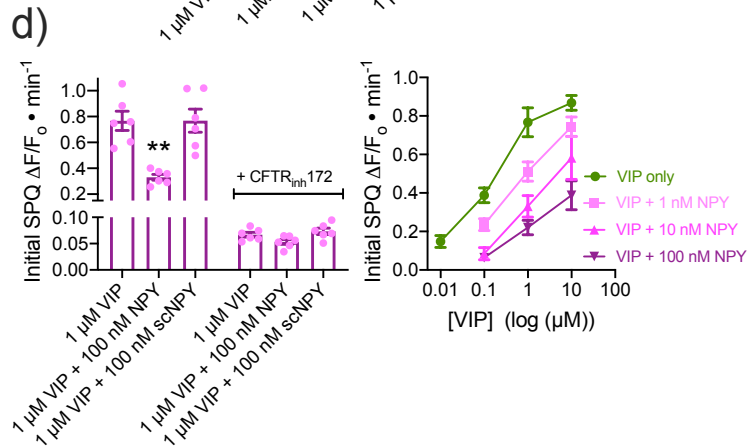
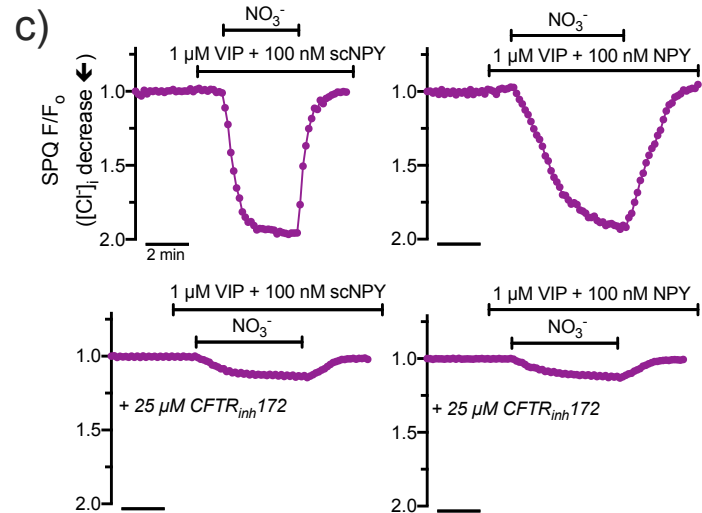
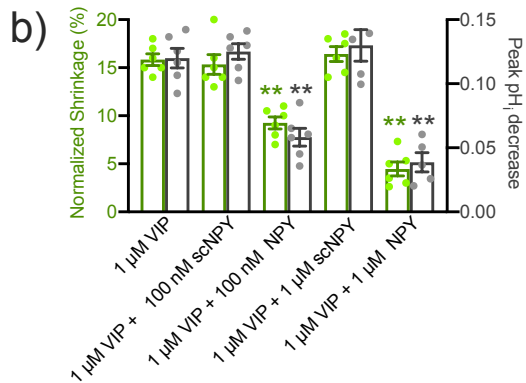
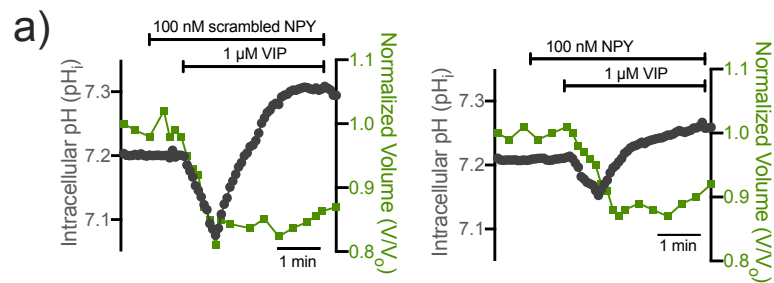
13. Groneberg DA, Heppt W, Cryer A, Wussow A, Peiser C, Zweng M, Dinh QT, Witt C, Fischer A. Toxic rhinitis-induced changes of human nasal mucosa innervation. *Toxicol Pathol* 2003; 31(3): 326-331.
14. Bowden JJ, Gibbins IL. Vasoactive intestinal peptide and neuropeptide Y coexist in non-noradrenergic sympathetic neurons to guinea pig trachea. *J Auton Nerv Syst* 1992; 38(1): 1-19.
15. Luts A, Uddman R, Alm P, Basterra J, Sundler F. Peptide-containing nerve fibers in human airways: distribution and coexistence pattern. *Int Arch Allergy Immunol* 1993; 101(1): 52-60.
16. Uddman R, Sundler F, Emson P. Occurrence and distribution of neuropeptide-Y-immunoreactive nerves in the respiratory tract and middle ear. *Cell Tissue Res* 1984; 237(2): 321-327.
17. Fang SY, Shen CL, Ohyama M. Presence of neuropeptides in human nasal polyps. *Acta Otolaryngol* 1994; 114(3): 324-328.
18. Fujiwara S, Hoshizaki M, Ichida Y, Lex D, Kuroda E, Ishii KJ, Magi S, Okada M, Takao H, Gandou M, Imai H, Hara R, Herzog H, Yoshimura A, Okamura H, Penninger JM, Slutsky AS, Uhlig S, Kuba K, Imai Y. Pulmonary phagocyte-derived NPY controls the pathology of severe influenza virus infection. *Nat Microbiol* 2019; 4(2): 258-268.
19. Li S, Koziol-White C, Jude J, Jiang M, Zhao H, Cao G, Yoo E, Jester W, Morley MP, Zhou S, Wang Y, Lu MM, Panettieri RA, Jr., Morrisey EE. Epithelium-generated neuropeptide Y induces smooth muscle contraction to promote airway hyperresponsiveness. *J Clin Invest* 2016; 126(5): 1978-1982.
20. Augustyniak D, Nowak J, Lundy FT. Direct and indirect antimicrobial activities of neuropeptides and their therapeutic potential. *Curr Protein Pept Sci* 2012; 13(8): 723-738.
21. Makinde TO, Steininger R, Agrawal DK. NPY and NPY receptors in airway structural and inflammatory cells in allergic asthma. *Exp Mol Pathol* 2013; 94(1): 45-50.
22. Lu Y, Ho R, Lim TK, Kuan WS, Goh DY, Mahadevan M, Sim TB, Van Bever HP, Larbi A, Ng TP. Neuropeptide Y may mediate psychological stress and enhance TH2 inflammatory response in asthma. *J Allergy Clin Immunol* 2015; 135(4): 1061-1063 e1064.
23. Macia L, Rao PT, Whewey J, Siervo F, Mackay F, Herzog H. Y1 signalling has a critical role in allergic airway inflammation. *Immunol Cell Biol* 2011; 89(8): 882-888.
24. Prod'homme T, Weber MS, Steinman L, Zamvil SS. A neuropeptide in immune-mediated inflammation, Y? *Trends Immunol* 2006; 27(4): 164-167.

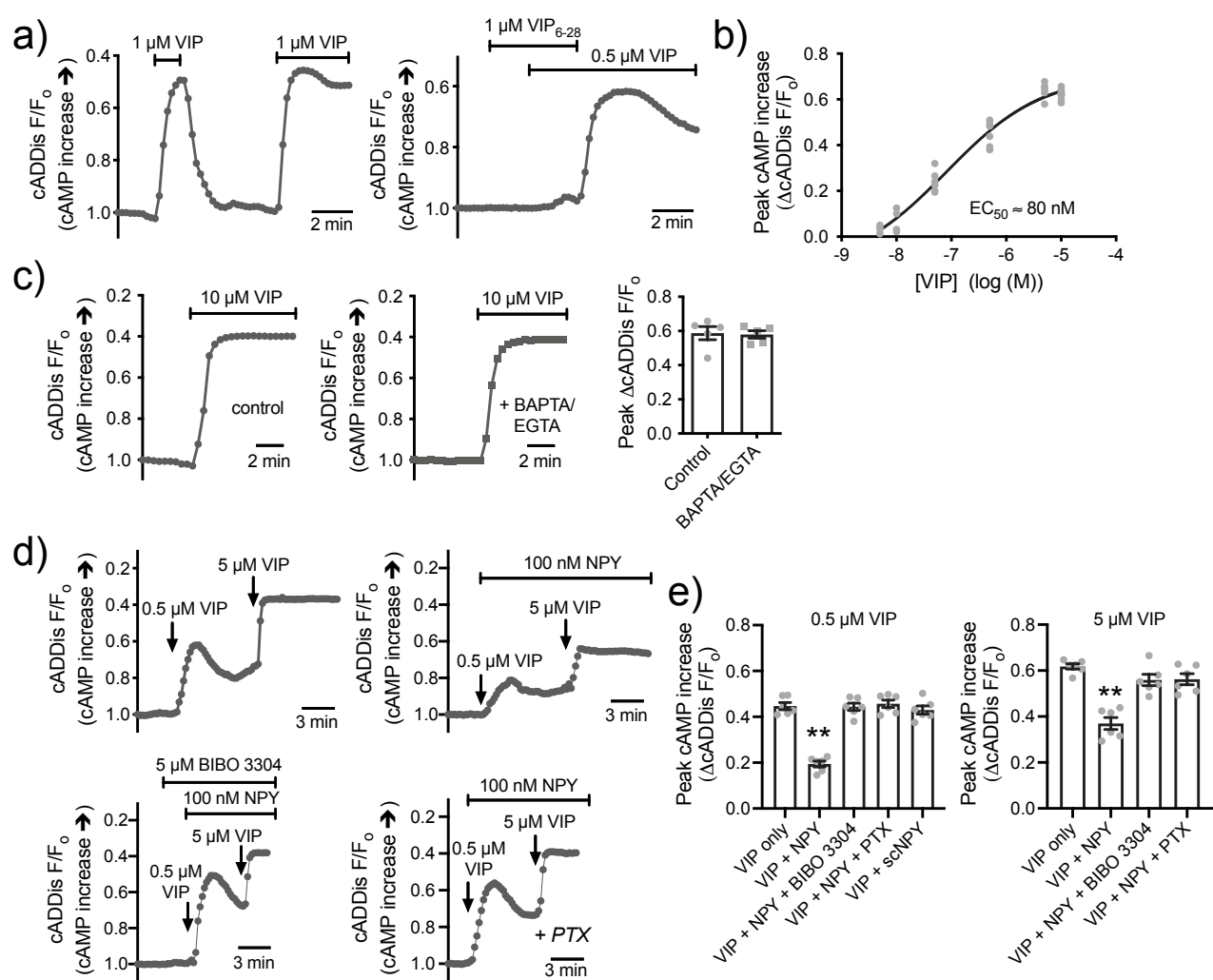
25. Buttari B, Profumo E, Domenici G, Tagliani A, Ippoliti F, Bonini S, Businaro R, Elenkov I, Rigano R. Neuropeptide Y induces potent migration of human immature dendritic cells and promotes a Th2 polarization. *FASEB J* 2014; 28(7): 3038-3049.
26. Mosimann BL, White MV, Hohman RJ, Goldrich MS, Kaulbach HC, Kaliner MA. Substance P, calcitonin gene-related peptide, and vasoactive intestinal peptide increase in nasal secretions after allergen challenge in atopic patients. *J Allergy Clin Immunol* 1993; 92(1 Pt 1): 95-104.
27. Lee RJ, Chen B, Doghramji L, Adappa ND, Palmer JN, Kennedy DW, Cohen NA. Vasoactive intestinal peptide regulates sinonasal mucociliary clearance and synergizes with histamine in stimulating sinonasal fluid secretion. *FASEB J* 2013; 27(12): 5094-5103.
28. Atanasova KR, Reznikov LR. Neuropeptides in asthma, chronic obstructive pulmonary disease and cystic fibrosis. *Respir Res* 2018; 19(1): 149.
29. Merten MD, Figarella C. Neuropeptide Y and norepinephrine cooperatively inhibit human tracheal gland cell secretion. *Am J Physiol* 1994; 266(5 Pt 1): L513-518.
30. Webber SE. The effects of peptide histidine isoleucine and neuropeptide Y on mucus volume output from the ferret trachea. *Br J Pharmacol* 1988; 95(1): 49-54.
31. Huang SC, Tsai MF. Receptors for peptide YY and neuropeptide Y on guinea pig pancreatic acini. *Peptides* 1994; 15(3): 405-410.
32. Chandrasekharan B, Nezami BG, Srinivasan S. Emerging neuropeptide targets in inflammation: NPY and VIP. *Am J Physiol Gastrointest Liver Physiol* 2013; 304(11): G949-957.
33. Lee RJ, Foskett JK. cAMP-activated Ca<sup>2+</sup> signaling is required for CFTR-mediated serous cell fluid secretion in porcine and human airways. *J Clin Invest* 2010; 120(9): 3137-3148.
34. Finkbeiner WE, Zlock LT, Mehdi I, Widdicombe JH. Cultures of human tracheal gland cells of mucous or serous phenotype. *In Vitro Cell Dev Biol Anim* 2010; 46(5): 450-456.
35. McMahon DB, Workman AD, Kohanski MA, Carey RM, Freund JR, Hariri BM, Chen B, Doghramji LJ, Adappa ND, Palmer JN, Kennedy DW, Lee RJ. Protease-activated receptor 2 activates airway apical membrane chloride permeability and increases ciliary beating. *FASEB J* 2018; 32(1): 155-167.
36. Huang J, Kim D, Shan J, Abu-Arish A, Luo Y, Hanrahan JW. Most bicarbonate secretion by Calu-3 cells is mediated by CFTR and independent of pendrin. *Physiol Rep* 2018; 6(5).

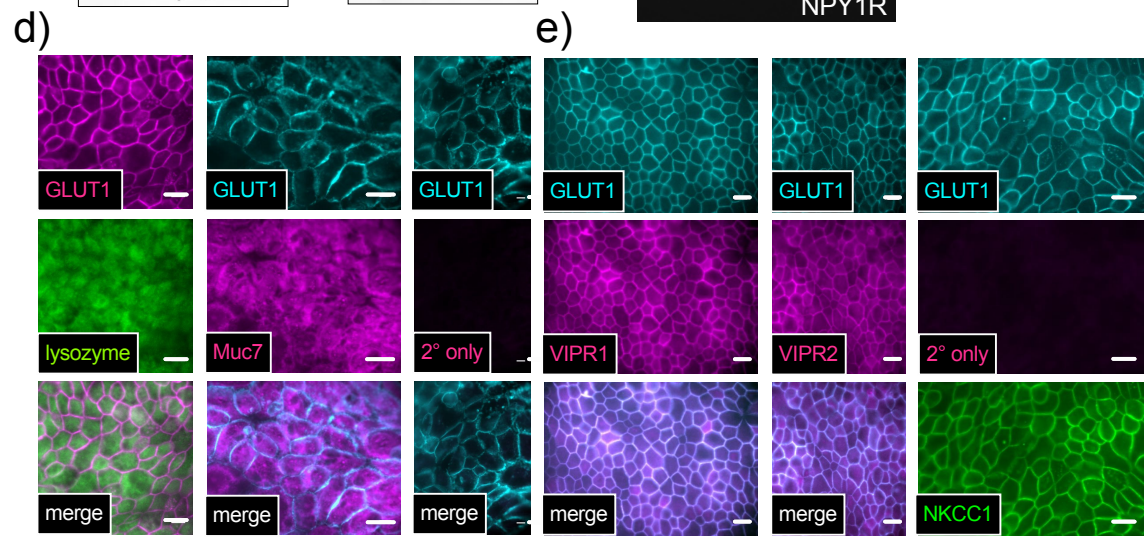
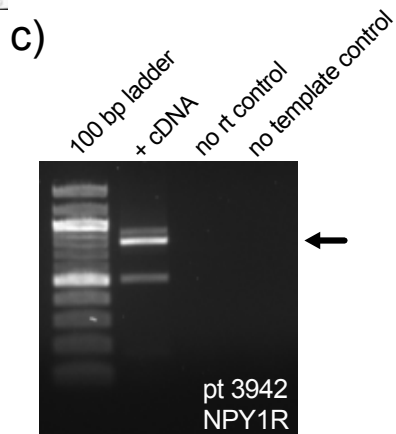
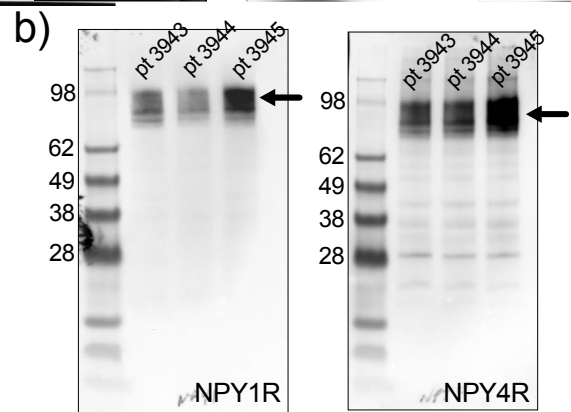
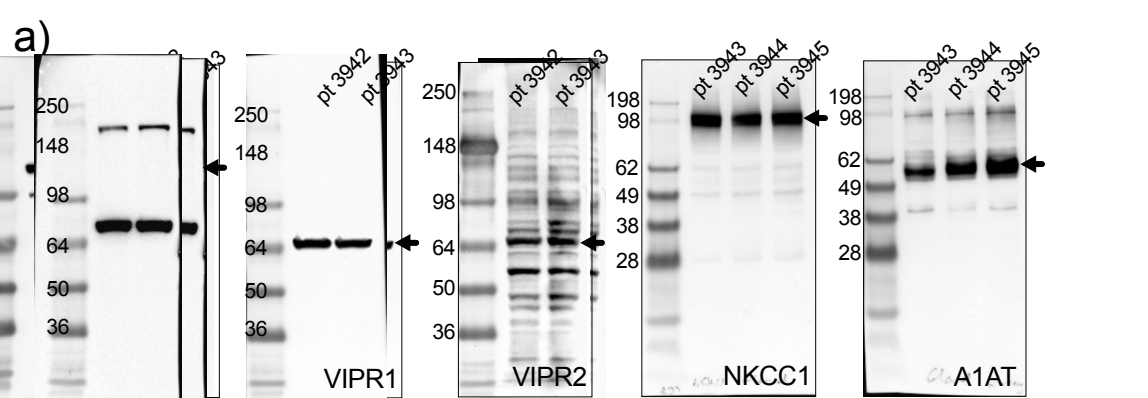
37. Tewson PH, Martinka S, Shaner NC, Hughes TE, Quinn AM. New DAG and cAMP Sensors Optimized for Live-Cell Assays in Automated Laboratories. *J Biomol Screen* 2016; 21(3): 298-305.
38. Kunzelmann K, Mehta A. CFTR: a hub for kinases and crosstalk of cAMP and Ca<sup>2+</sup>. *FEBS J* 2013; 280(18): 4417-4429.
39. Worthington EN, Tarran R. Methods for ASL measurements and mucus transport rates in cell cultures. *Methods Mol Biol* 2011; 742: 77-92.
40. Nakagami Y, Favoreto S, Jr., Zhen G, Park SW, Nguyenvu LT, Kuperman DA, Dolganov GM, Huang X, Boushey HA, Avila PC, Erle DJ. The epithelial anion transporter pendrin is induced by allergy and rhinovirus infection, regulates airway surface liquid, and increases airway reactivity and inflammation in an asthma model. *J Immunol* 2008; 181(3): 2203-2210.
41. Vanoni S, Scantamburlo G, Dossena S, Paulmichl M, Nofziger C. Interleukin-Mediated Pendrin Transcriptional Regulation in Airway and Esophageal Epithelia. *Int J Mol Sci* 2019; 20(3).
42. Dorschner RA, Lopez-Garcia B, Peschel A, Kraus D, Morikawa K, Nizet V, Gallo RL. The mammalian ionic environment dictates microbial susceptibility to antimicrobial defense peptides. *FASEB J* 2006; 20(1): 35-42.
43. Kreda SM, Seminario-Vidal L, van Heusden CA, O'Neal W, Jones L, Boucher RC, Lazarowski ER. Receptor-promoted exocytosis of airway epithelial mucin granules containing a spectrum of adenine nucleotides. *J Physiol* 2010; 588(Pt 12): 2255-2267.
44. Suzuki A, Iwata J. Molecular Regulatory Mechanism of Exocytosis in the Salivary Glands. *Int J Mol Sci* 2018; 19(10).
45. Veit G, Bossard F, Goepf J, Verkman AS, Galletta LJ, Hanrahan JW, Lukacs GL. Proinflammatory cytokine secretion is suppressed by TMEM16A or CFTR channel activity in human cystic fibrosis bronchial epithelia. *Mol Biol Cell* 2012; 23(21): 4188-4202.
46. Schnur A, Hegyi P, Rousseau S, Lukacs GL, Veit G. Epithelial Anion Transport as Modulator of Chemokine Signaling. *Mediators Inflamm* 2016; 2016: 7596531.
47. Zhang YL, Chen PX, Guan WJ, Guo HM, Qiu ZE, Xu JW, Luo YL, Lan CF, Xu JB, Hao Y, Tan YX, Ye KN, Lun ZR, Zhao L, Zhu YX, Huang J, Ko WH, Zhong WD, Zhou WL, Zhong NS. Increased intracellular Cl<sup>-</sup> concentration promotes ongoing inflammation in airway epithelium. *Mucosal Immunol* 2018; 11(4): 1149-1157.

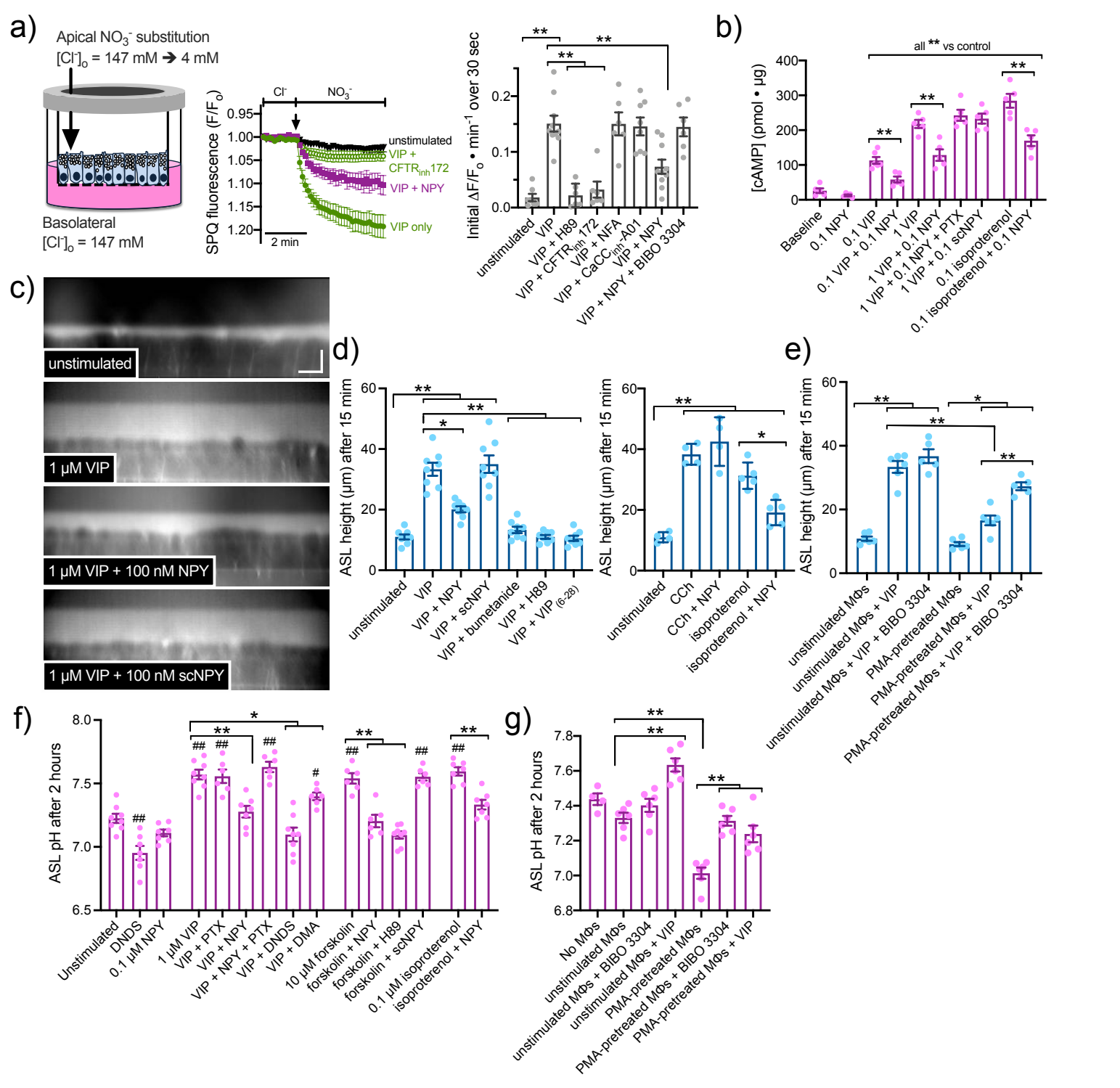
48. Armstrong DS, Hook SM, Jansen KM, Nixon GM, Carzino R, Carlin JB, Robertson CF, Grimwood K. Lower airway inflammation in infants with cystic fibrosis detected by newborn screening. *Pediatr Pulmonol* 2005; 40(6): 500-510.
49. Dhooghe B, Noel S, Huaux F, Leal T. Lung inflammation in cystic fibrosis: pathogenesis and novel therapies. *Clin Biochem* 2014; 47(7-8): 539-546.
50. Lee RJ, Workman AD, Carey RM, Chen B, Rosen PL, Doghramji L, Adappa ND, Palmer JN, Kennedy DW, Cohen NA. Fungal Aflatoxins Reduce Respiratory Mucosal Ciliary Function. *Sci Rep* 2016; 6: 33221.
51. Pfister S, Weber T, Hartig W, Schwerdel C, Elsaesser R, Knuesel I, Fritschy JM. Novel role of cystic fibrosis transmembrane conductance regulator in maintaining adult mouse olfactory neuronal homeostasis. *J Comp Neurol* 2015; 523(3): 406-430.
52. Tiringier K, Treis A, Fucik P, Gona M, Gruber S, Renner S, Dehlink E, Nachbaur E, Horak F, Jaksch P, Doring G, Cramer R, Jung A, Rochat MK, Hormann M, Spittler A, Klepetko W, Akdis CA, Szepfalusi Z, Frischer T, Eiwegger T. A Th17- and Th2-skewed cytokine profile in cystic fibrosis lungs represents a potential risk factor for *Pseudomonas aeruginosa* infection. *Am J Respir Crit Care Med* 2013; 187(6): 621-629.
53. Dios ID. Inflammatory role of the acinar cells during acute pancreatitis. *World J Gastrointest Pharmacol Ther* 2010; 1(1): 15-20.
54. Furukawa E, Ohrai T, Yamaya M, Suzuki T, Nakasato H, Sasaki T, Kanda A, Yasuda H, Nishimura H, Sasaki H. Human airway submucosal glands augment eosinophil chemotaxis during rhinovirus infection. *Clin Exp Allergy* 2004; 34(5): 704-711.



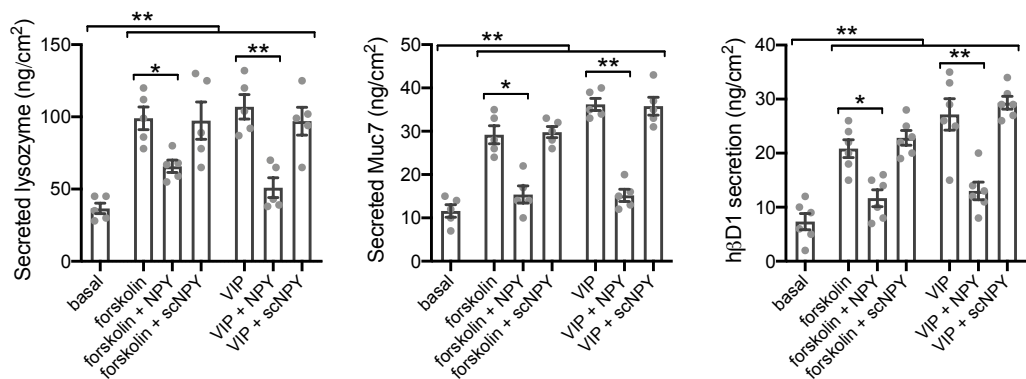




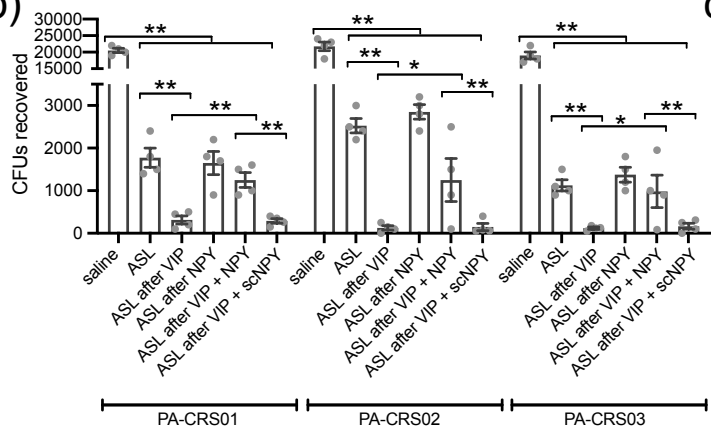




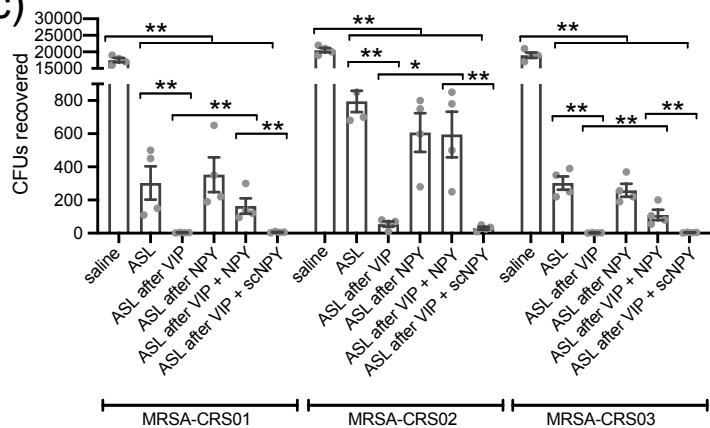
a)

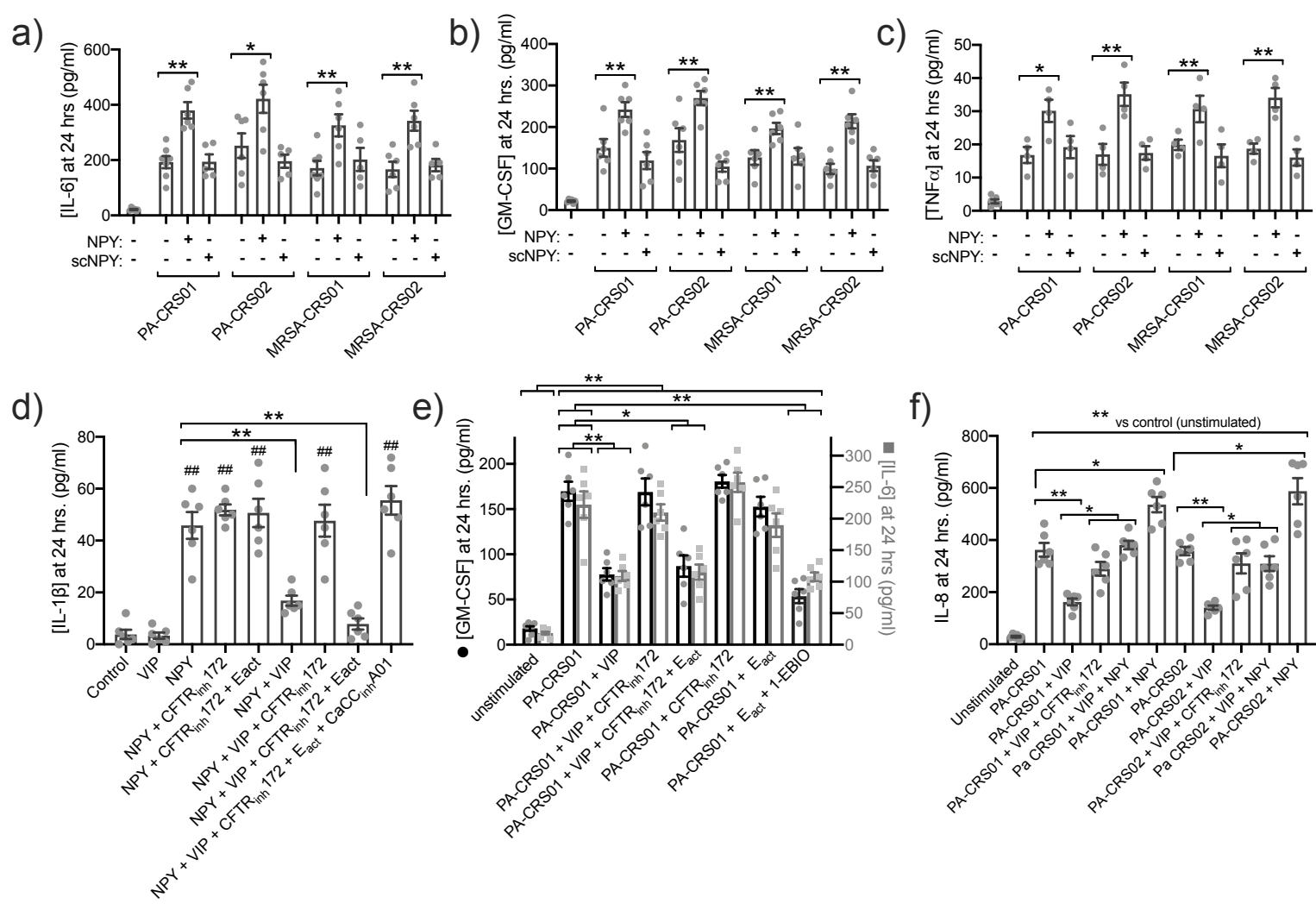


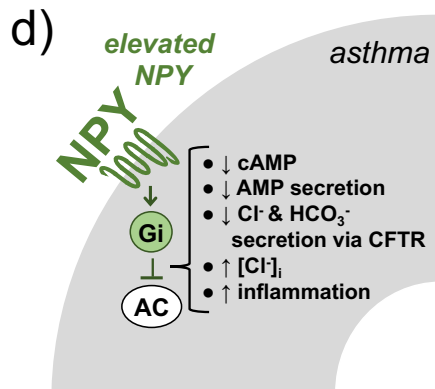
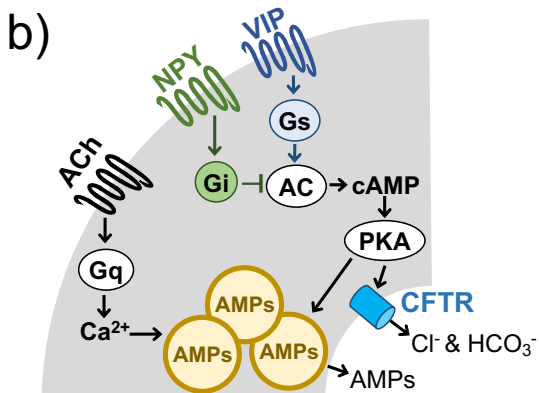
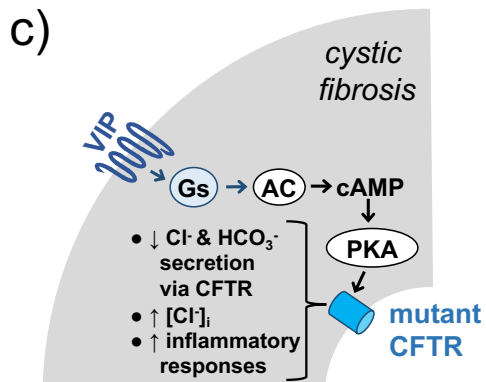
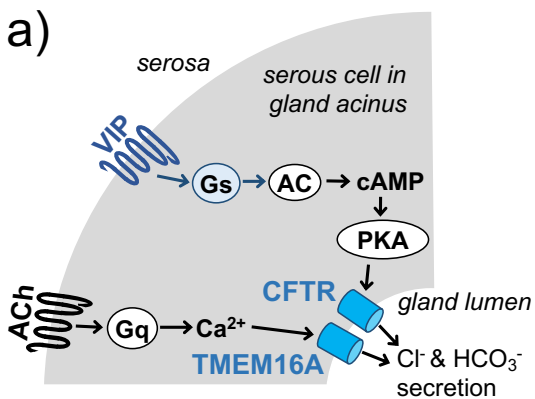
b)



c)







## SUPPLEMENTARY METHODS

### *Reagents and Solutions*

Reagents for fluorescence microscopy (SNARF-5F-AM, SNARF-1 dextran, 6-methoxy-N-(3-sulfopropyl)quinolinium [SPQ], Texas Red dextran [10,000 MW], BAPTA-AM, fura-2-AM) were from ThermoFisher Scientific. Calbryte 590-AM was from AAT Bioquest. ELISA development kits were from Peprotech (GM-CSF Cat # 900-K30, IL-6 Cat # 900-K16, TNF $\alpha$  Cat # 900-K25, IL-1 $\beta$  Cat # 900-K95, IL-33 Cat #900-K398, h $\beta$ D1 Cat #900-K202, h $\beta$ D2 Cat #900-K172) or BD Biosciences (IL-8 Cat #555244). Pre-coated ELISAs were from Aviva Systems Biology (Muc7 Cat # OKEH01290, Muc5B Cat # OKEH02841, Muc5AC Cat # OKEH02840, lysozyme Cat # OKCD01349, lactoferrin Cat # OKEH02822) or LSBio (NPY Cat # LS-F5407). Intracellular cAMP from lysed cells was measured using Amersham Biosciences cAMP Biotrak Enzyme Immunoassay system (GE Healthcare) per the manufacturer's instructions using the non-acetylation protocol (sensitivity of 25-6400 fmol per assay well). Live cell imaging of cAMP utilized downward green cADDis (Montana Molecular [1]) in a baculovirus modified for mammalian cells (BacMam; [2]). IL-4, IL-13, and LPS were from Cell Signaling Technologies and prepared with carrier BSA as per the manufacturer's instructions. Poly(I:C), NPY, scrambled NPY, BIBO 3304, VIP, VIP<sub>(6-28)</sub>, [D-p-CI-Phe<sup>6</sup>,Leu<sup>17</sup>]-VIP, were from Tocris. T16A<sub>inh</sub>-A01, CaCC<sub>inh</sub>-A01, CFTR<sub>inh</sub>-172, NPPB, 4,4'-diisothiocyanato-2,2'-silbenedisulfonic acid (DIDS), carbachol (CCh) were from Cayman Chemical. Inorganic salts for buffers, TNF $\alpha$ , bumetanide, forskolin, 4,4'-dinitrostilbene-2,2'-disulfonic acid (DNDS), 5-(N,N-dimethyl)amiloride (DMA), N-phenyl-1-naphthylamine (NPN), and all other reagents were from Sigma-Aldrich, unless otherwise indicated below.

Antibodies for lysozyme (BGN/06/96I; Cat # ab36362), lactoferrin (2B8, Cat # ab10110), Na<sup>+</sup>/K<sup>+</sup> ATPase (EP1845Y; Cat # ab76020), Muc7 (Cat # ab55542), Muc5AC (Cat # ab3649), alpha-1-antitrypsin (Cat # ab20830),  $\beta$ 2 adrenergic receptor (Cat # ab182136) and Glut1 (rabbit polyclonal; Cat# ab15039) were from Abcam. Mouse monoclonal antibody to Glut1 (SPM498; Cat # MS-10637)

was from Thermo. Antibodies to VIPR1 (Cat # AVR-001) and TMEM16A (Cat # ACL-011) were from Alomone Labs. Antibody to VIPR2 (Cat # PA3-114) was from Pierce. Antibody to NKCC1 (mouse monoclonal, clone T9) was from Developmental Studies Hybridoma Bank. Antibodies to CFTR were used as a cocktail (1:100 each); monoclonal clones 24-1 and M3A7 were from Novus Biologicals.

All solutions used were prepared as described [3, 4]. Krebs  $\text{HCO}_3^-$  buffer for isolated acinar cell experiments contained 125 NaCl, 5 KCl, 1.2  $\text{MgCl}_2$ , 1.2  $\text{NaH}_2\text{PO}_4$ , 11 glucose, and 25  $\text{NaHCO}_3$ , gassed with 95%  $\text{O}_2$  + 5%  $\text{CO}_2$ . Krebs  $\text{HCO}_3^-$ -free buffer contained 125 NaCl, 5 KCl, 1.2  $\text{MgCl}_2$ , 1.2  $\text{CaCl}_2$ , 1.2  $\text{NaH}_2\text{PO}_4$ , 11 glucose, 20 HEPES, 20 sucrose, pH 7.4, gassed with 100%  $\text{O}_2$ . Solutions for buffering capacity measurement, SNARF calibration, and SPQ calibration were as described [3, 4] and are indicated below. Hank's balanced salt solution (HBSS) contained (in mM) 138 NaCl, 5.3 KCl, 0.4  $\text{KH}_2\text{PO}_4$ , 0.34  $\text{NaHPO}_4$ , 0.41  $\text{MgSO}_4$ , 0.49  $\text{MgCl}_2$ , 1.8  $\text{CaCl}_2$ , 5.6 glucose, 20 mM HEPES pH 7.4. Unless indicated, all cell culture reagents were from Gibco. Bumetanide was used at 100  $\mu\text{M}$ , H89 at 10  $\mu\text{M}$ , BIBO 3304 at 1  $\mu\text{M}$ , DNDS at 30  $\mu\text{M}$ . Stocks were made at 1000x in DMSO.

### ***Serous cell isolation and culture***

Primary human nasal serous acinar cells were used to study  $\text{Cl}^-$ /fluid and  $\text{HCO}_3^-$  secretion. Studies of human turbinate submucosal gland serous cells are directly relevant to the understanding of mechanisms of CRS, particularly CF-related CRS, and turbinate gland serous cells approximate gland serous cells from the lower airway. We established that pig bronchial serous cell responses are identical to human turbinate serous cells [5, 6]. Working with human cells has important advantages over mice, as data from intact glands [7] and our own studies [3-6, 8, 9] have established important differences between mouse serous cells and those from pigs and humans.

Patients undergoing medically indicated sinonasal surgery were recruited from the Department of Otorhinolaryngology at the University of Pennsylvania with written informed consent as previously described [10-13]. Inclusion criteria were patients  $\geq 18$  years of age undergoing surgery for sinonasal disease (CRS) or other procedures (e.g., trans-nasal approaches to the skull base) where tissue was

classified as “control.” Exclusion criteria included history of systemic inheritable disease (e.g., granulomatosis with polyangiitis or systemic immunodeficiencies) with the exception of cystic fibrosis (CF). Members of vulnerable populations were not included.

Comparisons made here between non-CF and CF cell  $\text{Cl}^-$  and  $\text{HCO}_3^-$  secretion are valid, because SNARF and SPQ properties were identical between CF and non-CF cells, and both genotypes had identical resting  $[\text{Cl}^-]_i$ , resting  $\text{pH}_i$ , and intracellular  $\text{pH}_i$  buffering capacity (**supplementary figures S19-S20**). Moreover, non-CF and CF cells exhibited identical cAMP responses to VIP stimulation (**supplementary figure S6**).

Among non-CF patients, there was minimal patient-to-patient variability in the VIP-activated ion transport phenotype measured by cell shrinkage (**supplementary figure S21a-b**) once cells were removed from the tissue environment, as we previously described [6]. For ALI cultures of serous cells, we also observed minimal patient-to-patient variability in antimicrobial secretion in response to VIP (**supplementary figure s21c**) or IL-6 release in response to LPS (**supplementary figure S21d**). This is similar to surface epithelial cultures, where we find that once primary airway cells are removed from an inflammatory environment and expanded and cultured for 3-6 weeks in defined media, secondary disease-related phenotypes are removed and cells reflect a “healthy” baseline state, with responses overwhelmingly dictated by genetics, as previously described [10-18]. This allows disease-relevant *in vitro* manipulations (treatment with IL-13, NPY, etc.) with comparison of unmanipulated cells from the same patient as “control.” For these reasons and for logistical feasibility, some of the data points in each figure representing independent experiments used cells that originated from the same patient, as we have previously done [6, 10-14, 16, 19, 20]. An equal number of independent experiments, typically 2, was performed using cells from each patient to ensure that one patient could not skew results in any experiment, though minimal variability was observed as described above. All experiments shown utilized cells from multiple patients as indicated in the figure legends.

Isolated tissue was first placed in HBSS supplemented with 2 mM L-glutamine, MEM-vitamins MEM-amino acids, MEM non-essential amino acids, and 1% BSA. The epithelium was removed via

forceps and submucosal tissue was removed from the bone. The tissue was mechanically minced with scissors and then incubated for 90 min at room temperature in HBSS supplemented as above but with 1 mg/ml Collagenase P (Roche) and 10 µg/ml DNase I (Roche) with gentle shaking. Remaining intact tissue pieces were separated from dispersed acini and acinar cells by gravity (3 min). Gland acini were separated from single epithelial or immune cells by a short centrifugation (30 sec, 500x g). The isolation protocol yielded acini and strings of acinar cells. Acini were further dispersed by incubation with 0.5 mg/ml collagenase P as above for 60 min. Cells were pelleted and washed with HBSS before being seeded onto glass coverslips for imaging or collagen-coated transwells.

For culturing, acinar cells were washed with and resuspended in 1:1 MEME:Ham's F12K plus 20% FBS, 1x cell culture pen/strep supplement (GIBCO), gentamycin (100 µg/ml), and amphotericin B (2.5 µg/ml) modified from [21]. Cells were seeded ( $\sim 3 \times 10^5$  cells per  $\text{cm}^2$ ) on transparent Falcon filters (#353095; 0.3  $\text{cm}^2$ ; 0.4 µm pores) coated with human placental collagen. After confluence, the media was changed to 1:1 MEME:Lonza bronchial epithelial basal media (BEBM) including insulin (5 µg/ml), transferrin (5 µg/ml), hydrocortisone (0.5 µg/ml), triiodothyronine (20 ng/ml), and retinoic acid (50 nM) derived from Lonza bronchial epithelial cell culture Singlequot supplements (not using included EGF, epinephrine, BPE, or gentamycin/amphotericin mix), with added 2 mg/ml BSA, 2% NuSerum, and 1% cell culture penicillin/streptomycin supplement (modified from [21]). Media lacking EGF combined with the plastic type of these transwell filters was previously shown to differentiate cells into a serous phenotype [21, 22]. After 5 days of confluence, TEER reached  $\sim 300 - 500 \Omega \cdot \text{cm}^2$  and cells were fed with similar media except with 0.5% NuSerum on the basolateral side while the apical side was washed with PBS and exposed to air. Cells were used after 2-4 weeks at air-liquid interface. Unlike primary surface epithelial cells (isolated and cultured as described [13, 14, 19, 23]), serous cell ALIs did not exhibit motile cilia by light microscopy.

## **Surface epithelial cell isolation and culture**

Air-liquid-interface cultures of primary ciliated and goblet cells were derived from surface epithelium of middle turbinate as described [13, 14, 19, 20]. Cells were enzymatically dissociated and grown to confluence in 50% DMEM/Ham's F-12 plus 50% bronchial epithelial basal media (BEBM, Lonza) for 7 days [14, 19, 20]. Dissociated cells were then seeded on Transwell filters (Corning) coated with type I bovine collagen, fibronectin, and bovine serum albumin. Culture medium was removed from the upper compartment after 5-7 days, and cells were fed basolaterally with differentiation medium containing 50% DMEM and 50% BEBM plus Lonza B-ALI Singlequot supplements as provided supplemented with 100 U/ml penicillin, 100 µg/ml streptomycin, and retinoic acid B-ALI inducer (added fresh for each feeding) as described [13, 14, 19, 20].

## ***Imaging of intracellular cAMP dynamics in isolated nasal gland serous cells***

Isolated acinar cells were plated for 30 min on glass coverslips pre-coated with growth factor reduced Matrigel (diluted 1:30 in MEM; 24 hours at 37 °C), followed by washing and addition of serum-free Ham's F12K (Gibco) containing cADDiS expressing BacMam (Montana Molecular [1, 24]) plus 5 mM NaButyrate to enhance expression. Cells were imaged after 24 hrs incubation at 37 °C. Cells were imaged as above under CO<sub>2</sub>/HCO<sub>3</sub><sup>-</sup> conditions using a standard GFP/FITC filter set (Semrock) on a Nikon microscope (20x 0.75 Plan Apo objective) equipped with a QImaging Retiga R1 camera and XCite 110 LED illumination system. Data were acquired with Micromanager [25]. Experiments were done under ion substitution conditions (high K<sup>+</sup>) to reduce volume changes as previously described [3-6, 9] to ensure that cADDiS fluorescence changes were not artifacts of cell volume change during activation of secretion, confirmed by pilot experiments using mNeonGreen-only BacMam. For experiments with pertussis toxin (PTX), PTX was included with the BacMam virus infection reaction and included in media after removal of BacMam (~24 hours pretreatment).

### ***Primary culture of human monocyte-derived macrophages (M $\phi$ s)***

Monocytes were isolated from healthy apheresis donors by RosetteSep™ Human Monocyte Enrichment Cocktail (Stem Cell Technologies) by the University of Pennsylvania Human Immunology Core and provided as de-identified untraceable cells. Monocytes were differentiated into macrophages (M $\phi$ s) by 10 days of adherence culture in high glucose RPMI media containing 10% human serum. Differentiation to M $\phi$ s was confirmed by functional expression of markers including histamine H1 receptors determined by Ca<sup>2+</sup> imaging (**supplementary figure S22**) with specific antagonists as well as secretion of appropriate cytokines in response to M1 vs M2 polarization stimuli (**supplementary figure S10**). Induction of M $\phi$ s NPY production was carried out by incubation in PMA (100 nM) or vehicle (0.1% DMSO) for 24 hrs, followed by washing to remove PMA and further incubated for 24 hours in fresh 300  $\mu$ L media in a 24 well plate. This was based on previous work showing PMA increases M $\phi$  NPY production [26]. Phenol-red free media was used to facilitate ASL pH or height measurements.

### ***Immunofluorescence (IF)***

IF was carried out as previously described [10], with modifications outlined below. ALI cultures were fixed for 3 min in ice-cold methanol, followed by blocking in Dulbecco's phosphate buffered saline (DPBS) containing 1% bovine serum albumin (BSA), 5% normal donkey serum (NDS), 0.2% saponin, and 0.3% triton X-100 for 1 hour at 4°C. Primary antibody incubation was carried out at 4°C overnight. AlexaFluor-labeled donkey anti-mouse or rabbit secondary antibody incubation (1:1000) was carried out for 2 hours at 4°C. Transwell filters were removed from the plastic mounting ring and mounted with Fluoroshield with DAPI (Abcam). Images of ALIs were taken on an Olympus IX83 microscope (60x 1.4 NA objective) with spinning disc confocal unit (Olympus DSU). Images were analyzed using Metamorph software and/or the FIJI [27] version of ImageJ (W. Rasband, Research Services Branch, National Institute of Mental Health, Bethesda, MD). As VIPR1 and VIPR2

antibodies were both rabbit antibodies, co-staining was performed using Zenon antibody labeling kit (Thermo) per the manufacturer's instructions as described [19, 20].

### ***SNARF-5F, SPQ, and DIC live-cell imaging of primary isolated serous cells***

Isolation of primary serous acinar cells, immunofluorescence, and live cell imaging of acinar cell volume,  $pH_i$  (SNARF-5F), and  $Cl^-$  (SPQ) were carried out as described [3-6, 9]. After washing via gentle centrifugation and resuspension in  $HCO_3^-$  containing buffer, acinar cells were plated on Cell-Tak (BD Biosciences)-coated glass coverslips and allowed to adhere for 10–20 min in 5%  $CO_2$ . The isolation protocol yielded acini, single cells and strings of cells. Cells were identified based on visible morphology (size, polarized secretory granules, acinar structures) under DIC optics. The rationale and history of using changes in cell volume to track agonist-induced changes in secretory state is extensively described in [8, 28-30] and was performed as we previously described [3-6, 9].

Isolated acinar cells were loaded with SNARF-5F-acetoxymethyl ester (AM) for 15 min at room temperature in Krebs buffer containing 25 mM  $HCO_3^-$  gassed with 5%  $CO_2/95\% O_2$ . For experiments in the absence of  $HCO_3^-$ , cells were plated in Krebs buffer lacking  $NaHCO_3$  but containing 20 mM HEPES and gassed with 100%  $O_2$ . Solutions with 0- $Na^+$  had isosmotic replacement of NaCl with NMDG-Cl,  $NaH_2PO_4$  with  $KH_2PO_4$ , and  $NaHCO_3$  with NMDG- $HCO_3^-$ . Solutions used were exactly as previously described [4]. Ratiometric fluorescence measurements of SNARF-5F were carried out using 550/20 excitation filter, 570 long pass dichroic, and 585/20 and 640/20 emission filters (Chroma Technologies set 79010-ET) housed in a filter wheel (Sutter). Excitation light was generated with an X-Cite 120 Boost LED (Excelitas Technologies) and emission was captured with an ORCA Flash 4.0 sCMOS camera (Hamamatsu) with 2x2 pixel binning. Imaging was performed on a Olympus IX-83 microscope with 30x 1.05 NA UPlanSApo silicone oil immersion objective for single cell measurements or 10x 0.4 NA PlanApo lens for ASL measurements with cells on transwells. Single cells were continuously perfused with 37°C solution gassed with 95%  $O_2/5\% CO_2$  or 100%  $O_2$  as appropriate. Transwells were kept at 37°C with 5%  $CO_2$  using a Tokai Hit stage-top incubator.

For experiments blocking the driving force for  $\text{HCO}_3^-$  and  $\text{Cl}^-$  efflux (performed as described [4]), we assumed  $[\text{HCO}_3^-]_i = 16$  mM based on mean resting pH of 7.2 and  $[\text{HCO}_3^-]_o = 25$  mM, making the Nernst equilibrium potential ( $E_{\text{HCO}_3^-}$ )  $\sim 60\text{mV} \cdot \log(16/25) = -12$  mV. We have already demonstrated that the activation of secretion by serous cells results in efflux of KCl [3-6]. Mean resting  $[\text{Cl}^-]_i$  was measured at  $\sim 65$  mM in SPQ experiments, and with  $[\text{Cl}^-]_o$  in the Krebs buffer used here at 135 mM, for a  $E_{\text{Cl}^-} = -19$  mV.  $[\text{K}^+]_i$  was assumed to be 140 mM and  $[\text{K}^+]_o$  was calculated at 5 mM ( $E_{\text{K}^+} = -87$  mV). Using the Nernst equation, we calculated that a using  $[\text{Cl}^-]_o$  of 103 mM and  $[\text{K}^+]_o$  of 89 mM would set  $E_{\text{Cl}^-} = E_{\text{K}^+} = E_{\text{HCO}_3^-}$ , reducing the driving force for efflux of cellular KCl and  $\text{KHCO}_3$ . This solution contained (in mM) 41 NaCl, 57 KCl, 32 KGlucuronate, 1.2  $\text{MgCl}_2$ , 1  $\text{CaCl}_2$ , 1.2  $\text{NaH}_2\text{PO}_4$ , 11 glucose, 25  $\text{NaHCO}_3$ , pH 7.4 by gassing with 95%  $\text{O}_2/5\%$   $\text{CO}_2$  compared with control Krebs that contained (in mM) 125 NaCl, 5 KCl, 1.2  $\text{MgCl}_2$ , 1.2  $\text{CaCl}_2$ , 1.2  $\text{NaH}_2\text{PO}_4$ , 11 glucose, 25  $\text{NaHCO}_3$ , pH 7.4 by gassing with 95%  $\text{O}_2/5\%$   $\text{CO}_2$ .

SPQ measurement of  $[\text{Cl}^-]_i$  changes were carried out exactly as described [3-6, 9, 14]. Rates of SPQ fluorescence changes were extrapolated to relative anion permeability [31]. Upon substitution of extracellular  $\text{Cl}^-$  for  $\text{NO}_3^-$ , electroneutral influx of  $\text{NO}_3^-$  and efflux of  $\text{Cl}^-$  decreases intracellular  $[\text{Cl}^-]$  ( $[\text{Cl}^-]_i$ ) and causes an increase in intracellular SPQ fluorescence. Because most  $\text{Cl}^-$  channels are nearly equally permeable to  $\text{Cl}^-$  and  $\text{NO}_3^-$ , relative changes in the rate of SPQ fluorescence increase is roughly equivalent to relative changes in  $\text{Cl}^-$  permeability. Isolated acinar cells were incubated for 2 hours in 20 mM SPQ at room temperature. Acinar cell ALIs were incubated overnight with 20 mM SPQ on the apical side. SPQ was imaged using a standard DAPI filter set (350/50 ex, 400 long pass dichroic, 460/50 em; Chroma 49000 ET) with UV illumination from a xenon arc lamp (Sutter Lamda LS). Solutions used for  $\text{NO}_3^-$  substitution were as previously described [3, 5, 6, 9, 14]. For ALI experiments, control normal  $[\text{Cl}^-]_o$  apical solution contained (in mM) 138 NaCl, 5.3 KCl, 0.24  $\text{MgCl}_2$ , 1.3  $\text{CaCl}_2$  (total  $[\text{Cl}^-]_o = 147$ ), 20 HEPES pH 7.4. Low  $[\text{Cl}^-]_o$  solution contained (in mM) 138  $\text{NaNO}_3$  and 5.3  $\text{KNO}_3$  instead of NaCl and KCl, respectively (final  $[\text{Cl}^-]_o = 4$ ;  $\sim 37$ -fold less than normal  $[\text{Cl}^-]_o$ ). For isolated acinar cells, control solution contained (in mM), 136.2 NaCl, 3.8 KCl, 1.2  $\text{KH}_2\text{PO}_4$ , 1.2  $\text{CaCl}_2$ ,

1.2 MgCl<sub>2</sub>, 11 glucose, 10 HEPES pH 7.4. Low [Cl<sup>-</sup>]<sub>o</sub> solution contained NaCl replaced with NaNO<sub>3</sub> for a final [Cl<sup>-</sup>]<sub>o</sub> of 8.6 mM. Single cells were continuously perfused with 37°C solution gassed with 95% O<sub>2</sub>/5% CO<sub>2</sub> or 100% O<sub>2</sub> as appropriate. Transwell SPQ experiments were carried out at room temperature without gassing.

Cell volume was estimated by taking the cross-sectional area of the cell as imaged by differential interference contrast (DIC) to the 3/2 power (as described [3, 5, 6, 9, 30, 32, 33]). This method yields cell and small acini volume measurements faster than but indistinguishable from confocal 3D reconstructions [3]. Cell volumes are expressed as normalized volume (V) relative to initial cell volume (V<sub>o</sub>). DIC images were acquired sequentially by computer controlled shuttering off of the fluorescence light, rotating of the DIC polarizer into position, and shuttering on transmitted light. Imaging data was collected and analyzed in Metafluor and/or FIJI [27].

### ***Calibration of SNARF-5F and measurement of intracellular pH (pH<sub>i</sub>) buffering capacity***

Changes in SNARF 640/580 emission ratio were converted to pH<sub>i</sub> using SNARF-loaded cells exposed to high [K<sup>+</sup>]<sub>o</sub> solutions and the H<sup>+</sup>/K<sup>+</sup> exchanger nigericin to equilibrate extracellular pH (pH<sub>o</sub>) to pH<sub>i</sub> exactly as described [4] using solutions buffered to pH<sub>o</sub> 6.8, 7.2, and 7.6. SNARF-5F fluorescence varied linearly within the pH ranges observed during agonist stimulation.

Total pH<sub>i</sub> buffering capacity (β<sub>t</sub>) encompasses CO<sub>2</sub>-HCO<sub>3</sub><sup>-</sup> -dependent buffering capacity (β<sub>HCO<sub>3</sub><sup>-</sup></sub>) plus intrinsic CO<sub>2</sub>-independent intrinsic buffering capacity (β<sub>i</sub>) from cytoplasmic macromolecules and organelles [4, 34, 35]. Assuming the pKa of CO<sub>2</sub>-HCO<sub>3</sub><sup>-</sup> is 6.1 [4, 35, 36] and assuming that highly permeant [CO<sub>2</sub>]<sub>o</sub> = [CO<sub>2</sub>]<sub>i</sub> (1.2 mM in 5% CO<sub>2</sub> by Henry's Law), and using the Henderson-Hasselbach relationship, then [HCO<sub>3</sub><sup>-</sup>]<sub>i</sub> = 1.2 mM x 10<sup>pH-6.1</sup>, and β<sub>HCO<sub>3</sub><sup>-</sup></sub> = 2.3 x [HCO<sub>3</sub><sup>-</sup>]<sub>i</sub>. Because [CO<sub>2</sub>]<sub>i</sub> is constant (open buffering), β<sub>HCO<sub>3</sub><sup>-</sup></sub> rises exponentially as pH<sub>i</sub> increases [4].

Human serous acinar cell β<sub>t</sub> was empirically determined using observed pH<sub>i</sub> changes during exposure to NH<sub>4</sub>Cl in Na<sup>+</sup>/HCO<sub>3</sub><sup>-</sup> -free solutions to inhibit pH<sub>i</sub> regulatory mechanisms (as described; [4,

34, 35, 37]). Exposure of cells to solution containing  $\text{NH}_3$  and  $\text{NH}_4^+$  causes an initial alkalinization of  $\text{pH}_i$  due to entry of highly cell permeant  $\text{NH}_3$  and resulting  $\text{H}^+$  consumption as it is converted intracellularly to  $\text{NH}_4^+$ . After an experimental change in extracellular  $[\text{NH}_3]$  ( $[\text{NH}_3]_o$ ), the initial intracellular  $[\text{NH}_4^+]_i$  can be calculated by Henderson-Hasselbach with  $[\text{NH}_4^+]_i = [\text{NH}_3]_i \times 10^{9.2-\text{pH}_i}$ , assuming  $[\text{NH}_3]_o = [\text{NH}_3]_i$  are identical and  $\text{pKa} = 9.2$  [35]. Acinar cells were exposed to solutions containing (in mM) 0, 5, 10, and 20 mM  $[\text{NH}_4\text{Cl}]_o$ , which equilibrated to (in mM) 0, 0.6, 1.2, and 2.5  $[\text{NH}_3]_o$ . The base solution for  $\beta_i$  buffering experiments was (in mM) 120-140 NDMG-Cl, 5 KCl, 1.2  $\text{MgCl}_2$ , 1.2  $\text{CaCl}_2$ , 1.2  $\text{KH}_2\text{PO}_4$ , 11 glucose, 10 HEPES pH 7.4, and 0, 5, 10 or 20  $\text{NH}_4\text{Cl}$  gassed with 100%  $\text{O}_2$ . Mean  $\beta_i$  was calculated as the units of acid of base equivalent required to change the  $\text{pH}_i$  by one unit around the midpoint of the pH change as described [4]. Raw data points for  $\beta_i$  were taken from experiments of 12 cells of each genotype (4 patients; 3 experiments per patient) and fit with an exponential decay function in Prism. The sum of the  $\beta_i$  and  $\beta_{\text{HCO}_3^-}$  curves was used to calculate  $\beta_t$ .

### **Measurements of ASL pH and ASL height**

ASL height and pH measurement was carried out as described [10-14, 16, 19, 20, 38]. Cultures were imaged at  $37^\circ\text{C}$  in a Tokai Hit stage top incubator. For pH measurements, cells were incubated in serum-free phenol-red-free low glucose DMEM (Gibco) on the basolateral side and gassed with 5%  $\text{CO}_2$ , 20%  $\text{O}_2$ , 80%  $\text{N}_2$ . For “thin film” ASL pH measurements (main text) SNARF-1 dextran (~1 mg/ml) was sonicated in perfluorocarbon and 100  $\mu\text{L}$  was added to the top of each culture. For longer-term  $\text{HCO}_3^-$  secretion experiments (**supplementary figure S11**), 100  $\mu\text{L}$  of 1 mg/ml SNARF dextran in low buffering capacity solution was added (HBSS with 1 mM HEPES, as described [38]). ASL pH was calibrated by overlaying 1 mg/ml SNARF dextran on top of cultures in  $\text{HCO}_3^-$  conditions in solutions buffered with 20 mM HEPES at pH 6.8, 7.2, 7.6, and 7.8. SNARF 1 dextran pH changes were linear over the pH range observed here (~7-7.8).

ASL height was measured similarly and as previously described [11], but in  $\text{HCO}_3^-$ -free conditions (100%  $\text{O}_2$  with basolateral HBSS buffered with 20 mM HEPES) using Texas red dextran (10,000 MW) as previously described [11]. When corrected for refractive index mismatch ( $1.52 \eta_{\text{oil}}/1.33 \eta_{\text{water}} = \sim 1.14$ ), an observed change in ASL height of  $\sim 30 \mu\text{m}$  with agonist stimulation is in reality  $30/1.14 = 26 \mu\text{m}$ . Treating the ALI as a cylinder, where volume = area x height, a change in ASL height of  $\sim 26 \mu\text{m}$  over 15 min equals a secretion volume of  $2.6 \mu\text{L}/\text{cm}^2$  ( $2.6 \times 10^{-5} \text{ m} \times 1 \times 10^{-4} \text{ m}^2 = 2.6 \times 10^{-9} \text{ m}^3 = 2.6 \times 10^{-6} \text{ L}$ ) or  $\sim 10 \text{ uL} \cdot \text{cm}^{-2} \cdot \text{hr}^{-1}$ . Calu-3 cells were previously reported to secrete fluid at a rate of 4 or  $5.4 \text{ uL} \cdot \text{cm}^{-2} \cdot \text{hr}^{-1}$  when stimulated with forskolin or VIP, respectively, using a virtual gland technique [39]. The fact that measurements of primary serous cells here using the Texas red ASL technique are within an order of magnitude of measurements of Calu-3 cells using a different technique suggests the ASL height measurements made here are reasonable within the context of cellular fluid secretion capabilities.

### **Quantitative (q) PCR**

RNA was isolated from ALI cultures as previously described [10] and qPCR was performed using a QuantStudio5 qPCR machine and TaqMan primer assays (Applied Biosystems/ThermoFisher Scientific) for human CFTR (Hs00357011\_m1), lysozyme (Hs00426232\_m1), lactoferrin (Hs00914334\_m1), Muc5AC (Hs01365616\_m1), Muc5B (Hs00861595\_m1), Muc7 (Hs00379529\_m1), Ano1 (Hs00216121\_m1), pendrin (SLC26A4; Hs01070627\_m1), alpha-1-antitrypsin (Hs00164575\_m1),  $\beta$ -actin (Hs01060665\_g1), beta-defensin 1 (DEFB1 Hs00608345), beta-defensin 2 (DEFB4; Hs00823638\_m1), IL-6 (Hs00174131\_m1), IL-8 (Hs00174103\_m1), and IL-1 $\beta$  (Hs01555410\_m1) and/or GAPDH (Hs02786623\_g1) in separate reactions. Relative expression was calculated by means of the  $2^{-\Delta\Delta C_t}$  method. Comparison of  $\beta$ -actin with GAPDH was used as a control to validate suitability of GAPDH as a housekeeping gene in these cells.

### **Generation of Calu-3 air-liquid interface (ALI) cultures**

Calu-3 bronchial epithelial cells (shown in **supplementary figures S7, S8, and part of S9**) were obtained from ATCC and cultured in T75 flasks in minimal essential medium (MEM) with Earl's salts and 1 mM L-glutamine, 10% fetal bovine serum, and 1% penicillin/streptomycin mix. Cells were lifted with 0.25% trypsin and plated on 1.1 cm<sup>2</sup> cell culture inserts (Greiner BioOne Thincerts, transparent, 0.4 μm pore size). Cells were grown to confluence for 5 days, followed by apical exposure to air and subsequent 3 weeks for full differentiation/polarization before use. Only ALIs with transepithelial resistances (TEERs) of >250-300 Ω•cm<sup>2</sup> were used.

### **Bacterial growth assays**

Bacterial growth assays were carried out as previously described [23, 40]. *Pseudomonas aeruginosa* strains PAO1 (HER-1018; ATCC BAA-47) and clinical isolates of methicillin-resistant *Staphylococcus aureus* (MRSA) and *P. aeruginosa* were isolated by the Philadelphia VA Medical Center Microbiology Laboratory and grown in LB or tryptic soy broth (TSB; Gibco/Thermo Scientific), respectively.

Bacterial 1-N-phenyl-naphthylamine (NPN) fluorescence assay was modified from previous descriptions [41-44]. *P. aeruginosa* were grown to an OD<sub>600</sub> of 0.5 in LB, centrifuged, and resuspended at half volume of 10 mM HEPES, 5 mM glucose, 0.1 mM EDTA, pH 8. Bacteria were then aliquoted and mixed with an equal volume of diluted airway surface liquid secretions or antibiotics, and then pipetted into a plate reader containing an equal volume of 25% PBS containing 20 μM NPN (final NPN 10 μM, final OD<sub>600</sub> 0.25). Samples were then incubated for 10 min and read on a Tecan 10M plate reader at 350 nm excitation and 450 nm emission. Samples were read in triplicate, with averages of ≥3 independent experiments reported.

CFU antimicrobial assays with Calu-3 ASL washings were carried out similarly to a previously published protocol [12, 45] and modified based on our own antimicrobial ASL protocols used in our lab [12, 40]. Cultures were washed copiously with PBS and transferred to antibiotic-free MEME for 48

hrs. before use. Calu-3 cell secretions were collected from 3 week old ALIs stimulated basolaterally with 100  $\mu$ M isoproterenol for 72 hours, followed by washing of the apical surface with 30  $\mu$ L 25% PBS. While washing a 1.1  $\text{cm}^2$  ALIs with 30  $\mu$ L significantly dilutes the ASL fluid ( $\sim$ 1  $\mu$ L per  $\text{cm}^2$  of surface area [46]), washings retained antibacterial activity and were thus sufficient to be used for this assay. ASL washings (30  $\mu$ L per culture) were pooled and mixed with bacteria resuspended in 25% PBS, adjusted to 0.1 OD, then diluted 1:1000 in 25% PBS). Bacteria and ASL mixture was incubated statically in a 96-well plate at 37  $^{\circ}$ C for 2 hrs, followed by 4 serial 10-fold dilutions and spot plating onto LB plates. After overnight incubation at 37  $^{\circ}$ C, CFUs were manually counted.

CFU antimicrobial assays with primary serous cell ASL washings were carried out as above, but cultures were not pre-treated with isoproterenol. Cultures were unstimulated or stimulated for 30 min with VIP  $\pm$  NPY  $\pm$  scrambled NPY on the basolateral side. Afterward, the surface of a 0.33  $\text{cm}^2$  transwell was washed with 50  $\mu$ L 25% saline (thus ASL was  $\sim$ 5x more dilute than used in Calu-3 experiments).

Live-dead staining was carried out with BacLight Live/Dead kit (ThermoFisher Scientific) consisting of Syto9 (live cell stain) and propidium iodide (dead cell stain), as previously used with *P. aeruginosa* [10]. Bacteria were adjusted to an OD = 0.1. Bacterial suspension was mixed with ASL (25  $\mu$ L each) in a black microplate and incubated for indicated time at 37  $^{\circ}$ C. 50  $\mu$ L 2x Live-Dead staining solution was then added, followed by further 10 min incubation at room temp and reading on a fluorescence microplate reader (Tecan Spark 10M) at 488 excitation and dual emission wavelengths as indicated. Control calibration of live dead staining was carried out by mixing heat-killed (as below) with live bacteria at the indicated ratios to a final OD of 0.1 followed by mixing with 25 % saline only and incubation as above prior to live dead staining.

### ***Production of heat-killed bacteria***

Bacteria were heat killed according to a previously published protocol [47]. *P. aeruginosa* or MRSA strains were grown overnight at 37 $^{\circ}$ C in LB broth, then resuspended in LB and grown for 2-4

hours to an OD<sub>600</sub> of 1. Bacteria were heat killed for 20 min at 95°C. Cells were treated with bacteria diluted to OD<sub>600</sub> = 0.005 (200x dilution) in 100 uL PBS on the apical side only. Unstimulated control cultures were treated with 1:200 LB media only.

### ***Western blotting of primary gland cells***

Serous ALIs were washed 3x with PBS (apical and basolateral sides), then scrapped and pelleted with a pulse spin on a tabletop microfuge. Pellets were lysed using RIPA Buffer (20 mM Tris pH 7.5, 150 mM NaCl, 1% IgePal, 1% deoxycholate, 1 mM DTT, Complete protease inhibitor cocktail (Roche); 60ug of post 800xg cell lysate was separated on a 4-12% Bis-Tris NuPage SDS-PAGE gels using MOPS (Muc5B, Muc7, VIPR1, VIPR2) or MES (NKCC1, A1AT, NPY1R, NPY4R) running buffer with See-Blue Plus2 markers (Thermo). Different marker molecular weights are due to MOPS vs MES running buffers. As we found that NPY1R and NPY4R aggregated at the top of the gel when boiled (common for hydrophobic transmembrane GPCRs), we ran these samples without heating, which likely reflects why these proteins were observed as dimers (also common for GPCRs). Antibodies were used at a 1:1000 dilution followed by secondary HRP-linked antibodies and BioRad Clarity western ECL substrate.

**SUPPLEMENTARY TABLE S1** Characteristics of CF (blue; n = 9) and non-CF (green; n = 42) patients from whom samples were used in this study.

Patient	Age at Surgery	Gender	Ethnicity	Primary Diagnosis	# Prior FESS	Polyps	Lund-Mackay	SNOT-22	Smoking History	Asthma	AFS	Abx	Steroids	Comorbidities	CF genotype
CF1	26	Female	Caucasian	CRS	1	No	N/A	78	No	Yes	No	No	No	CF, GERD, DM	F508del/F508del
CF2	23	Male	Caucasian	CRS	1	Yes	N/A	N/A	No	No	No	No	No	CF, GERD	F508del/F508del
CF3	33	Female	Caucasian	CRS	1	Yes	13	8	No	No	No	No	No	CF, Double Lung Transplant, Allergies, GERD, HTN, DM	F508del/F508del
CF4	32	Female	Caucasian	CRS	1	Yes	N/A	77	No	Yes	No	No	No	CF, GERD	F508del/F508del
CF5	58	Female	Caucasian	CRS	2	Yes	18	27	No	Yes	No	No	No	CF, Allergies, GERD, HTN	F508del/F508del
CF6	27	Female	Caucasian	CRS	0	No	N/A	59	No	Yes	No	No	No	CF	F508del/G542X
CF7	28	Female	Caucasian	CRS	0	Yes	12	45	No	Yes	No	No	No	CF, Allergies	F508del/F508del
CF8	38	Female	Caucasian	CRS	1	Yes	16	93	No	No	No	No	Yes	CF, Lung transplant, DM	F508del/F508del
CF9	42	Male	Caucasian	CRS	1	No	14	33	No	Yes	No	Yes	No	CF, Lung transplant, DM, GERD, HTN	F508del/E585X
non-CF1	34	Male	Caucasian	CRS	0	Yes	N/A	N/A	No	No	No	No	No	Allergies	N/A
non-CF2	56	Female	Caucasian	CSF leak	0	No	N/A	N/A	No	No	No	No	No	Hypothyroid	N/A
non-CF3	65	Male	Caucasian	IP	0	Yes	4	N/A	No	No	No	No	Yes	N/A	N/A
non-CF4	71	Male	Caucasian	CRS	2	Yes	24	8	No	Yes	No	No	Yes	Samter's triad, Hypothyroid	N/A
non-CF5	71	Male	Caucasian	CRS	4	Yes	18	13	No	No	No	No	No	Samter's triad, Allergies, GERD, AERD, OSA, HTN	N/A
non-CF6	60	Male	Caucasian	CRS	1	Yes	11	57	No	No	No	No	Yes	N/A	N/A
non-CF7	59	Female	Caucasian	CRS	0	No	N/A	61	No	No	No	No	No	DM, GERD, HTN	N/A
non-CF8	66	Male	Caucasian	CRS	0	Yes	N/A	18	No	No	No	No	Yes	N/A	N/A
non-CF9	76	Female	Caucasian	Pituitary microadenoma	0	No	N/A	N/A	No	No	No	No	No	HTN, CAD, PVD	N/A
non-CF10	60	Male	Caucasian	CRS	0	Yes	N/A	N/A	No	Yes	No	No	No	N/A	N/A
non-CF11	46	Female	Hispanic, Latino	CRS	1	Yes	N/A	95	No	Yes	No	No	Yes	Obesity	N/A
non-CF12	48	Male	Caucasian	CRS	0	No	N/A	N/A	No	No	No	No	Yes	OSA, COPD	N/A
non-CF13	56	Female	Caucasian	CRS	0	Yes	N/A	27	No	No	No	No	No	N/A	N/A
non-CF14	69	Male	Caucasian	CRS	3	Yes	N/A	12	No	No	No	No	No	N/A	N/A
non-CF15	34	Male	Caucasian	CRS	0	Yes	N/A	N/A	No	No	No	No	No	Allergies	N/A
non-CF16	56	Female	Caucasian	CSF leak	0	No	N/A	N/A	No	No	No	No	No	hypothyroid	N/A
non-CF17	65	Male	Caucasian	IP	0	Yes	4	N/A	No	No	No	No	Yes	N/A	N/A
non-CF18	71	Male	Caucasian	CRS	2	Yes	24	8	No	Yes	No	No	Yes	Samter's triad, hypothyroid	N/A
non-CF19	78	Female	African American	Control/skull base tumor	0	No	N/A	19	No	No	No	No	No	HTN, Allergies	N/A
non-CF20	19	Male	Caucasian	CRS	1	Yes	N/A	41	No	Yes	No	No	No	Allergies	N/A
non-CF21	44	Female	Caucasian	CRS	0	No	6	27	No	Yes	No	No	Yes	Pacemaker	N/A
non-CF22	70	Female	Caucasian	CRS	0	No	8	61	No	No	No	Yes	Yes	HTN	N/A
non-CF23	57	Male	Caucasian	CRS	0	Yes	15	16	No	No	No	Yes	No	Allergies	N/A
non-CF24	37	Male	Caucasian	CRS	1	Yes	18	68	Yes	No	No	No	No	Allergies, Sinusoidal Trauma	N/A
non-CF25	60	Female	Caucasian	Control/skull base tumor	0	Yes	14	9	Yes	Yes	No	No	Yes	DM, HTN, OSA, IP	N/A
non-CF26	24	Female	Caucasian	CRS	0	No	13	69	No	No	No	No	No	Allergies, GERD	N/A
non-CF27	83	Male	Caucasian	CRS	1	Yes	3	10	No	No	No	No	No	HTN	N/A
non-CF28	52	Male	Caucasian	Fungal Ball	0	Yes	15	35	No	No	Yes	No	No	Allergies	N/A
non-CF29	60	Female	Caucasian	CRS	2	Yes	16	53	No	Yes	No	No	No	Samter's Triad, Allergies	N/A
non-CF30	61	Female	Caucasian	CRS	0	Yes	N/A	46	Yes	Yes	No	Yes	Yes	HTN	N/A
non-CF31	65	Male	Caucasian	CRS	1	No	N/A	52	No	Yes	No	No	Yes	HTN, GERD	N/A
non-CF32	62	Female	Native American	CRS	2	No	6	45	Yes	No	No	No	No	HTN	N/A
non-CF33	49	Male	Caucasian	CRS	1	No	14	56	No	Yes	No	No	Yes	OSA, HTN, MI, GERD	N/A
non-CF34	72	Female	Caucasian	CRS	3	No	9	49	No	Yes	Yes	No	Yes	GERD, HTN	N/A
non-CF35	51	Female	Caucasian	CRS	1	No	4	7	No	No	No	No	No	COPD, DM, OSA, GERD, Allergies	N/A
non-CF36	40	Male	Caucasian	CRS	1	No	13	27	No	No	No	No	No	Allergies	N/A
non-CF37	42	Male	Caucasian	CRS	0	No	5	68	No	No	No	No	No	HTN, OSA	N/A
non-CF38	57	Female	Caucasian	CRS	0	No	5	14	No	No	No	No	No	GERD	N/A
non-CF39	79	Male	Caucasian	CRS	0	Yes	11	22	No	No	No	No	No	Afib, CAD, HTN	N/A
non-CF40	57	Male	Caucasian	CRS	0	No	7	11	Yes	No	No	No	No	OSA	N/A
non-CF41	54	Male	Caucasian	CRS	0	No	7	78	No	No	No	No	No	GERD	N/A
non-CF42	38	Male	Caucasian	CRS	0	No	3	5	No	No	No	No	No	GERD	N/A

**Abbreviations:** Abx, antibiotics; AERD, aspirin-exacerbated respiratory disease; AFS, allergic fungal sinusitis; CF, cystic fibrosis; COPD, chronic obstructive pulmonary disease; CRS, chronic rhinosinusitis; CSF, cerebrospinal fluid; DM, diabetes mellitus; FESS, functional endoscopic sinus surgery; GERD, gastroesophageal reflux disease; HTN, hypertension; IP, inverted papilloma; Lund-Mackay, sinonasal staging algorithm score [48, 49]; N/A, not available; OSA, obstructive sleep apnea; SNOT-22, 22 question sinonasal outcomes test [50]

**SUPPLEMENTARY TABLE S2** Gene expression output from the Cancer Cell Line Encyclopedia (accessed 26 April, 2019; <https://portals.broadinstitute.org/ccle> [51]) for NPY receptors, VIP receptors, and serous cell markers lysozyme (LYZ) and CFTR. Note that Calu-3 cells, a bronchial adenocarcinoma line frequently used as a model of serous cells due to high CFTR and lysozyme expression, express the highest amount of NPY1R relative to other airway cancer cell lines.

Affyematrix

Gene	NPY1R	NPY2R	NPY5R	VIPR1	VIPR2	LYZ	CFTR
A549_LUNG	3.97359	3.910246	4.316899	5.347613	4.442829	3.861464	3.98063
CALU1_LUNG	4.150831	3.587063	4.239859	7.542943	4.087702	3.718109	3.854273
<b>CALU3_LUNG</b>	<b>7.168295</b>	3.803298	4.45895	6.922686	4.311346	11.0784	10.05969
CALU6_LUNG	3.512282	3.750993	4.158273	8.829339	4.305164	6.284744	4.588329
NCIH292_LUNG	3.553423	3.486564	3.898884	6.090106	4.314193	3.713948	3.729571
NCIH441_LUNG	3.701913	3.58951	4.291047	7.25233	4.440556	3.726355	4.128871
NCIH520_LUNG	3.952049	3.850606	4.148694	5.315201	4.260294	4.190855	4.465682
NCIH522_LUNG	3.666311	3.629025	4.243514	5.523483	4.433325	3.896822	3.716021

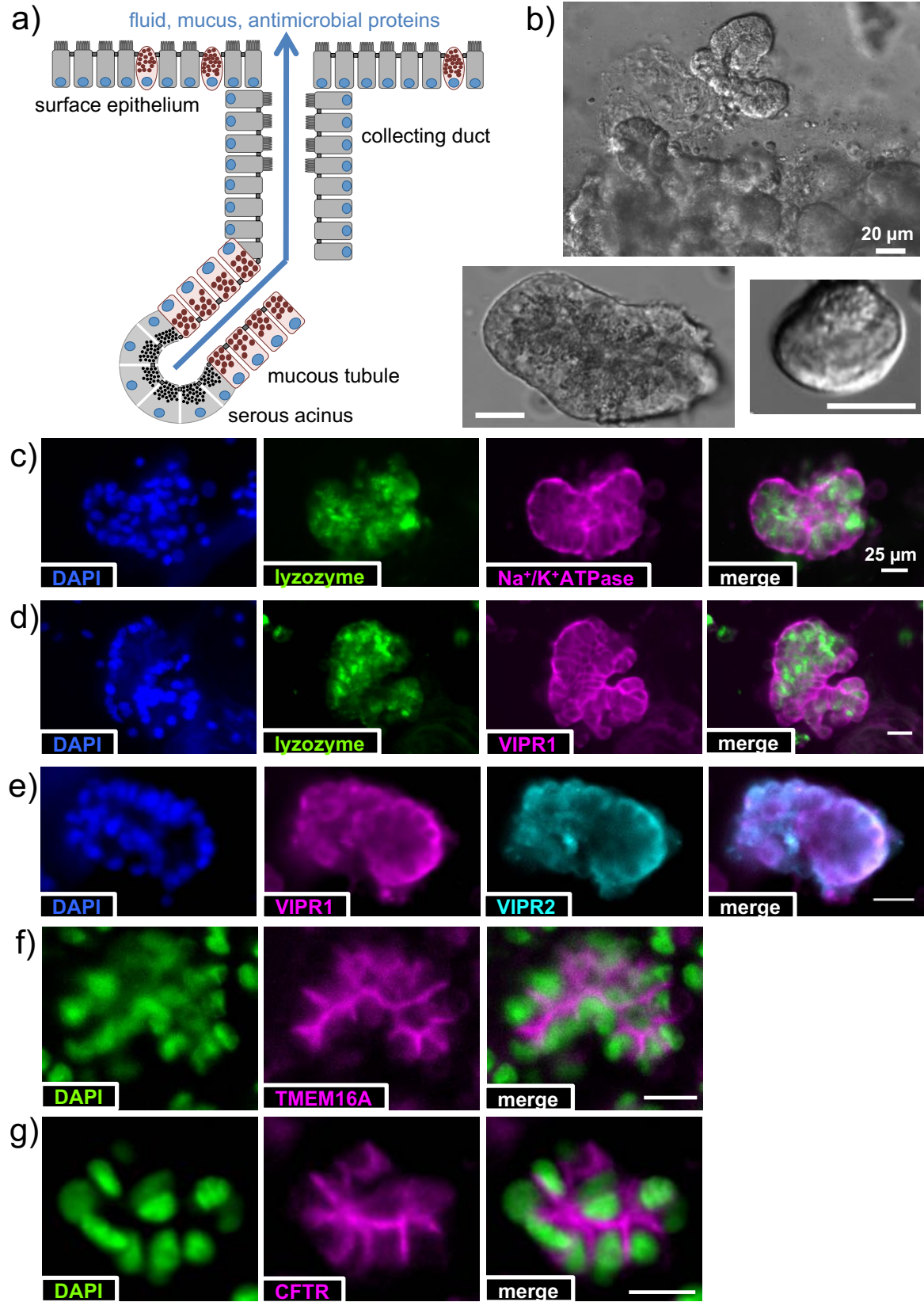
RNAseq

Gene	NPY1R	NPY2R	NPY4R	NPY5R	VIPR1	VIPR2	LYZ	CFTR
A549_LUNG	-5.3022356	-3.1772462	5.69438127	-13	-4.4839539	-8.4031139	-4.837362	-6.4493319
CALU1_LUNG	-1.6370841	-13	-0.0247348	-13	1.83239394	-13	-3.4844883	-4.3859648
<b>CALU3_LUNG</b>	<b>0.76601676</b>	-13	-2.4547363	-1.7320273	0.81640217	-13	7.36181905	6.44949113
CALU6_LUNG	-4.1292877	-7.6433373	-5.1671067	-6.7017855	3.62349708	-9.1687653	1.71665862	0.66432141
NCIH292_LUNG	-8.8698593	-13	0.67477717	-13	0.85130002	-0.6510655	-2.2350607	-7.3064622
NCIH441_LUNG	-13	-13	-4.4713423	-13	1.79193401	-6.2665501	-3.3788701	-5.7721996
NCIH520_LUNG	-4.5970396	-13	-6.0181873	-13	-3.6856484	-9.4348835	-0.494092	-3.896139
NCIH522_LUNG	-7.686093	-13	-6.7853125	-13	-3.0377362	-6.6170462	-1.6362569	-5.7076583

**SUPPLEMENTARY TABLE S3** Gene expression output from MERAV database (accessed 11 July 2018; <http://merav.wi.mit.edu/> [52]). Similar to the Cancer Cell Line Atlas data above, MERAV suggested Calu-3 cells expressed the highest amount of NPY1R among frequently used lung cancer cell lines.

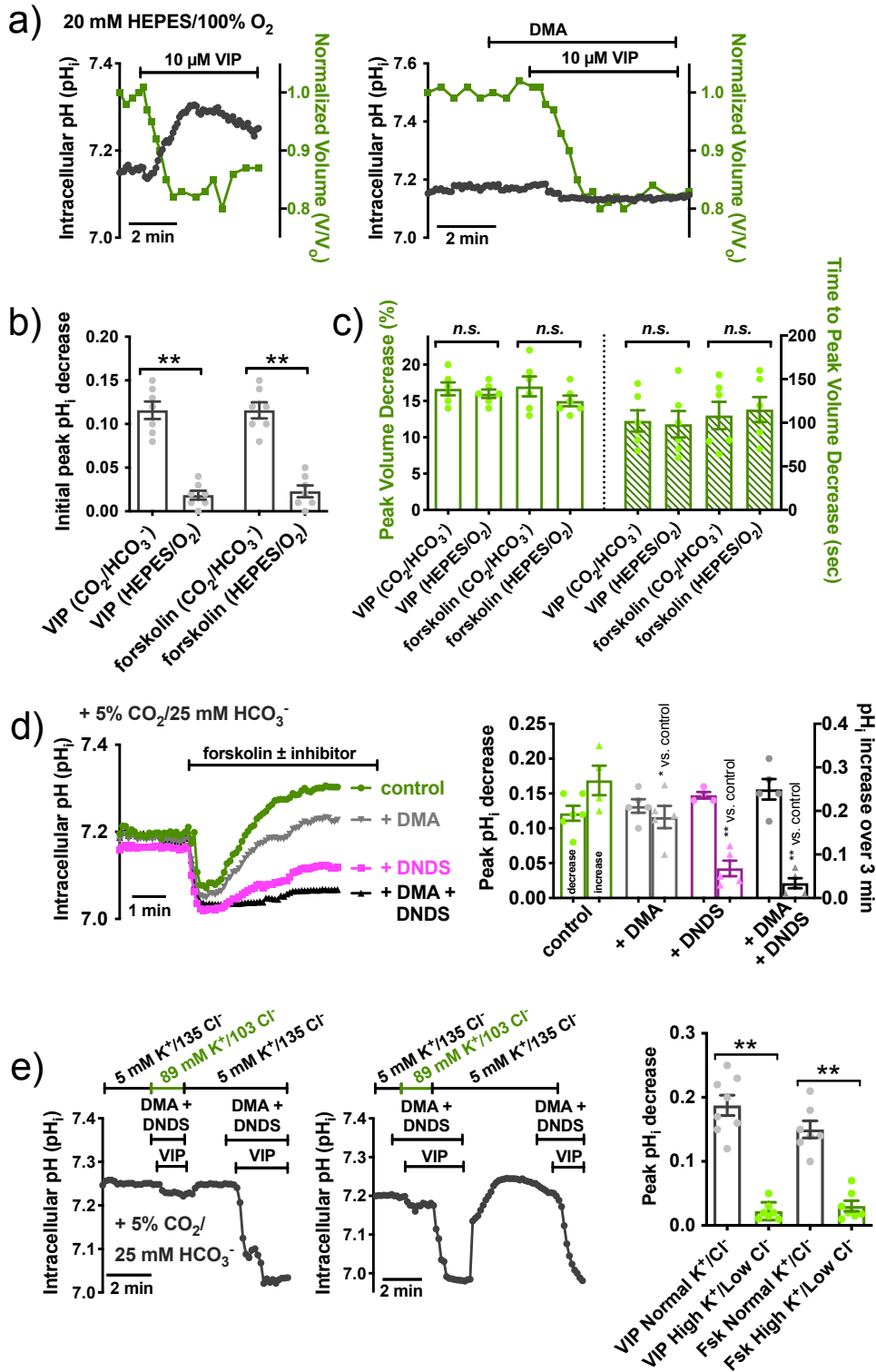
GENE	NPY1R	NPY2R	NPY4R	NPY5R	NPY6R	VIPR1	VIPR2	LYZ	CFTR
A549 Lung_Cancer.Cell.Line.Large_A549_Non-Small.Cell.Lung.Carcinoma: METIS_p_NCLE_RNA1_Human_U133_Plus_2_0_H01_241018	20.28	19.39	104.89	29.99	64.41	69.52	54	28.38	24.6
A549 Lung_Cancer.Cell.Line.Large_A549_Non-Small.Cell.Lung.Carcinoma: GSM139646	16.49	17.66	78.19	20.19	66.14	73.3	58.19	26.4	24.02
A549 Lung_Cancer.Cell.Line.Large_A549_Non-Small.Cell.Lung.Carcinoma: GSM253203	26.74	19.48	46.55	43.68	136.8	130.62	54.08	24.67	24.66
A549 Lung_Cancer.Cell.Line.Large_A549_Non-Small.Cell.Lung.Carcinoma: GSM274739	18.43	17.99	111.42	36.73	87.56	81.09	50.29	25.34	24.33
A549 Lung_Cancer.Cell.Line.Large_A549_Non-Small.Cell.Lung.Carcinoma: GSM274740	20.94	20.97	141.78	35.76	83.06	77.51	42.31	24.14	24.59
A549 Lung_Cancer.Cell.Line.Large_A549_Non-Small.Cell.Lung.Carcinoma: GSM433024	55.74	20.57	76.52	39.55	70.34	95.51	55.45	25.13	26.5
A549 Lung_Cancer.Cell.Line.Large_A549_Non-Small.Cell.Lung.Carcinoma: GSM433025	57.1	24.58	81.78	31.01	66.64	92.39	52.3	28.06	20.06
<b>Calu3 Lung_Cancer.Cell.Line.Large_Calu-3_Adenocarcinoma: WATCH_p_NCLE_RNA8_HG-U133_Plus_2_A02_474612</b>	<b>128.77</b>	18	45.06	34.25	66.32	195.12	47.65	872.07	708.73
Calu6 Lung_Cancer.Cell.Line.Large_Calu-6_Adenocarcinoma: BRAKE_p_NCLE_RNA2_HG-U133_Plus_2_E04_241144	13.41	16.41	50.21	26.83	94.21	447.11	44.95	68.77	32.67
Calu6 Lung_Cancer.Cell.Line.Large_Calu-6_Adenocarcinoma: Calu-6_SS474757_HG-U133_Plus_2_HCHP-225882	17.07	15.34	32.14	40.08	73.67	564.18	45.56	105.84	26.02
Calu-6 Lung_Cancer.Cell.Line.Large_Calu-6_Adenocarcinoma: Calu-6_SS474758_HG-U133_Plus_2_HCHP-225883	16.23	17.07	30.89	36.32	79.62	567.31	44.38	109.59	25.33
Calu-6 Lung_Cancer.Cell.Line.Large_Calu-6_Adenocarcinoma: Calu-6_SS474759_HG-U133_Plus_2_HCHP-225884	19.51	17.4	34.71	32.74	69.48	552.72	47.16	104.84	25.04
H292 Lung_Cancer.Cell.Line.Large_NCI-H292_Mucoepidermoid.Carcinoma: GSM274745	15.82	14.98	44.11	39.69	75.71	116.55	48.99	27.7	21.59
H292 Lung_Cancer.Cell.Line.Large_NCI-H292_Mucoepidermoid.Carcinoma: GSM274746	15.69	16.33	47.04	34.49	74.92	89.52	50.44	24.76	22.58
H441 Lung_Cancer.Cell.Line.Large_NCI-H441_Bronchioloalveolar.Adenocarcinoma: METIS_p_NCLE_RNA1_Human_U133_Plus_2_0_E05_240954	14.87	16.62	49.04	34.08	87.71	212.35	48.29	18.77	24.56
H441 Lung_Cancer.Cell.Line.Large_NCI-H441_Bronchioloalveolar.Adenocarcinoma: GSM274741	16.59	14.5	38.25	45.12	72.27	119.51	47.77	26.89	22.77
H441 Lung_Cancer.Cell.Line.Large_NCI-H441_Bronchioloalveolar.Adenocarcinoma: GSM274742	14.95	15.78	44.38	37.62	71.5	116.88	44.24	25.52	21.04
H441 Lung_Cancer.Cell.Line.Large_NCI-H441_Bronchioloalveolar.Adenocarcinoma: NCI-H441_SS475525_HG-U133_Plus_2_HCHP-225837	15.89	18.07	48.6	28.07	69.86	263.85	43.29	23.61	28.88
H441 Lung_Cancer.Cell.Line.Large_NCI-H441_Bronchioloalveolar.Adenocarcinoma: NCI-H441_SS475527_HG-U133_Plus_2_HCHP-225839	19.1	16.67	50.57	27.93	68.59	226.22	44.21	26.03	27.01
H520 Lung_Cancer.Cell.Line.Large_NCI-H520_Squamous.Cell.Carcinoma: BRAKE_p_NCLE_RNA2_HG-U133_Plus_2_D02_241116	19.37	17.66	59.98	28.5	76.65	67.04	44.04	33.57	34.41
H520 Lung_Cancer.Cell.Line.Large_NCI-H520_Squamous.Cell.Carcinoma: GSM274798	16.5	15.8	48.05	30.93	78.98	87.21	46.82	36.39	21.66
H520 Lung_Cancer.Cell.Line.Large_NCI-H520_Squamous.Cell.Carcinoma: GSM274831	20.61	16.66	47.85	34.97	77.36	82.98	45.82	32.57	25.09
H522 Lung_Cancer.Cell.Line.Large_NCI-H522_Adenocarcinoma: NIECE_p_NCLE_RNA3_HG-U133_Plus_2_B08_296028	14.91	17.14	42.85	31.33	98.42	94.97	57.63	24.73	21.26
H522 Lung_Cancer.Cell.Line.Large_NCI-H522_Adenocarcinoma: GSM274754	17.07	17.13	48.65	38.8	86.16	65.48	48.6	28.98	23.56
H522 Lung_Cancer.Cell.Line.Large_NCI-H522_Adenocarcinoma: GSM274753	16.1	15.3	42.23	36.5	81.83	76.29	53.99	31.59	21.85
H522 Lung_Cancer.Cell.Line.Large_NCI-H522_Non-Small.Cell.Lung.Carcinoma: NCI-H522_SS181856_HG-U133_Plus_2_HCHP-167900	14.4	16.48	43.98	22.48	68.53	77.74	70.22	20.51	22.26
H522 Lung_Cancer.Cell.Line.Large_NCI-H522_Non-Small.Cell.Lung.Carcinoma: NCI-H522_SS181857_HG-U133_Plus_2_HCHP-167901	15.77	16.37	39.13	22.04	110.03	67.85	54.42	22.81	23.76

**SUPPLEMENTARY FIGURE S1**



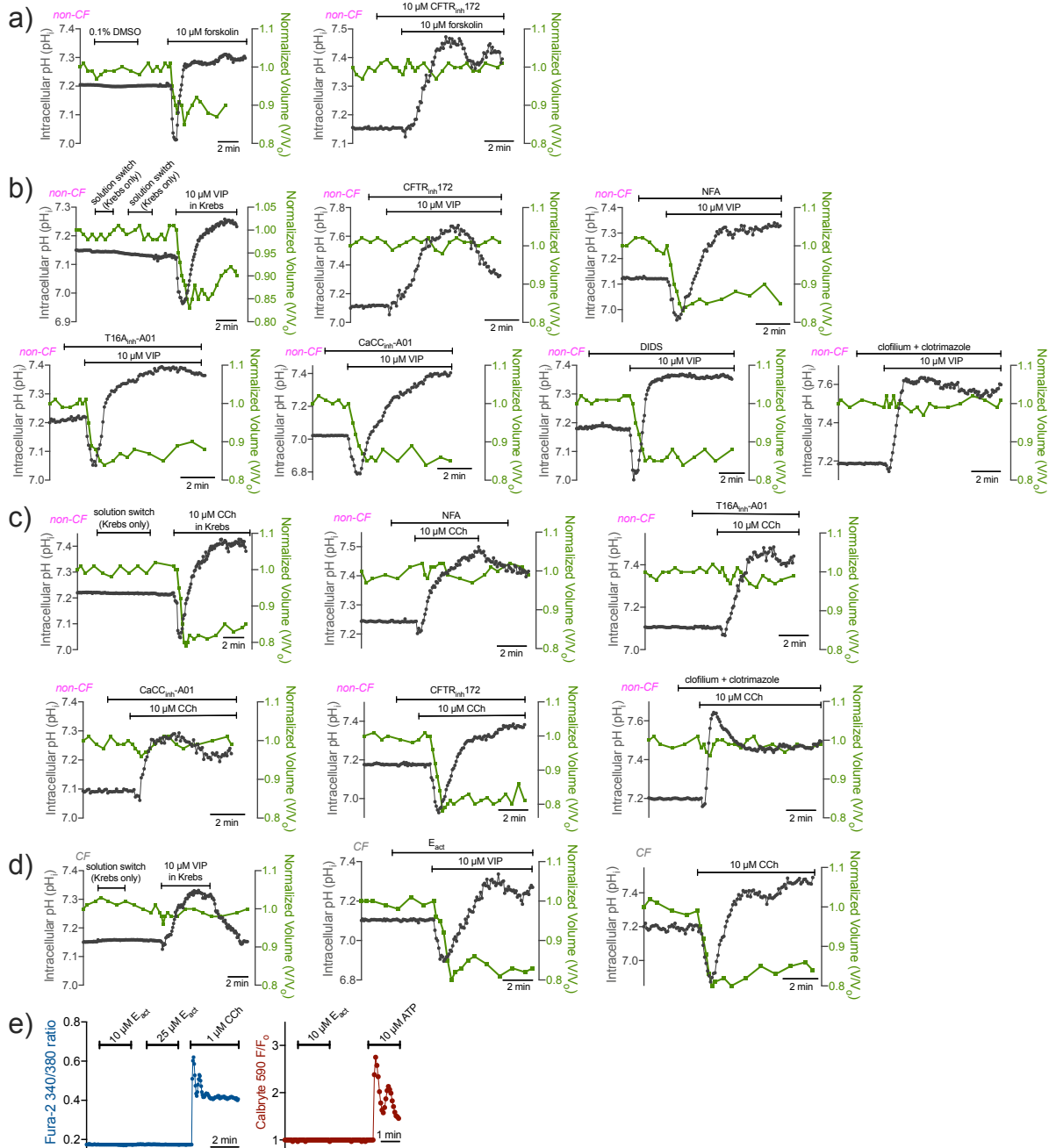
**SUPPLEMENTARY FIGURE S1** Isolated airway serous acinar cells. **a)** Representative diagram showing serous acinar cells at the distal ends of submucosal glands, which secrete the bulk of fluid in response to agonists that utilize cAMP or Ca<sup>2+</sup> as second messengers. **b)** Representative spinning disk confocal images of primary human serous acini and acinar cells isolated from human middle turbinate samples plated on CellTak coated coverslips. **c-e)** Isolated serous acini exhibited punctate granular immunofluorescence for lysozyme (*c-d*) as well as basolateral membrane staining for Na<sup>+</sup>/K<sup>+</sup> ATPase (*c*), VIPR1 (*d-e*), and VIPR2 (*e*). **f-g)** Apical membrane staining was observed for secretory Cl<sup>-</sup> channels TMEM16A (*f*) and CFTR (*g*), as previously described [3-6, 9]. Results are representative of immunofluorescence experiments using cells from ≥3 patients. Scale bars are 20 μm in *b* and 25 μm in *c-g*. CFTR, lysozyme, and TMEM16A immunofluorescence matched previous studies [3-6, 9] of airway submucosal gland serous cells.

SUPPLEMENTARY FIGURE S2



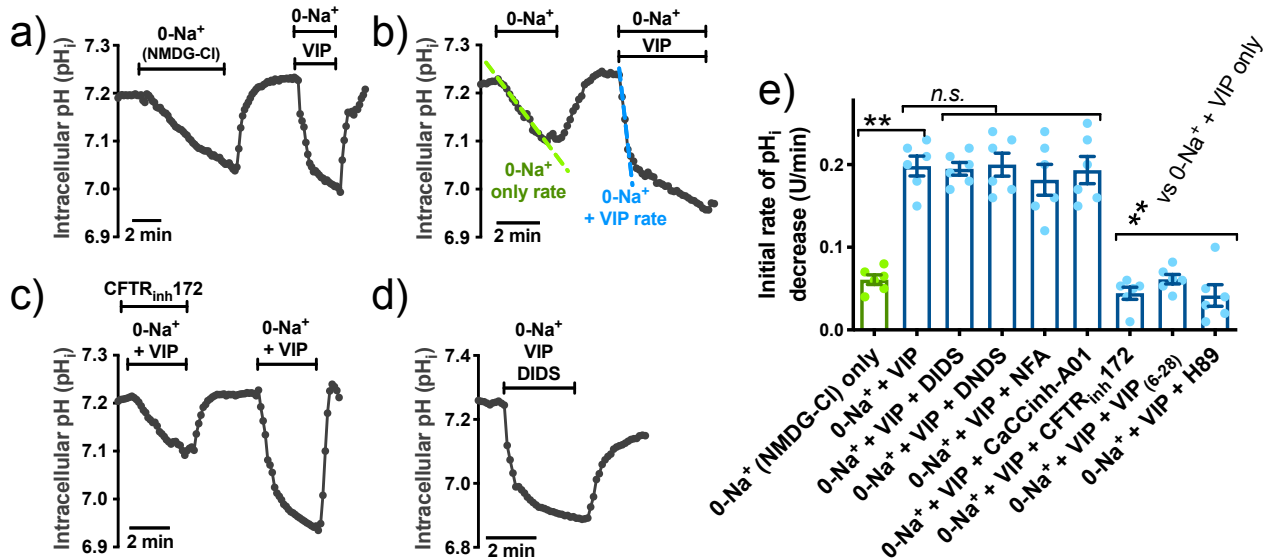
**SUPPLEMENTARY FIGURE S2** VIP-induced acidification reflects conductive  $\text{HCO}_3^-$  efflux, while subsequent alkalinization reflects  $\text{HCO}_3^-$  uptake via  $\text{Na}^+\text{HCO}_3^-$  cotransporter (NBC). **a)** In the absence of  $\text{HCO}_3^-$  (20 mM HEPES-buffered conditions gassed with 100%  $\text{O}_2$ ), VIP-induced acidification is eliminated. However, cells still shrink at a normal magnitude and rate. Residual  $\text{pH}_i$  increase is blocked by DMA, suggesting it reflects NHE activity. **b-c)** Bar graphs (mean  $\pm$  SEM) showing peak  $\text{pH}_i$  decrease (*b*) or volume decrease magnitude and kinetics (*c*) during VIP or forskolin stimulation in the presence or absence of  $\text{CO}_2/\text{HCO}_3^-$ . Significance determined by one-way ANOVA with Bonferroni posttest;  $**p < 0.01$  and *n.s.* = no statistical significance. These data demonstrate that VIP-induced  $\text{pH}_i$  decrease requires  $\text{HCO}_3^-$ , suggesting it reflects  $\text{HCO}_3^-$  efflux. However, the magnitude of initial cell shrinkage is not  $\text{HCO}_3^-$ -dependent; as previously shown, shrinkage primarily reflects  $\text{Cl}^-$  efflux [3-6, 8, 9]. This is likely due to the relative magnitude of  $\text{Cl}^-$  and  $\text{HCO}_3^-$  solute lost during secretion. A serous cell has resting  $[\text{Cl}^-]_i = \sim 65$  mM (supplementary figure S19 and [3]) and loses  $>50\%$  of cellular  $\text{Cl}^-$  content ( $>40$  meq $\cdot\text{L}^{-1}$ ) during  $\sim 20\%$  volume decrease [3, 33]. However, the actual  $\text{HCO}_3^-$  content lost from the cell during secretion is smaller; a 7.2 to 7.0  $\text{pH}_i$  change would drop  $[\text{HCO}_3^-]_i$  from  $\sim 16$  mM to 12 mM (calculated via Henderson Hasselbach). Taking into account the cell volume loss (20%) but ignoring non-osmotically active volume for simplicity, this is a loss of cellular  $\text{HCO}_3^-$  content of  $(1 \times 16 \text{ meq}\cdot\text{L}^{-1}) - (0.8 \times 12 \text{ meq}\cdot\text{L}^{-1}) = \sim 6.4$  meq $\cdot\text{L}^{-1}$   $\text{HCO}_3^-$ . Thus, cell volume is primarily an indicator of  $\text{Cl}^-$  secretion while  $\text{pH}_i$  is primarily an indicator of  $\text{HCO}_3^-$ , as previously observed [4, 53]. **d)** In the presence of  $\text{HCO}_3^-$ , serous cell  $\text{pH}_i$  increases (after initial decrease) were substantially reduced by NBC inhibitor 4,4'-dinitrostilbene-2,2'-disulfonic acid (DNDS; 100  $\mu\text{M}$ ). Alkalinization was not significantly reduced by  $\text{Na}^+/\text{H}^+$  exchanger (NHE) inhibitor dimethyl amiloride (DMA; 30  $\mu\text{M}$ ) alone. All experiments done at  $37^\circ\text{C}$  in the presence of 5%  $\text{CO}_2$ . Representative traces shown on left. Bar graph right shows mean  $\pm$  SEM;  $** = p < 0.01$  by one-way ANOVA with Bonferroni posttest. These data suggest NBC drives serous cell alkalinization during VIP stimulation, likely as a way to sustain  $\text{HCO}_3^-$  secretion due the basolateral localization of NBC in exocrine acinar cells [54-58], similar to what was previously observed with NHE sustaining  $\text{HCO}_3^-$  secretion during cholinergic-evoked secretion [4]. By keeping  $[\text{HCO}_3^-]_i$  elevated during VIP stimulation, basolateral NBC will increase the driving force for  $\text{HCO}_3^-$  efflux across the apical membrane through CFTR. **e)** In the presence of high  $\text{K}^+/\text{low Cl}^-$  conditions designed to block conductive  $\text{HCO}_3^-$  efflux by clamping  $E_{\text{K}^+} = E_{\text{Cl}^-} = E_{\text{HCO}_3^-} = V_m$  (described in the supplementary methods and [4]), VIP-induced acidification is blocked. Bar graph in *b* shows mean  $\pm$  SEM with significance ( $**p < 0.01$ ) determined via Student's *t* test. DMA (30  $\mu\text{M}$ ) + DNDS (100  $\mu\text{M}$ ) were used to prevent alkalinization so we could observe only the acidification ( $\text{HCO}_3^-$  efflux). Thus, the VIP-induced acidification likely reflects conductive  $\text{HCO}_3^-$  efflux, likely through an ion channel like CFTR and not a  $\text{Cl}^-/\text{HCO}_3^-$  exchanger.

## SUPPLEMENTARY FIGURE S3



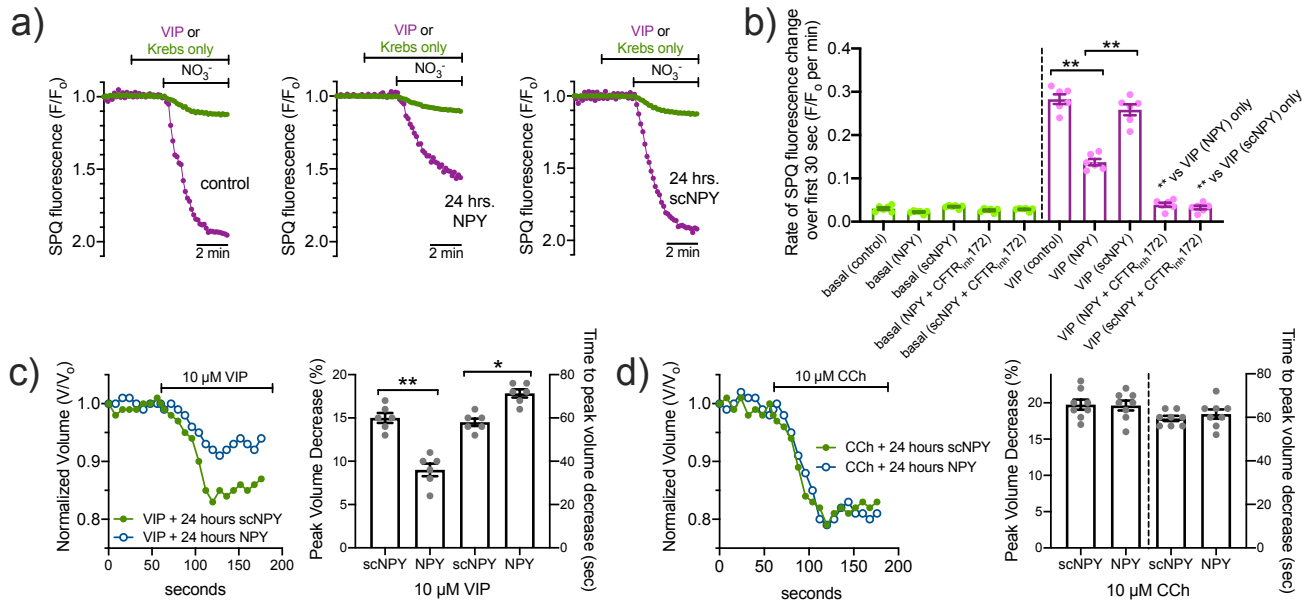
**SUPPLEMENTARY FIGURE S3** Representative traces of responses summarized in main text figure 1. **a)** Representative traces of responses summarized in figure 1e. **b)** Representative traces of responses summarized in main text figure 1f. **c)** Representative traces of responses summarized in figure 1g. **d)** Representative traces of responses summarized in main text figure 1h. **e)** Eact was recently suggested to be an indirect activator of TMEM16A via TRPV4 activation and elevation of Ca<sup>2+</sup> [59]. Serous cells were loaded with either fura-2 or Calbryte 590 by incubation in the AM ester form for 20 min as described [3, 5, 6] and imaged using fura-2 or TRITC filter sets, respectively. No evidence of changes in [Ca<sup>2+</sup>]<sub>i</sub> were observed with concentrations of E<sub>act</sub> used in this study, despite changes with sub-saturating cholinergic or purinergic stimulation. Traces are representative of experiments using 3-5 serous acini from 3 individual patients (9-15 experiments total with each dye). Two dyes were used to confirm no effects on [Ca<sup>2+</sup>]<sub>i</sub>.

## SUPPLEMENTARY FIGURE S4



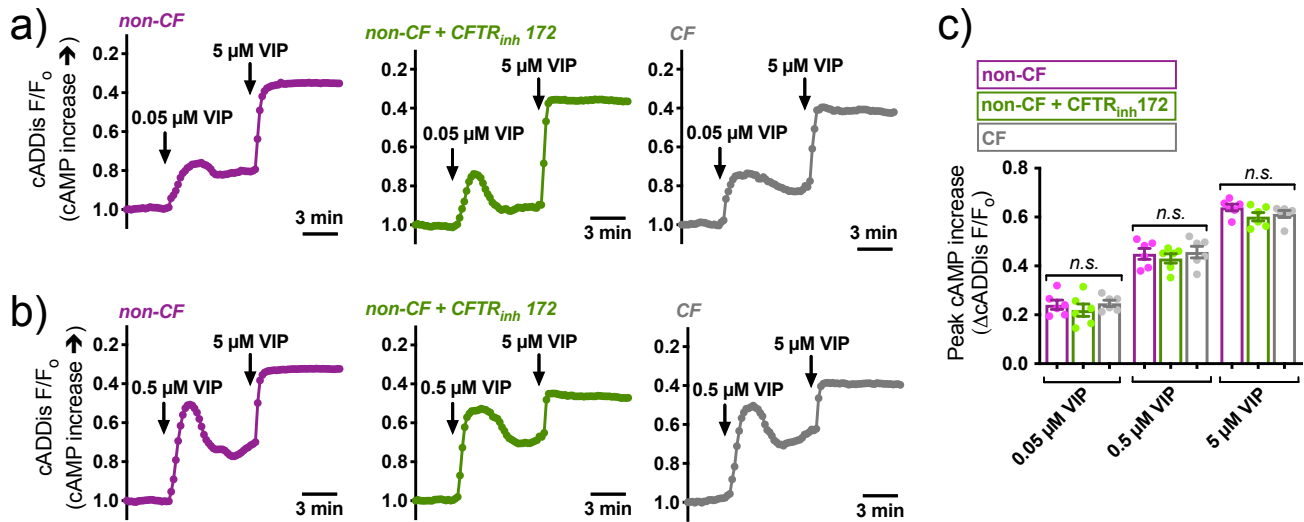
**SUPPLEMENTARY FIGURE S4** Isolation of the VIP-induced HCO<sub>3</sub><sup>-</sup> efflux pathway under 0-Na<sup>+</sup> conditions. **a-b**) To better isolate VIP-induced acidification, we performed experiments in 0-Na<sup>+</sup> to prevent alkalinization by Na<sup>+</sup> dependent mechanisms (NHE, NBC) in serous cells from non-CF patients. In the absence of Na<sup>+</sup> (isosmotic substitution with NMDG<sup>+</sup>; solutions used described in the supplementary methods and [4]), cells exhibited a slow acidification. VIP (1 μM) nonetheless still increased the acidification rate under these conditions. Panel B shows comparisons of rates ± VIP (blue vs green). **c-d**) The VIP-induced increased in acidification was inhibited by CFTR<sub>inh</sub>172 (20 μM; c), but not by Ca<sup>2+</sup>-activated Cl<sup>-</sup> channel (CaCC) and/or Cl<sup>-</sup>/HCO<sub>3</sub><sup>-</sup> exchanger (e.g., pendrin [60]) inhibitors like 4,4'-diisothiocyano-2,2'-stilbenedisulfonic acid (DIDS; d; 1 mM), DNDS (30 μM), NFA (100 μM), or CaCC<sub>inh</sub>-A01. **e**) Bar graphs showing rates measured from experiments as in A-D. VIP-induced acidification was inhibited only by CFTR<sub>inh</sub>172, VIP receptor antagonist VIP<sub>(6-28)</sub>, or PKA inhibitor H89 (10 μM). Graph shows mean ± SEM with significance determined by one-way ANOVA with Bonferroni posttest; \*\**p* < 0.01 and *n.s.* = no statistical significance. All experiments done at 37°C in 5% CO<sub>2</sub>/25 mM HCO<sub>3</sub><sup>-</sup>. These data show that inhibitors of TMEM16A/CaCC [61-63] or pendrin [60] do not inhibit VIP-induced acidification. Along with ion substitution (**supplementary figure S1**) and data from CF patient cells (**figure 1**), these data support CFTR conduction as the primary HCO<sub>3</sub><sup>-</sup> efflux pathway in serous cells during VIP stimulation.

## SUPPLEMENTARY FIGURE S5



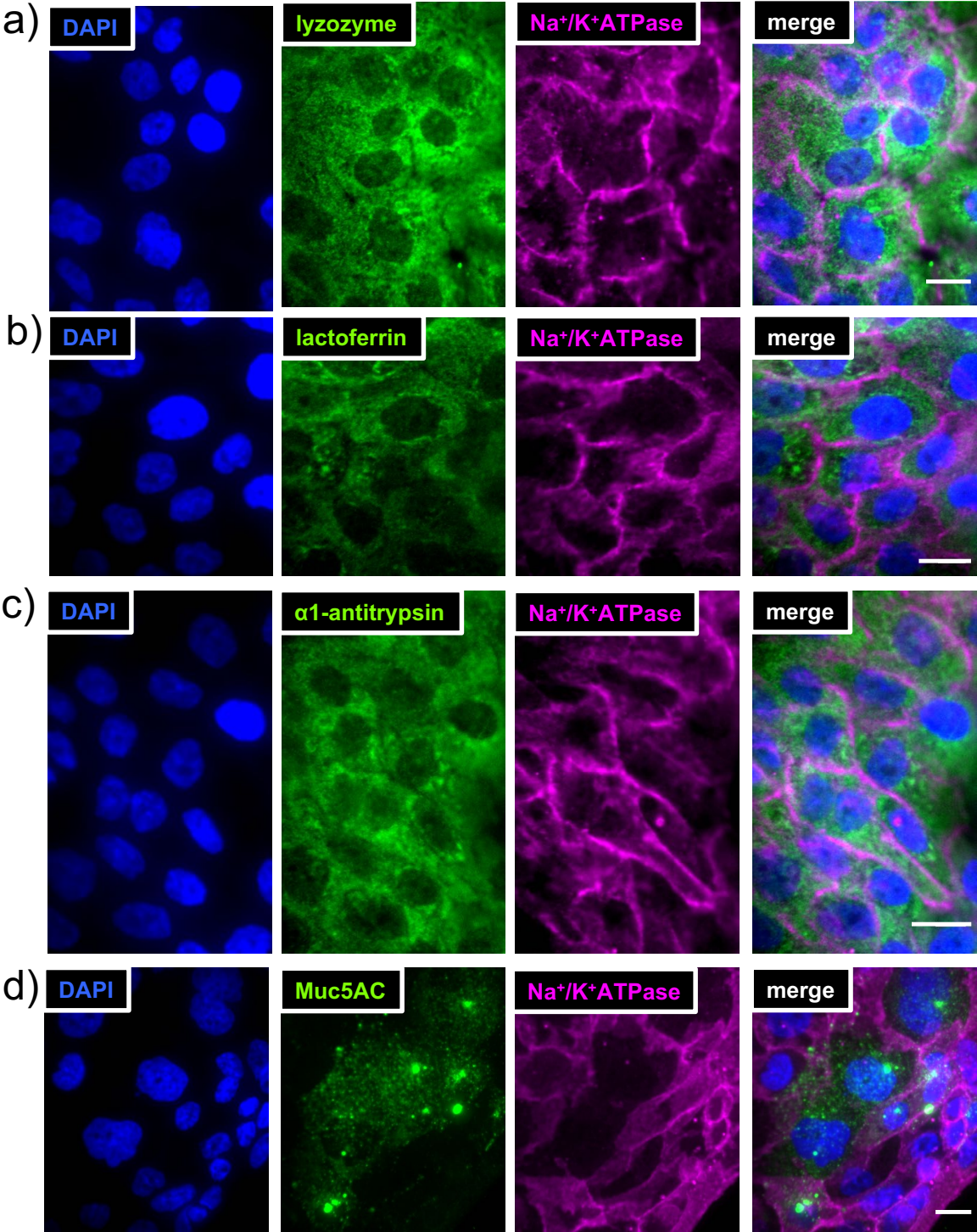
**SUPPLEMENTARY FIGURE S5** Effects of 24 hours NPY stimulation on Cl<sup>-</sup> ion transport phenotypes. **a)** Representative traces of SPQ fluorescence from isolated serous cells in the presence of 5 μM VIP after 24 hrs prior stimulation with media only (control), 1 μM NPY, or scrambled NPY (scNPY). Cells were isolated and plated on Matrigel-coated coverslips (1:30 dilution of growth factor reduced Matrigel) and stimulated in serum-free MEME for 24 hours. Cells were loaded with SPQ 2 hours prior to the experiments, done in the continued presence of NPY or scNPY as applicable. Unstimulated SPQ fluorescence (no VIP) changes are shown in green and VIP-stimulated fluorescence changes shown in magenta (separate experiments). As described in the text, supplementary methods, and previous studies [3-6, 9, 11, 14], SPQ is quenched by Cl<sup>-</sup> but no NO<sub>3</sub><sup>-</sup>. Upon substitution of extracellular Cl<sup>-</sup> for NO<sub>3</sub><sup>-</sup>, intracellular [Cl<sup>-</sup>] decreases via electroneutral exchange of Cl<sup>-</sup> for NO<sub>3</sub><sup>-</sup> via diffusion and SPQ fluorescence increases. As most Cl<sup>-</sup> channels have roughly equal permeability to Cl<sup>-</sup> and NO<sub>3</sub><sup>-</sup>, the relative rate of SPQ fluorescence change is roughly equal to relative anion permeability. **b)** Bar graph showing initial rate of SPQ fluorescence change over first 30 sec of NO<sub>3</sub><sup>-</sup> substitution. NPY, but not scNPY, significantly reduced SPQ fluorescence changes under VIP-stimulated conditions but not unstimulated conditions. Data points for each bar are 6 independent experiments using cells from 3 patients (2 experiments per patient); \*\**p* < 0.01 by 1-way ANOVA with Bonferroni posttest. **c)** Cells were stimulated with NPY or scNPY as above and then VIP cell volume responses were immediately imaged in the continued presence of NPY or scNPY (representative traces from independent experiments shown on left). The peak cell shrinkage and time to peak shrinkage in response to 10 μM VIP was reduced in the presence of NPY (bar graph on right). **d)** Similar experiments were carried out as c but with stimulation with 10 μM CCh. No inhibition of secretion was observed with CCh. Significance in *c* and *d* by 1-way ANOVA with Bonferroni posttest with paired comparisons as indicated; \**p* < 0.05 and \*\**p* < 0.01. Data points for each bar are 6 independent experiments using cells from 3 patients (2 experiments per patient); \*\**p* < 0.01 by 1-way ANOVA with Bonferroni posttest. Together with experiments in the main text, these data suggest NPY reduces anion secretion in response to cAMP-elevating VIP but does not affect anion secretion in response to CCh.

## SUPPLEMENTARY FIGURE S6



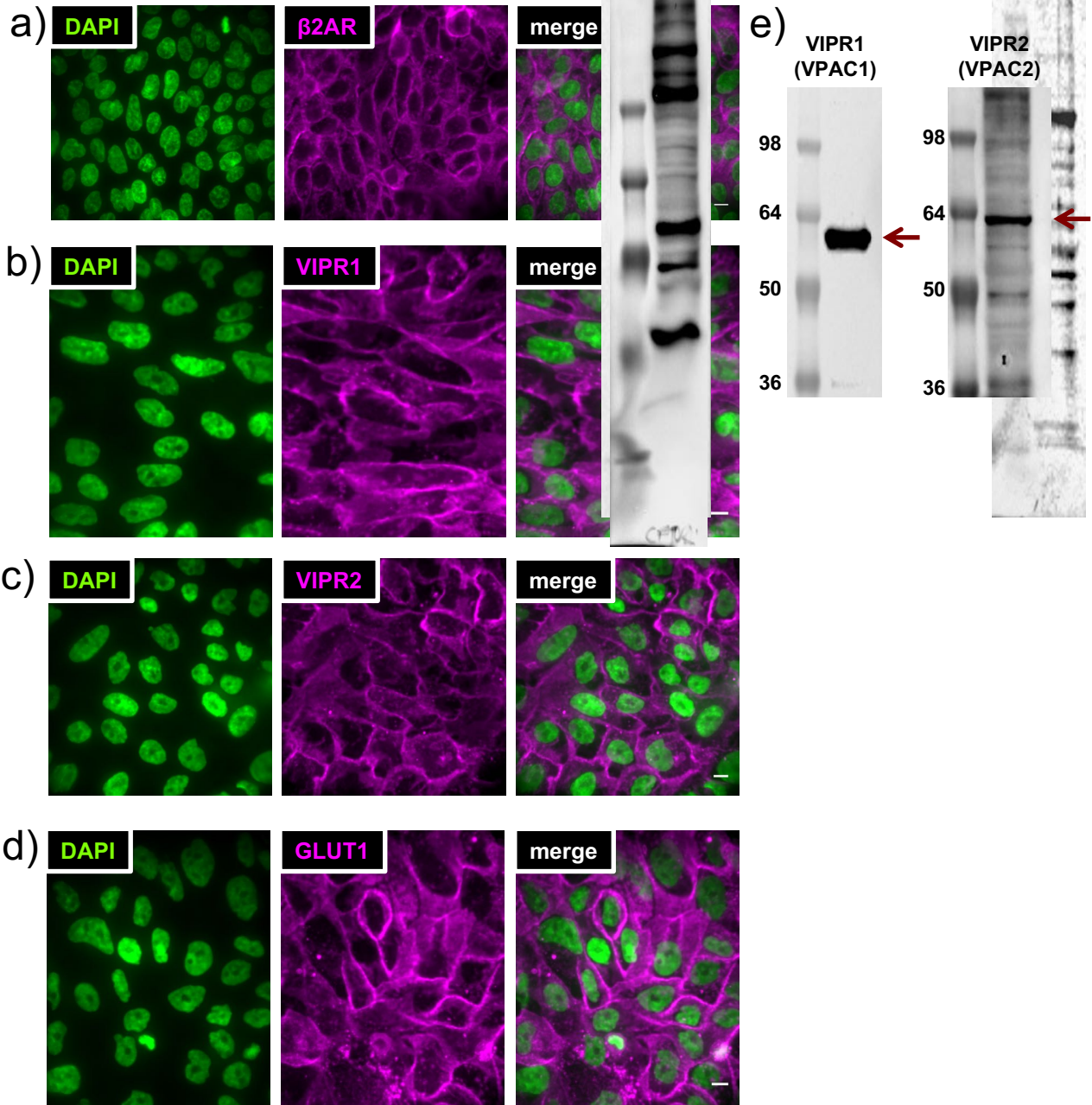
**SUPPLEMENTARY FIGURE S6** Comparison of VIP-induced cAMP signaling in CF vs non-CF cells. CFTR has been proposed to act as a hub for kinases and other signaling proteins. We used a fluorescent cAMP biosensor to visualize VIP-activated cAMP increases in CF and non-CF serous cells. We utilized a baculovirus pseudotyped for mammalian cells (BacMam) vector [2], as BacMam was previously used to express proteins in primary lacrimal gland acinar cells [64-66]. Serous acinar cells were isolated, seeded onto CellTak-coated coverslips, and transduced for 6 hrs with a BacMam expressing an mNeonGreen-based fluorescent cAMP biosensor (downward cADDIs; Montana Molecular, Bozeman MT; [1]) under a CMV promoter followed by 18-24 hrs incubation. Single transduced cells and acini were imaged using GFP filters. A decrease in F/F<sub>0</sub> (plotted inversely, thus shown as an upward deflection of trace) equals an increase in cAMP (as indicated by the arrow on the axis). **a-b)** We examined if CF serous cells exhibited alterations in cAMP signaling in response to 0.05, 0.5, and 5 μM VIP. No differences were observed between CF and non-CF patients. This suggests that VIP-evoked cAMP signaling, at least at a global cytoplasmic level, is intact in CF serous cells. We also treated non-CF cells with CFTR<sub>inh</sub>172, and found no alterations of cAMP signals. **c)** Bar graph of peak responses (absolute values are plotted) from representative experiments as shown in *a-b* (3-5 patients samples used for each group, ≥2 experiments per patient per group). 1-way ANOVA with Bonferroni posttest suggested no statistically significant differences. Bar graph shows mean ± SEM; *n.s.* = no statistical significance.

**SUPPLEMENTARY FIGURE S7**



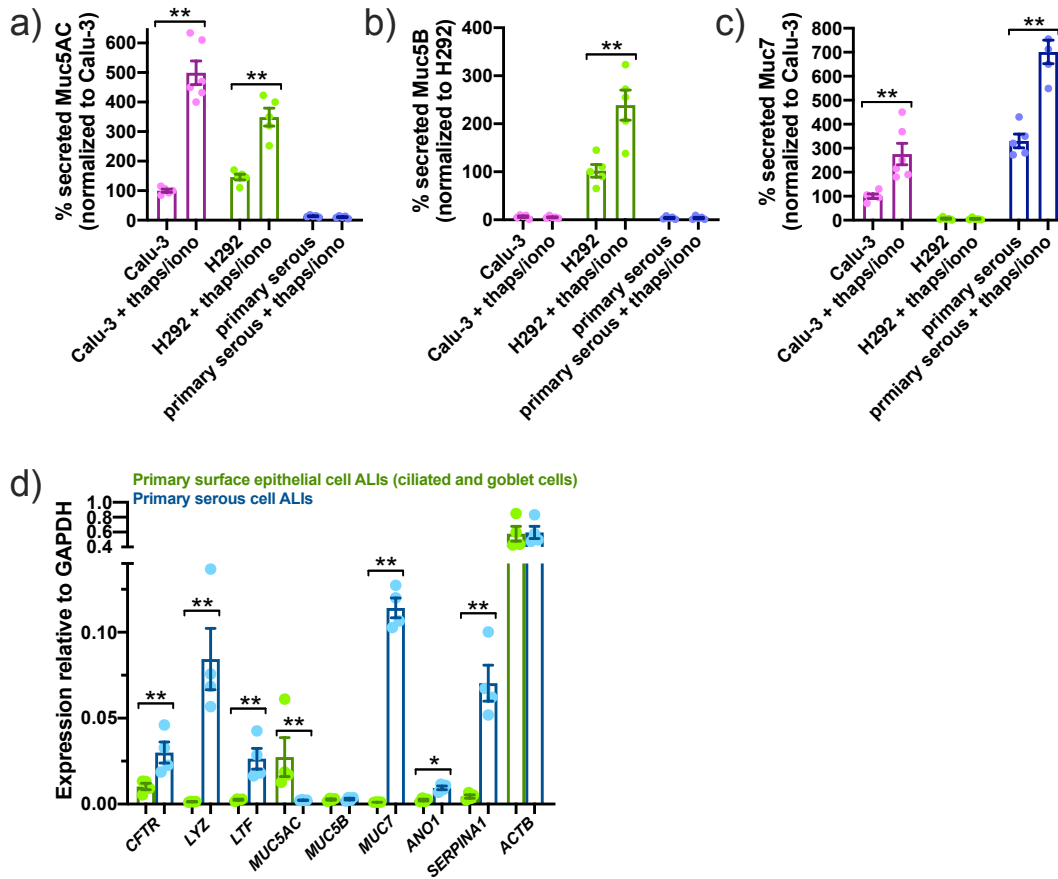
**SUPPLEMENTARY FIGURE S7** Expression of serous cell markers lysozyme (a), lactoferrin (b), and alpha-1-antitrypsin (c) in Calu-3 cells as well as goblet cell marker Muc5AC (d). Cells were seeded and grown as a monolayer on collagen coated glass bottom dishes (MatTek), and confluent monolayers were fixed in ice cold MeOH for 3 min before immunostaining as described in the supplementary methods. Antibody against Na<sup>+</sup>/K<sup>+</sup> ATPase was used as a positive plasma membrane control.

**SUPPLEMENTARY FIGURE S8**



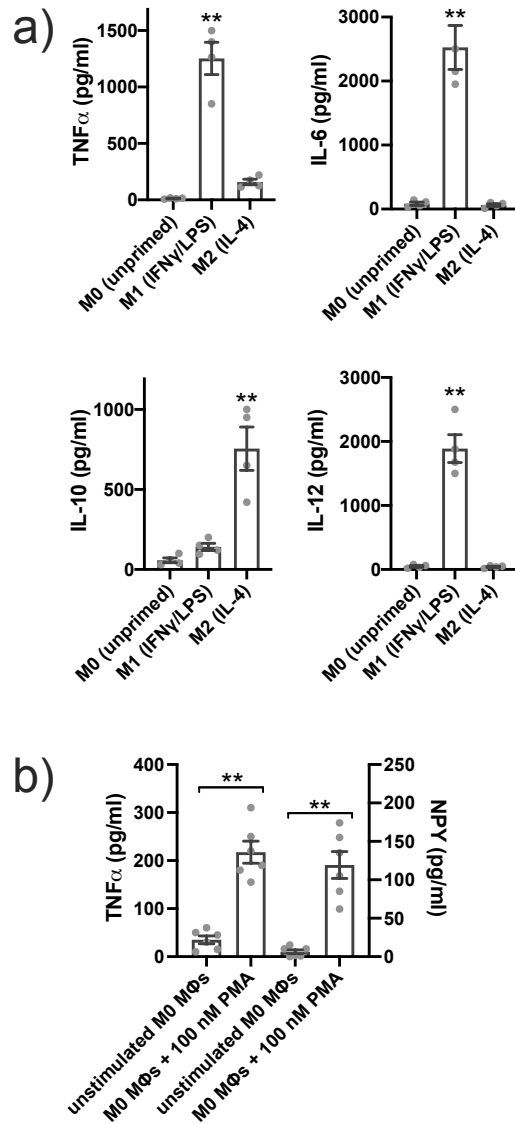
**SUPPLEMENTARY FIGURE S8** Expression of both VIPR1 (VPAC1) and VIPR2 (VPAC2) in Calu-3 cells. **a-d)** Cells were seeded and grown as a monolayer on collagen coated glass bottom dishes (MatTek), and confluent monolayers were fixed in ice cold MeOH for 3 min before immunostaining as described in the supplementary methods. GLUT1 and  $\beta$ 2AR1 were used as plasma membrane controls. **e)** Western blot showing bands corresponding to VIPR1 and VIPR2 using antibodies from *b* and *c* and as used in the main text.

## SUPPLEMENTARY FIGURE S9



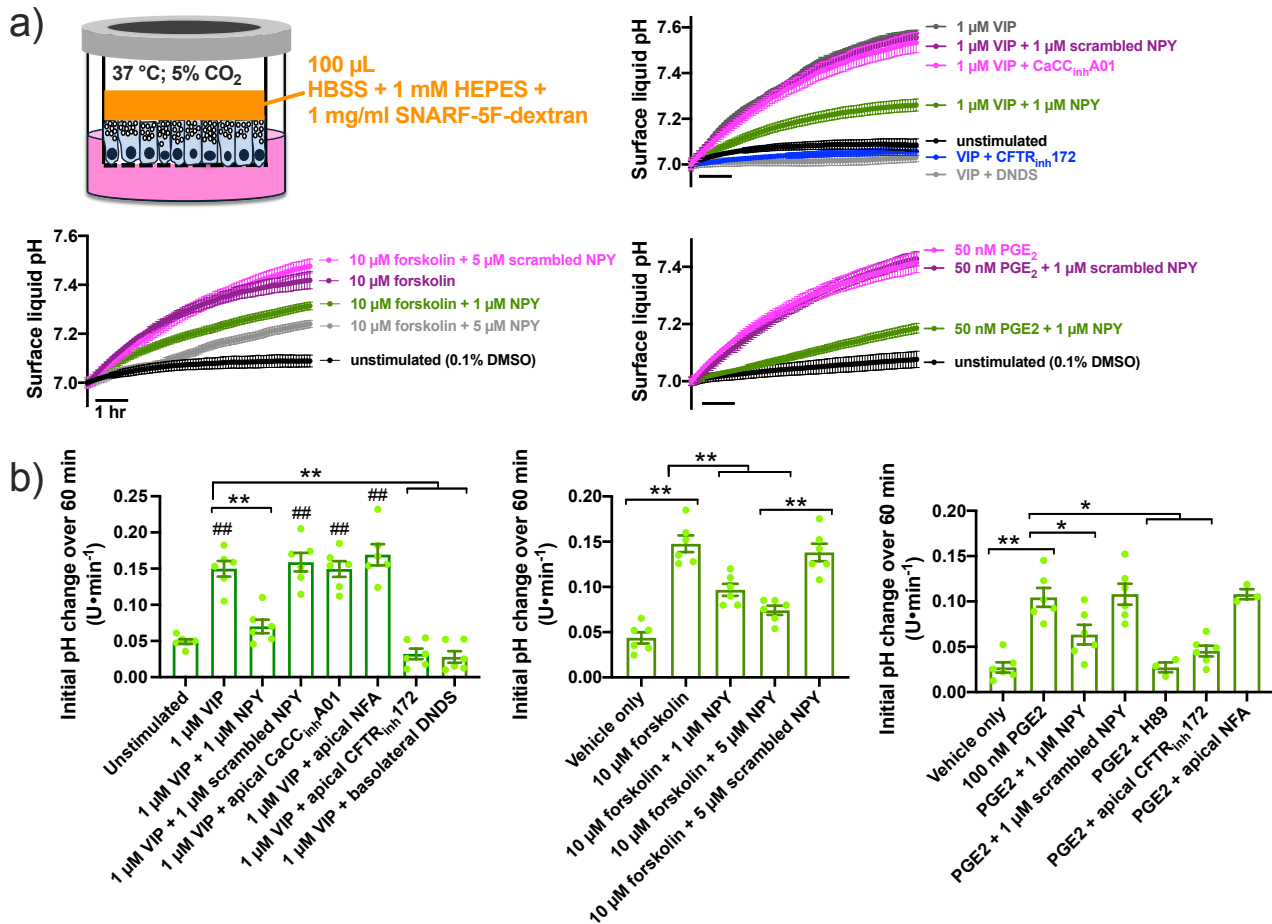
**SUPPLEMENTARY FIGURE S9** Verification of Muc7, but not Muc5AC or Muc5B, production from primary human nasal serous cell cultures, suggesting maintenance of serous phenotype. ASL was collected  $\pm$  stimulation with thapsigargin and ionomycin (10  $\mu\text{g}/\text{ml}$  each; 30 min, basolaterally) to maximally elevate  $\text{Ca}^{2+}$  and activate acute secretion. **a)** Calu-3 cells produced goblet cell Muc5AC [67] as previously reported [68-70], as did H292 cells, as previously reported [71-74]. **b)** H292 cells produced mucous cell-marker Muc5B [75, 76], as previously reported [77-80]. Calu-3 and serous cells did not make detectible Muc5B. **c)** Both Calu-3 and primary serous cells produced serous cell marker Muc7 [75, 76]. H292 cells did not. Secretion of all mucins was increased acutely after basolateral stimulation with thapsigargin and ionomycin. **d)** Primary surface epithelial cells (cultured as described [13, 14, 19, 20] to generate primarily ciliated and goblet cells) and serous cells were cultured from the same patients for three weeks after air exposure. Expression of CFTR, lysozyme (LYZ), lactoferrin (LTF), Muc5AC, Muc5B, Muc7, Ano1 (TMEM16A), alpha-1-antitrypsin (SERPINA1), and actin were compared with GAPDH. Serous cell cultures expressed higher levels of CFTR and serous cell markers lysozyme, lactoferrin, alpha-1-antitrypsin, and Muc7 than surface epithelial cells. Surface epithelial cells expressed higher levels of goblet cell Muc5AC. Mucous cell Muc5B was not expressed at high levels in either type of culture. All data are mean  $\pm$  SEM of 3-5 independent experiments using primary serous cells from 3-5 separate non-CF patients.

## SUPPLEMENTARY FIGURE S10



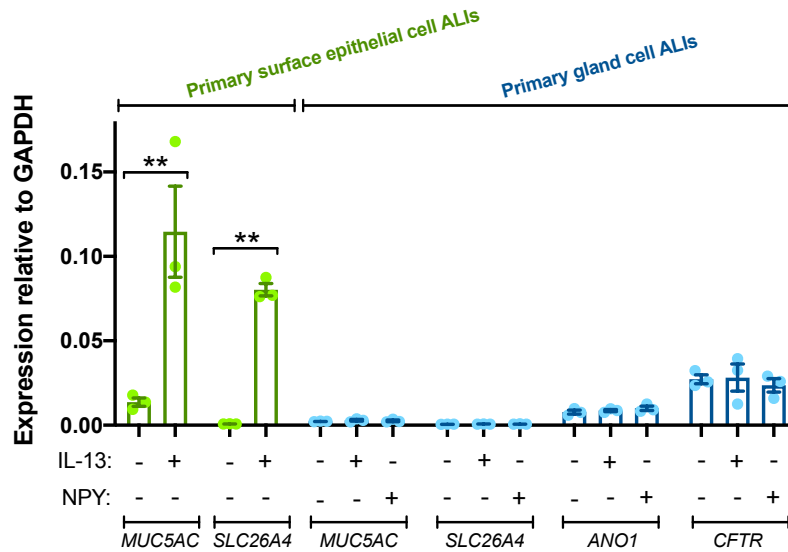
**SUPPLEMENTARY FIGURE S10** Confirmation of macrophage (M $\phi$ ) differentiation by production of appropriate cytokines in response to M1 vs M2 polarization. **a)** Human monocyte-derived M $\phi$  were cultured as described in the text, and stimulated as indicated in the graphs for the final 3 days of the 10 day differentiation. M1 polarization (IFN  $\gamma$  + LPS [81, 82]) resulted in robust secretion of TNF $\alpha$ , IL-6, and IL-12, while M2 polarization (IL-4 [81, 82]) resulted in robust secretion of IL-10, as determined by ELISA. **b)** Stimulation of M0 (unpolarized) M $\phi$ s by PMA for 48 hrs. resulted in secretion of TNF $\alpha$  (left two bars) as well as NPY (right two bars), as previously reported [26, 83-86], as determined by ELISA. Add data are from 6 independent experiments from M $\phi$ s isolated from 3 separate individuals (2 experiments per individual). Significance determined by 1-way ANOVA with Bonferroni posttest; \*\* $p$ <0.01.

## SUPPLEMENTARY FIGURE S11



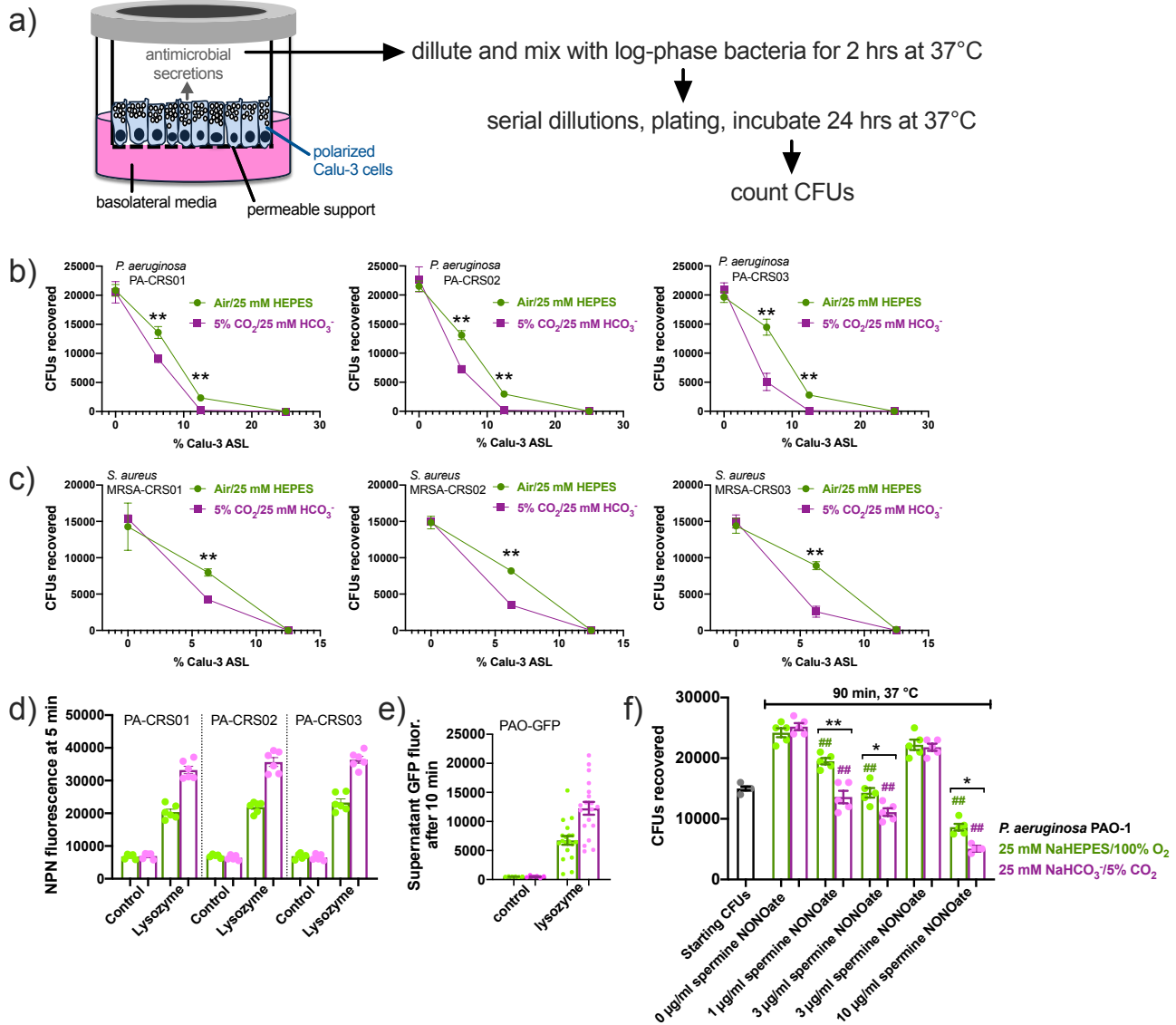
**SUPPLEMENTARY FIGURE S11** VIP, forskolin, or prostaglandin E<sub>2</sub> (PGE<sub>2</sub>) increased apical secretion of HCO<sub>3</sub><sup>-</sup> over >8 hours, while NPY reduced secretion in response to all three agonists. **a)** Non-CF serous cell ALIs were imaged in a stage top incubator (Tokai Hit, Tokyo, Japan) at 37 °C with 5% CO<sub>2</sub>. 100 µL of 1 mg/ml SNARF dextran in low buffering capacity solution was added (HBSS with 1 mM HEPES, as described [38]), and pH was measured every 10 min. These experiments facilitated addition of inhibitors to the apical side. Shown are representative traces (average of 3 ALIs, 3 fields per ALI) from single experiments. **b)** Bar graphs (mean ± SEM) of 6 individual experiments from ≥3 patients. Left bar graph shows inhibition of VIP-induced pH<sub>i</sub> increase by NPY but not scrambled NPY as well as by CFTR<sub>inh</sub>172 (15 µM) but not by apical TMEM16A inhibitors CaCC<sub>inh</sub>-A01 (15 µM) or niflumic acid (NFA; 100 µM). Block by basolateral DNDS (25 µM) suggests surface liquid pH<sub>i</sub> increases are due to HCO<sub>3</sub><sup>-</sup> secretion sustained by Na<sup>+</sup>HCO<sub>3</sub><sup>-</sup> co-transporter (NBC) activity. Middle bar graph shows reduction of forskolin-induced ASL pH<sub>i</sub> increase by NPY but not scrambled NPY. Right bar graph shows inhibition of PGE<sub>2</sub>-induced HCO<sub>3</sub><sup>-</sup> secretion by NPY, protein kinase A inhibitor H89 (10 µM), or CFTR<sub>inh</sub>172. Significance determined by 1-way ANOVA with Bonferroni posttest; \*\**p*<0.01 vs bracketed bars and ##*p*<0.01 vs unstimulated control. These data support the hypothesis that cAMP-elevating agonists like VIP, forskolin, and PGE<sub>2</sub> activates HCO<sub>3</sub><sup>-</sup> secretion through apical CFTR sustained by basolateral NBC and support results from the main text that NPY has an inhibitory effect on this process.

## SUPPLEMENTARY FIGURE S12



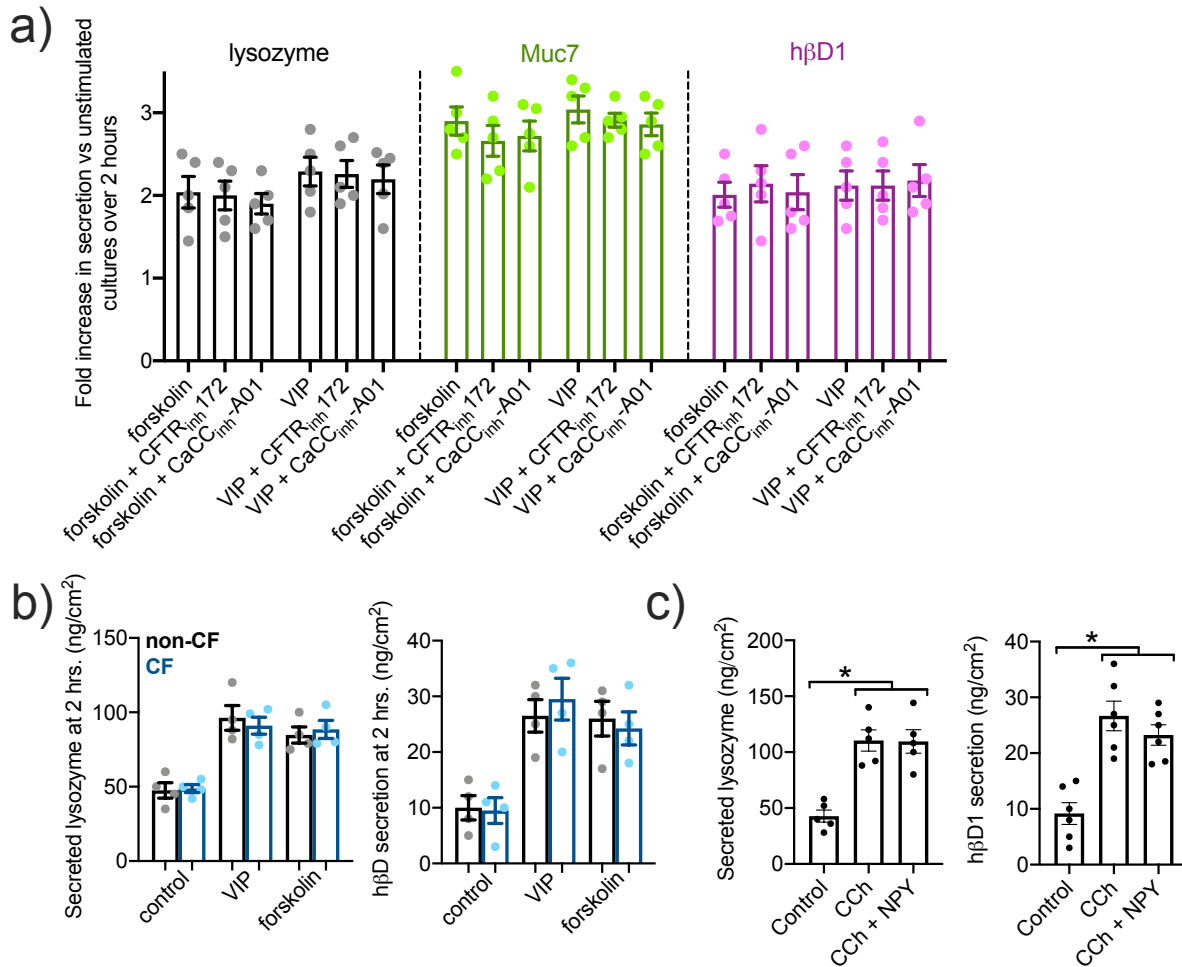
**SUPPLEMENTARY FIGURE S12** Primary serous cell air-liquid interface (ALI) cultures or surface epithelial cell ALIs (primarily ciliated and goblet cells) were grown and stimulated with IL-13 or NPY as indicated in the figure and main text. Quantitative PCR was carried out for the indicated genes as described in the supplementary methods. Three ALIs from three individual patients were used for each condition as independent experiments. The same patients were used for surface epithelial and gland cultures. Significance determined by Bonferroni posttest with paired comparisons; \*\* $p < 0.01$ .

## SUPPLEMENTARY FIGURE S13



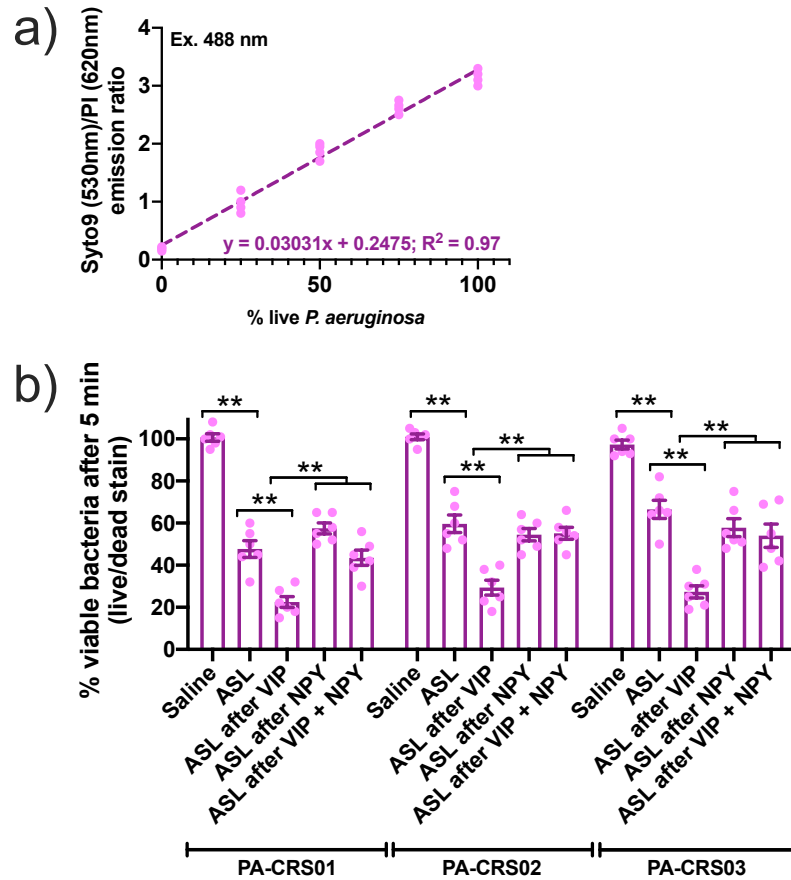
**SUPPLEMENTARY FIGURE S13**  $\text{HCO}_3^-$  increases antimicrobial efficacy of Calu-3 secretions against clinical *Pseudomonas aeruginosa* strains isolated from chronic rhinosinusitis (CRS) patients.  $\text{HCO}_3^-$  has been suggested to be critical to efficacy of antimicrobial peptides secreted by serous cells [8, 87-91]. Antimicrobial assays were carried out as described ([40] modified from [45]) using ASL from Calu-3 bronchial cell cultures. **a-c**) Apical washings (collected with either 25% PBS + 20 mM HEPES or 25% PBS + 25 mM  $\text{HCO}_3^-$ ) were mixed with clinical CRS isolates of *P. aeruginosa* (b) or methicillin-resistant *S. aureus* (c) and incubated at 37°C in room air (HEPES-buffered washings) or 5%  $\text{CO}_2$  ( $\text{HCO}_3^-$ -buffered washings) followed by serial dilutions and spotting on plates for CFU counting. At low dilutions (6.25-12.5%), antimicrobial activity was greater in the presence of 5%  $\text{CO}_2$ . **d**) NPN fluorescence (reflecting uptake due to cell wall damage) of clinical *P. aeruginosa* strains was measured after 5 min of lysozyme treatment (as described [40]) in the presence (pink) or absence of  $\text{HCO}_3^-$  (green). **e**) GFP-release of GFP-expressing *P. aeruginosa* (PAO-GFP) was measured during lysozyme treatment in the presence (pink) or absence (green) of  $\text{HCO}_3^-$ . **f**) *P. aeruginosa* lab type strain PAO-1 was mixed in the presence (pink) or absence (green) of  $\text{HCO}_3^-$  with various concentrations of NO donors, which have anti-bacterial effects (as described [92]). Overall, the presence of  $\text{HCO}_3^-$  had small but significant pro-bactericidal effect in all assays tested.

## SUPPLEMENTARY FIGURE S14



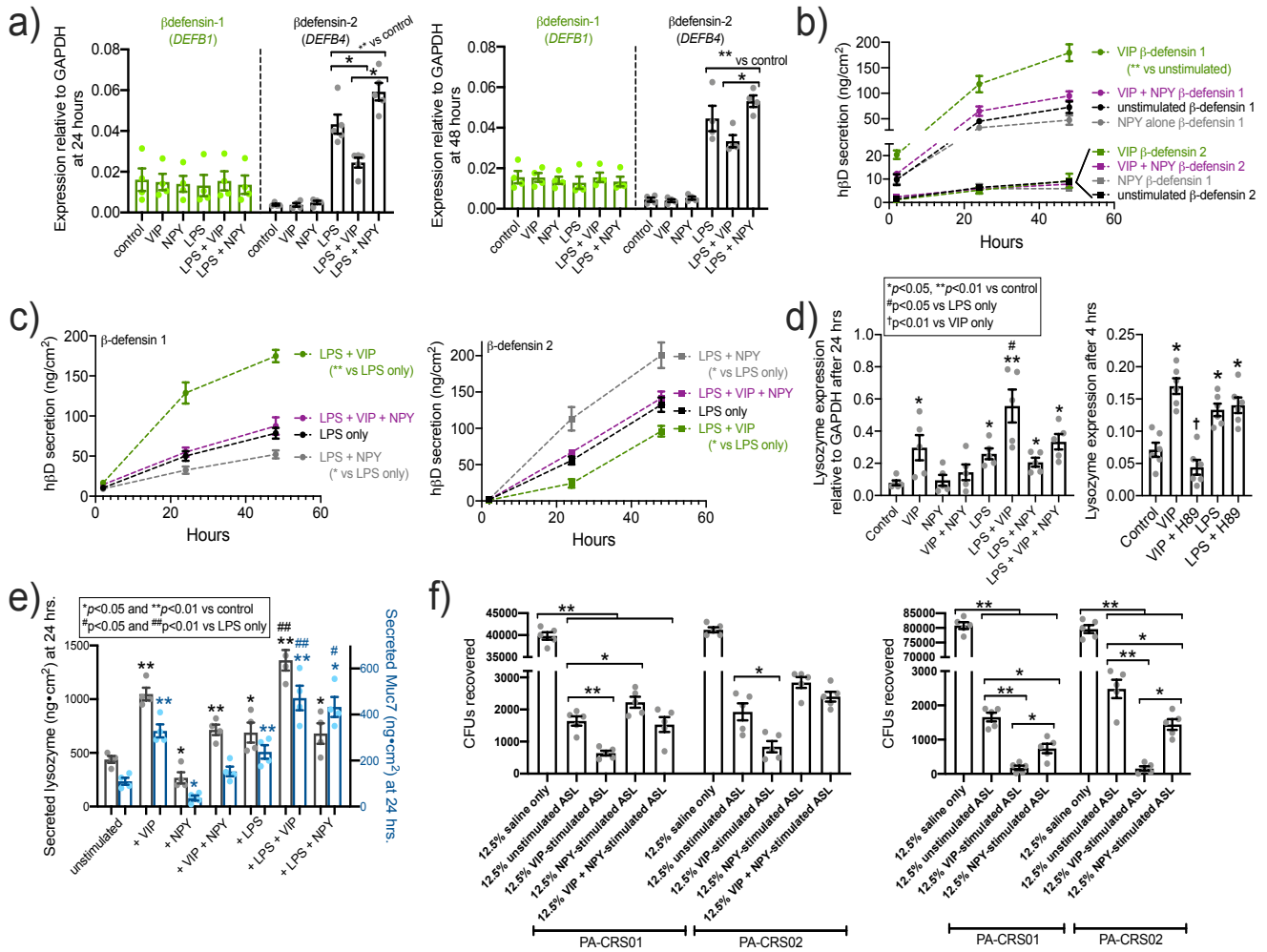
**SUPPLEMENTARY FIGURE S14 a)** Lysozyme, Muc7, and  $\beta$ -defensin 1 ( $h\beta D1$ ) secretion was quantified by ELISA as in the main text. Fold increase in secretion from 5 individual experiments (using ALIs from 5 individual patients) was plotted. No significant reduction of secretion was observed to forskolin (10  $\mu M$ ) or VIP (5  $\mu M$ ) stimulation in the presence of apical CFTR<sub>inh</sub>172 (10  $\mu M$ ) or CaCC<sub>inh</sub>-A01 (10  $\mu M$ ), determined by one-way ANOVA with Bonferroni posttest. **b)** ALIs grown from non-CF (gray) or CF (blue) tissue were stimulated with VIP (5  $\mu M$ ) or forskolin (10  $\mu M$ ) and assayed for lysozyme or  $h\beta D1$  as above. No difference was observed in baseline or stimulated secretion between CF and non-CF patients by 1-way ANOVA with Bonferroni posttest with paired comparisons. Data shown are from 4 independent experiments using ALIs from 2 CF and 2 non-CF patients (2 ALIs per patient per condition). **c)** Lysozyme and  $h\beta D1$  were assayed after 2 hours stimulation with 10  $\mu M$  carbachol (CCh), a cholinergic agonist that activates Ca<sup>2+</sup>-dependent, TMEM16A-dependent, CFTR-independent secretion from serous cells (this study and [3-6, 8, 9]). No significant inhibition of secretion was observed with NPY (1  $\mu M$ ), determined by one-way ANOVA with Bonferroni posttest. Each condition shows data points from independent experiments using ALIs from separate individual patients (5 experiments per condition); \* $p < 0.05$ .

## SUPPLEMENTARY FIGURE S15



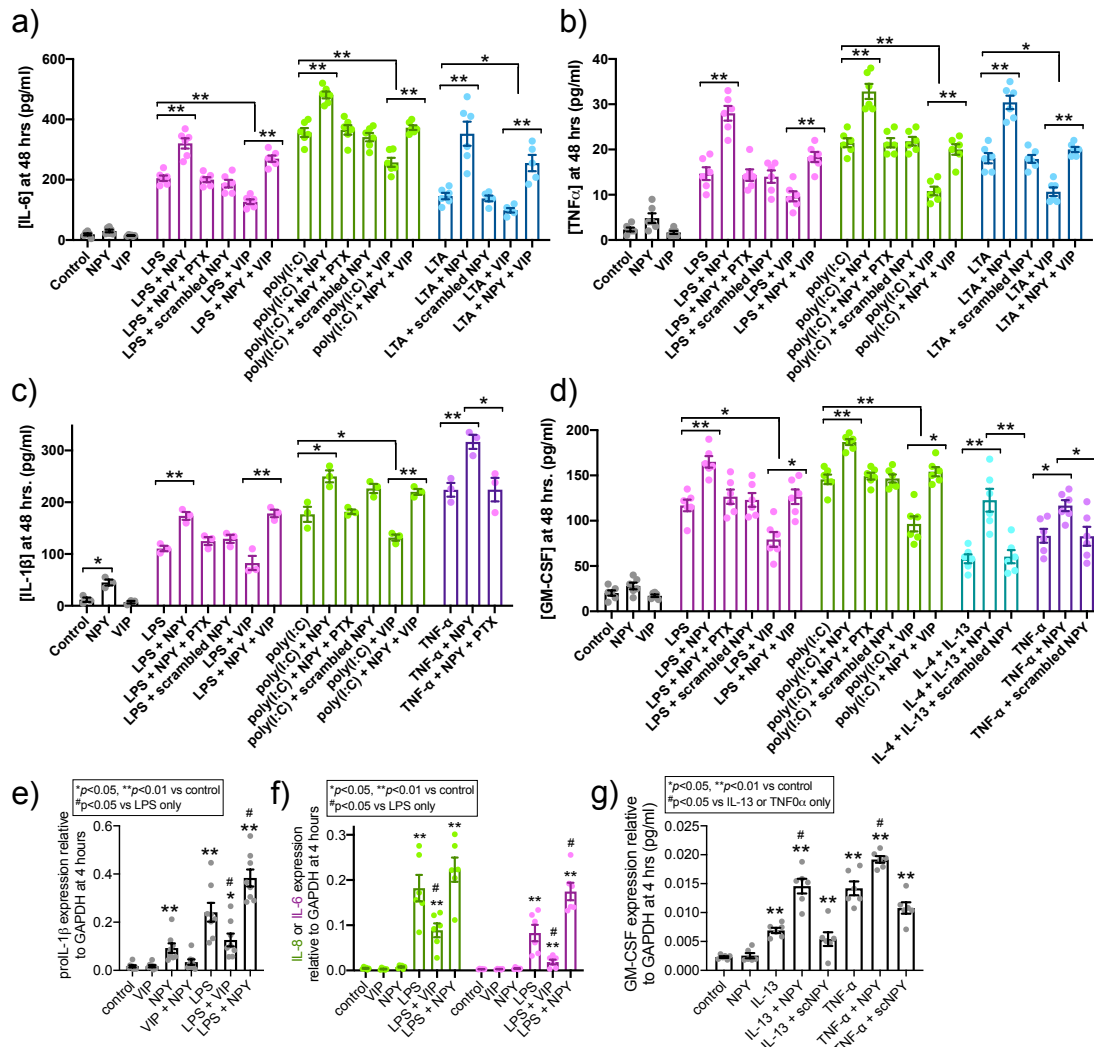
**SUPPLEMENTARY FIGURE S15** Confirmation of neuropeptide-induced changes in ASL antimicrobial efficacy by live-dead staining. **a)** Incubation of dilutions of live and heat-killed *P. aeruginosa* (PAO-1) showed a linear relationship of Syto9 (live cell stain) and propidium iodide (PI; dead cell stain). Strain PA-CRS01 was used for calibration. **b)** Live bacteria were mixed with ASL washings from primary serious ALI cultures stimulated as indicated, stained with Syto9 and PI, and read on a plate reader using 488 nm excitation and ratiometric emission (530 and 620 nm). Calibration from **a)** was used to convert fluorescence ratio into viability. Bar graph shows mean  $\pm$  SEM from 5-6 independent experiments using ALI washings from  $\geq 3$  separate patients. Three clinical isolates of *P. aeruginosa* isolated from CRS patients were used. Significance determined by 1-way ANOVA with Bonferroni posttest; \*\* $p < 0.01$ .

# SUPPLEMENTARY FIGURE S16



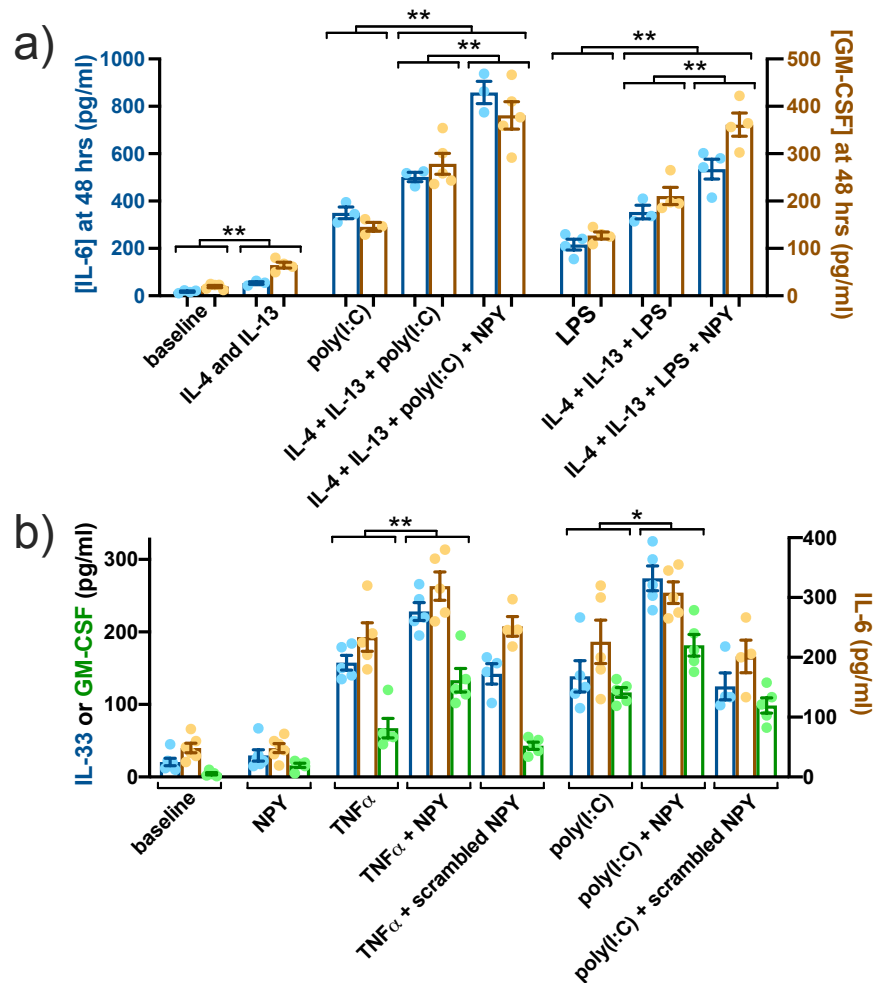
**SUPPLEMENTARY FIGURE S16** Longer-term alterations of antimicrobial peptide production, secretion, and efficacy in serous ALI cultures. **a)** Expression of  $\beta$ -defensin 1 (*DEFB1* gene) and  $\beta$ -defensin 2 (*DEFB4* gene) was measured by qPCR TaqMan assay at 24 hours  $\pm$  VIP,  $\pm$  NPY,  $\pm$  LPS (100 ng/ml). As expected, LPS increased NF $\kappa$ B-regulated  $\beta$ -defensin 2 but not constitutive  $\beta$ -defensin 1 [93, 94]. NPY (100 nM) and VIP (1  $\mu$ M) had no effects on expression alone. VIP reduced  $\beta$ -defensin 2 expression at 48 hours. While LPS + NPY was significantly different from LPS + VIP conditions, LPS + NPY was not significantly different from LPS alone. Significance by 1-way ANOVA with Bonferroni posttest. Each bar graph shows mean  $\pm$  SEM of 4 independent experiments using cultures from 4 different patients. **b)** Measurement of  $\beta$ -defensins 1 and 2 secretion into the ASL by ELISA as described in the methods and text. VIP increased secretion of  $\beta$ -defensin 1 over 48 hours (VIP  $p < 0.01$  vs unstimulated) while NPY eliminated the effect of VIP (VIP + NPY  $p < 0.01$  vs VIP alone).  $\beta$ -defensin 2 was not significantly increased by any stimulation. Significance determined by 1-way ANOVA with Bonferroni posttest comparing all points at 48 hours. Data are mean  $\pm$  SEM of 4 independent experiments per condition per timepoint using cultures from 4 different patients. **c)** Measurement of  $\beta$ -defensins 1 and 2 secretion into the ASL by ELISA in the presence of LPS. LPS had minimal effect on  $\beta$ -defensins 1, but NPY reduced  $\beta$ -defensin 1 secretion ( $p < 0.05$  vs LPS only) while VIP enhanced it ( $p < 0.01$  vs LPS only). In contrast, LPS enhanced secretion of  $\beta$ -defensin 2, and this was further enhanced ( $p < 0.05$ ) with NPY + LPS. VIP reduced the effect of LPS on  $\beta$ -defensin 2 ( $p < 0.05$  vs LPS only). Significance determined by 1-way ANOVA with Bonferroni posttest comparing all points at 48 hours. Data are mean  $\pm$  SEM of 4 independent experiments per timepoint per condition using cultures from 4 different patients. **d)** Left bar graph: lysozyme expression was measured  $\pm$ VIP  $\pm$ NPY  $\pm$ LPS. VIP increased expression of lysozyme while VIP + NPY together did not increase lysozyme expression over control (unstimulated). LPS also increased lysozyme expression, and this was potentiated by VIP but not NPY. Right bar graph: Increase of lysozyme expression by VIP was inhibited by H89 (1  $\mu$ M) while increase in response to LPS was not. This suggest that effects of VIP may be mediated by cAMP-activated transcription factor CREB, which can increase lysozyme transcription [95, 96]. Significance determined by 1-way ANOVA with Bonferroni posttest comparing all points at 48 hours. Data are mean  $\pm$  SEM of 5 independent experiments using cultures from 5 different patients for each time point. **e)** Lysozyme and Muc5AC secretion was measured at 24 hours by ELISA as described in the text. Secretion was enhanced by VIP and reduced by NPY. VIP also increased lysozyme and Muc7 secretion in the presence of LPS. Significance determined by 1-way ANOVA with Bonferroni posttest comparing all points at 48 hours. Data are mean  $\pm$  SEM of 4 independent experiments using cultures from 4 different patients for each time point. **f)** CFU assays were carried out as described in the text and using airway surface liquid (ASL) washings after 24 hours (left bar graph) and 48 hours (right bar graph). Two clinical strains of *P. aeruginosa* were used. At both time points, VIP increased antimicrobial efficacy while NPY reduced it. Significance determined by 1-way ANOVA with Bonferroni posttest comparing all points at 48 hours. Data are mean  $\pm$  SEM of 5 independent experiments using cultures from 5 different patients for each time point. Due to the increased antimicrobial capacity of culture secretion at 24 and 48 hours (vs 2 hours as shown in the main text), we altered the parameters of the assay to be able to measure CFUs. 40,000 and 80,000 CFUs were used as the starting inputs for 24 hour and 48 hour ASL experiments, respectively (vs 20,000 at 2 hours in the main text). ASL was also diluted 1:2 compared with the main text. These alterations allowed the CFUs obtained in this assay to be within a countable range.

## SUPPLEMENTARY FIGURE S17



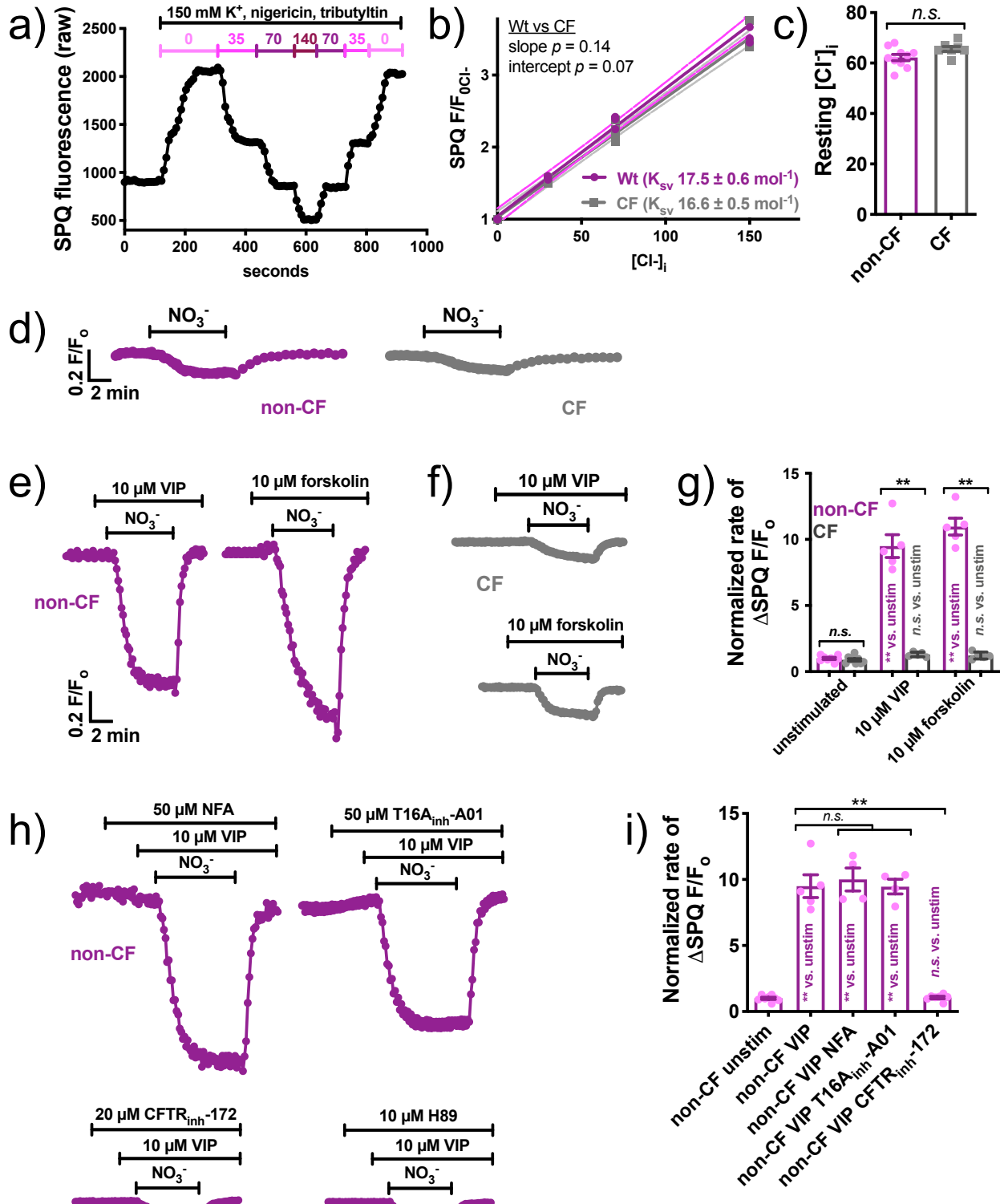
**SUPPLEMENTARY FIGURE S17** Pro-inflammatory effects of NPY and anti-inflammatory effects for VIP. Acinar cells from parotid and pancreatic exocrine glands can make and release cytokines [97-100]. Infection of isolated human tracheal submucosal gland cells with rhinovirus, which can activate TLR3 [101], increases IL-1 $\alpha$ , IL-1 $\beta$ , IL-6, and IL-8 [102]. TLR4 is also expressed in pig tracheal acinar cells [103], and submucosal TLR4 levels may be elevated in CF [104]. Both VIP and NPY are immunomodulatory [105]. **a-d)** As described in the text, serous cell cultures were stimulated with TLR4 agonist LPS (1  $\mu$ g/ml), TLR3 agonist poly(I:C) (5  $\mu$ g/ml), TLR2 agonist LTA (1  $\mu$ g/ml), TNF $\alpha$  (100 ng/ml) or a Th2 cocktail of IL-4 and IL-13 (20 ng/ml each; [106]) on the apical side only, with VIP (1  $\mu$ M) and/or NPY (100 nM) or scrambled NPY (100 nM) on the basolateral side, or followed by collection of basolateral media and determination of IL-6 (a), TNF $\alpha$  (b), IL-1 $\beta$  (c), or GM-CSF (d) concentration by ELISA. In most cases, NPY potentiated inflammatory responses while VIP reduce them. The only cytokine affected by either VIP or NPY alone was IL-1 $\beta$ , which was increased by NPY. Bar graphs show individual experiments using at least 6 ALI cultures from at least 3 patients (2 ALIs per patient); Significance by 1-way ANOVA with Bonferroni posttest comparing secretion of each specific cytokine among bars within each color-matched group (LPS, poly(I:C), LTA, TNF $\alpha$ , or IL-4 and IL-13; \* $p$ <0.05 and \*\* $p$ <0.01. These data agree with other studies showing VIP having anti-inflammatory or protective effects in parotid acini [105, 107-110] and NPY having pro-inflammatory effects in leukocytes [111]. GM-CSF and IL-1 $\beta$  that are important in allergic inflammation [112], neutrophil or eosinophil infiltration [113], and Th2 polarization [114]. Note that NPY itself increased IL-1 $\beta$ , and IL-1 $\beta$  polymorphisms may contribute to CF [115] or CRS [116]. It remains to be determined if these polymorphisms affect expression or secretion of IL-1 $\beta$  from gland acini. **e-g)** Cytokine mRNA was examined in serous ALIs stimulated as indicated for 4 hours. Isolated RNA was subject to reverse transcription quantitative PCR (qPCR) using TaqMan primers as indicated in the supplementary methods. Concentrations of agonists used are the same as in a-d. Significance by one-way ANOVA with Bonferroni posttest.

## SUPPLEMENTARY FIGURE S18



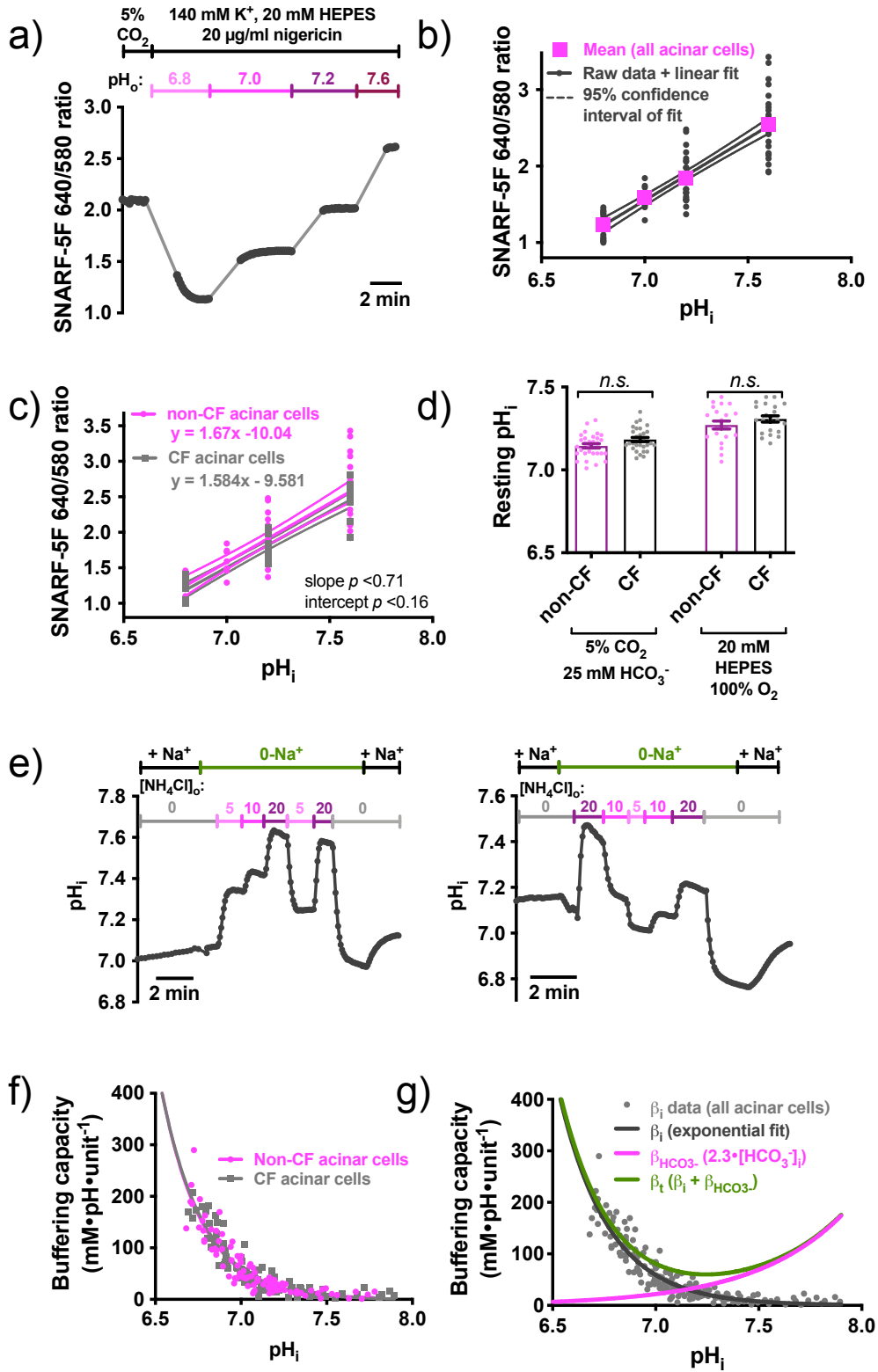
**SUPPLEMENTARY FIGURE S18** Pro-inflammatory effects of NPY in cultured (A) and acutely isolated (B) airway gland serous cells. **a)** A strong Th2 environment by itself may increase other inflammatory responses in airway cells [117]. IL-6 and GM-CSF secretion was measured by ELISA using non-CF primary serous cell ALIs stimulated with a Th2 cytokine cocktail (IL-4 + IL-13) as well as TLR3 agonists poly(I:C) or TLR4 agonist (LPS)  $\pm$  NPY for 48 hrs. IL-4 + IL-13 increased responses to poly(I:C) and LPS, and NPY had a further pro-inflammatory effect even in the presence of IL-4 and IL-13, suggesting that NPY can augment inflammatory responses even in the strong Th2 environment that accompanies many inflammatory airway diseases. Bar graphs show mean  $\pm$  SEM from 3-5 individual experiments each using an ALI from a separate non-CF patients. Significance determined by 1-way ANOVA with Bonferroni posttest; \* $p$ <0.05 and \*\* $p$ <0.01. **b)** Isolated acinar cells were stimulated with TNF $\alpha$  or poly(I:C)  $\pm$  NPY or scrambled NPY. NPY, but not scrambled NPY, increased secretion of IL-33, GM-CSF, and IL-6 (measured via ELISA) in response to both TNF $\alpha$  or poly(I:C) but had minimal effect on its own, supporting data from cultured cells. Bar graphs show mean  $\pm$  SEM from 6 individual experiments using 2 ALIs each from 3 non-CF patients. Significance determined by 1-way ANOVA with Bonferroni posttest; \* $p$ <0.05 and \*\* $p$ <0.01.

SUPPLEMENTARY FIGURE S19



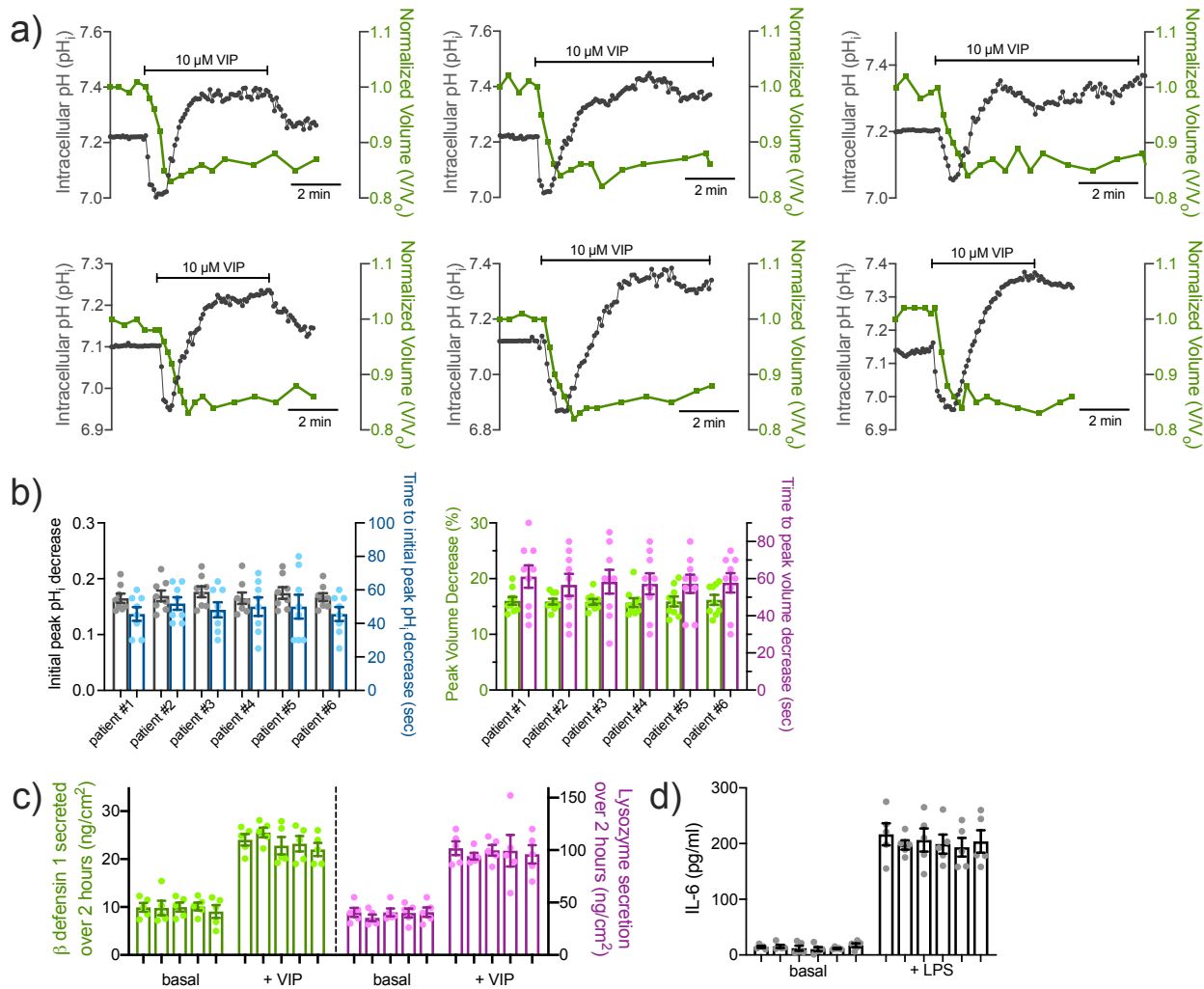
**SUPPLEMENTARY FIGURE S19** Resting  $[Cl^-]_i$  is not different in non-CF and CF serous cells, but CF serous cells lack VIP/cAMP-stimulated  $Cl^-$  permeability. Non-CF and CF serous cells were obtained and isolated from patient samples and loaded with  $Cl^-$ -sensitive dye SPQ as described in the supplementary methods and [3, 5, 6]. **a)** Representative trace of calibration of SPQ fluorescence at various  $[Cl^-]_i$  values was carried out using high extracellular  $K^+$  solution and  $H^+/K^+$  exchanger nigericin and anion exchanger tributyltin. **b)** Stern-Volmer plot (as described [3]) showed Stern-Volmer constant ( $K_{SV}$ ) values of  $\sim 17/mol$  for both genotypes and revealed similar resting  $[Cl^-]_i$ . **c)** Bar graph of resting  $[Cl^-]_i$  (mean  $\pm$  SEM) in non-CF and CF serous cells, which not significantly different by Student's  $t$  test. **d-g)** We examined  $Cl^-$  permeability using extracellular  $NO_3^-$  substitution with SPQ loaded cells. SPQ is quenched by  $Cl^-$  but not by  $NO_3^-$ , and  $Cl^-$  channels are nearly equally permeable to  $Cl^-$  and  $NO_3^-$ .  $NO_3^-$  substitution ( $0-Cl^-_o$ ) revealed identical resting  $Cl^-$  permeabilities in non-CF and CF cells (*d, g*). However, when stimulated with VIP or forskolin,  $Cl^-$  permeability increased in non-CF but not CF cells (*e-g*). A downward deflection of traces reflects a decrease in  $[Cl^-]_i$  (increase in SPQ  $F/F_o$ ). Bar graph in *g* shows mean  $\pm$  SEM; \* and \*\* =  $p < 0.05$  and  $0.01$ , respectively (one-way ANOVA with Bonferroni posttest). All data points are independent experiments from 3-4 CF and 3-5 non CF patients (at least 2 independent acinar cell experiments per patient). These data show that cAMP-activated  $Cl^-$  permeability is absent in CF serous cells. **h-i)** In non-CF cells, increased  $Cl^-$  permeability in response to VIP was inhibited by CFTR<sub>inh</sub>172 (CFTR inhibitor) or H89 (PKA inhibitor) but not by niflumic acid (NFA) or T16A<sub>inh</sub>-A01 ( $Ca^{2+}$ -activated  $Cl^-$  channel inhibitors). Bar graph in *l* shows mean  $\pm$  SEM; \* and \*\* =  $p < 0.05$  and  $0.01$ , respectively by one-way ANOVA with Bonferroni posttest. Thus, VIP-activated  $Cl^-$  permeability is cAMP-dependent and is blocked by CFTR inhibition.

SUPPLEMENTARY FIGURE S20



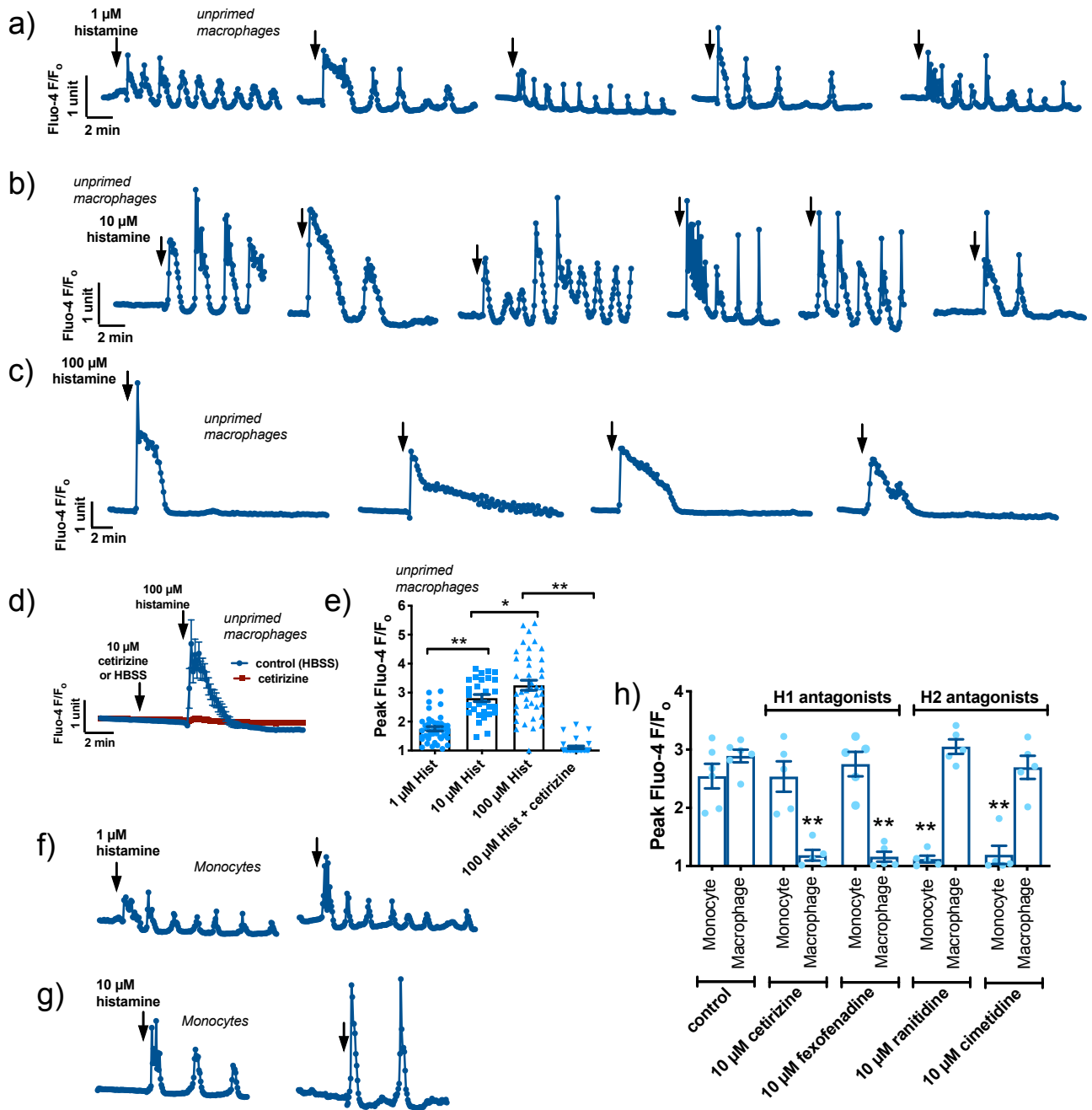
**SUPPLEMENTARY FIGURE S20** Measurement of intracellular pH ( $pH_i$ ) in serous cells from CF and non-CF patients. **a-c)** Non-CF and CF serous cells were loaded with the ratiometric intracellular pH ( $pH_i$ ) indicator SNARF-5F. SNARF-5F fluorescence was calibrated using high  $K^+$  solutions of known pH containing  $H^+/K^+$  exchanger nigericin (as described in [4]). Example calibration shown in (a). *b* shows calibration of acinar cells of all genotypes and *c* shows CF vs non-CF cells. No differences were observed between CF and non-CF acinar cells ( $n = 3$  patients each), allowing comparison of the SNARF responses in the two groups. **(D)**. Resting  $pH_i$  was extrapolated from experiments in the presence or absence of  $HCO_3^-$ . No significant difference was observed in CF vs non-CF cells. Mean  $\pm$  SEM; *n.s.* = not significantly different by one-way ANOVA with Bonferroni posttest. All data points are independent experiments from 3-4 CF and 3-5 non CF patients (at least 2 independent acinar cell experiments per patient). **e-g)** Intrinsic ( $HCO_3^-$ -independent)  $pH_i$  buffering capacity ( $\beta_i$ ) was measured using  $NH_3/NH_4$  pulse method [described in [4, 35]] under 0- $Na^+$  conditions to reduce  $pH_i$  regulatory mechanisms. Because of marked variation in buffering capacity of various cell types due to size and organelle composition,  $\beta_i$  must be experimentally determined. Representative calibration experiments shown in (e). Pooled buffering capacity measurements were used to compare CF and non-CF acinar cells (f). No significant difference in  $\beta_i$  was observed between the two cells. This means  $pH_i$  changes similarly represent  $OH^-$  eq fluxes in the two groups;  $pH_i$  changes can thus be compared between the two groups.  $\beta_i$  was fit with an exponential decay curve (g) and combined with  $HCO_3^-$ -dependent buffering ( $\beta_{HCO_3^-}$ ) to calculate total buffering capacity ( $\beta_t$ ) to convert  $pH_i$  changes to  $OH^-$  eq fluxes (not shown here). We measured  $pH_i$  changes in cells exposed to solutions of various  $[NH_4Cl]_o$ . Exposure of cells to a solution of  $NH_3-NH_4^+$  leads to rapid entry of membrane-permeant  $NH_3$  into the cell, causing  $pH_i$  alkalization as  $H^+$  is consumed as intracellular  $NH_3$  converts to  $NH_4^+$ . This is followed by a slower acidification, likely  $NH_4^+$  entry through  $K^+$  channels or the  $Na^+/K^+$  ATPase [34, 118]. Upon changing  $[NH_3]_o$ , the  $[NH_4^+]_i$  can be calculated using Henderson-Hasselbach with  $[NH_4^+]_i = [NH_3]_i \times 10^{pK_a - pH_i}$  with  $pK_a$  of  $NH_3/NH_4^+ = 9.2$  [35]. Solutions containing 0, 5, 10, and 20 mM  $[NH_4Cl]_o$  contained 0, 0.6, 1.2, and 2.5 mM  $[NH_3]_o$ , respectively, at  $pH_o = 7.4$ . Buffering was calculated after an experimental change in  $[NH_3]_o$  using the initial fast  $pH_i$  increase or decrease to estimate buffering power around the midpoint of the  $pH_i$  change  $\Delta[NH_4^+]/\Delta pH_i$  (units of  $mmol \cdot L^{-1}$  of acid or base equivalent required to change  $pH_i$  by one unit). Raw data points from experiments as in e were fit with an exponential decay function (f). No difference was observed between CF and non-CF acinar cells in  $\beta_i$ . Total buffering capacity ( $\beta_t$ ; g) was calculated using all data points (both genotypes) and adding the  $\beta_i$  curve to  $\beta_{HCO_3^-}$  ( $2.3 \times [HCO_3^-]$ , with  $[HCO_3^-]_i$  calculated from Henderson Hasselbach with  $CO_2$  clamped at 5%). See the supplementary methods and [4, 35] for more experimental information.

## SUPPLEMENTARY FIGURE S21



**SUPPLEMENTARY FIGURE S21** Minimal patient-to-patient variability of responses in primary serous cells acutely isolated (*a-b*) and cultured at air-liquid interface (ALI) for 4 weeks (*c-d*). **a)** Representative responses to of intracellular  $\text{pH}_i$  (to track  $\text{HCO}_3^-$  secretion) and cell volume (to track  $\text{Cl}^-$  secretion) in primary ALIs from six different patients. **b)** quantification of responses from 9 independent acini imaged from each patient. No significant differences were observed by 1-way ANOVA. Note that resolution of time to peak shrinkage and time to peak  $\text{pH}_i$  decrease values are limited by the 4 sec sampling frequency, used to limit phototoxicity and photobleaching during fluorescence live cell imaging experiments (as described in supplementary methods and [3, 5, 6, 30]). **c)** Quantification of  $\beta$  defensin 1 and lysozyme secretion in 4-week serous cell ALIs over 2 hours in unstimulated (basal) conditions and 10  $\mu\text{M}$  VIP-stimulated conditions. No significant differences were observed by 1-way ANOVA. **d)** Quantification of IL-6 secretion at baseline (unstimulated) and after stimulation with 1  $\mu\text{g}/\text{ml}$  LPS for 24 hours. No significant differences among patients were observed by 1-way ANOVA. Each bar graph in *c* and *d* shows mean  $\pm$  SEM of 5 independent experiments from each patient. Together, these data suggest that culture-to-culture variability rather than patient-to-patient variability is the main variable factor in these types of experiments. In our experience with surface epithelial ALI cultures [10-18], we find that once primary cells are expanded and cultured for 3-6 weeks in defined media, secondary disease-related phenotypes are removed and cells reflect a “healthy” baseline state, with responses overwhelmingly dictated by genetics. This allows disease-relevant *in vitro* manipulations (treatment with IL-13, NPY, etc.) with comparison of unmanipulated cells from the same patient as “control.”

SUPPLEMENTARY FIGURE S22



**SUPPLEMENTARY FIGURE S22** Confirmation of M $\phi$  differentiation by functional H1 receptor expression.

Differentiation of monocytes into M $\phi$ s is accompanied by switch of histamine receptor expression from H2 to H1 isoform [119-121]. **a-c)** Representative Ca<sup>2+</sup> oscillations induced in individual Fluo-4 loaded M $\phi$ s by 1, 10  $\mu$ M histamine as well as larger transients with 100  $\mu$ M histamine in M $\phi$ s differentiated for 10 days as indicated in the text. **d)** Average representative traces (~25 M $\phi$ s) of response to 100  $\mu$ M histamine in the absence (blue) or presence of 10  $\mu$ M cetirizine (H1 antagonist). (E) Plot of responses from individual M $\phi$ s from  $\geq 3$  independent experiments using M $\phi$ s from  $\geq 3$  individuals. **f-g)** Representative Ca<sup>2+</sup> oscillations from freshly isolated monocytes imaged on Cell-Tak-coated coverslips. **h)** Bar graph of individual experiments (n = 3-6 from  $\geq 3$  patients) showing inhibition of Ca<sup>2+</sup> responses to 10  $\mu$ M histamine by H1 antagonists cetirizine or fexofenadine in M $\phi$ s and H2 antagonists ranitidine and cimetidine in monocytes. Bar graphs are mean  $\pm$  SEM with significance determined by 1-way ANOVA with Bonferroni posttest; \* $p < 0.05$  and \*\* $p < 0.01$ .

## SUPPLEMENTARY REFERENCES

1. Tewson PH, Martinka S, Shaner NC, Hughes TE, Quinn AM. New DAG and cAMP Sensors Optimized for Live-Cell Assays in Automated Laboratories. *J Biomol Screen* 2016: 21(3): 298-305.
2. Kost TA, Kemp CW. Fundamentals of Baculovirus Expression and Applications. *Adv Exp Med Biol* 2016: 896: 187-197.
3. Lee RJ, Limberis MP, Hennessy MF, Wilson JM, Foskett JK. Optical imaging of Ca<sup>2+</sup>-evoked fluid secretion by murine nasal submucosal gland serous acinar cells. *J Physiol* 2007: 582(Pt 3): 1099-1124.
4. Lee RJ, Harlow JM, Limberis MP, Wilson JM, Foskett JK. HCO<sub>3</sub><sup>-</sup> secretion by murine nasal submucosal gland serous acinar cells during Ca<sup>2+</sup>-stimulated fluid secretion. *J Gen Physiol* 2008: 132(1): 161-183.
5. Lee RJ, Foskett JK. Mechanisms of Ca<sup>2+</sup>-stimulated fluid secretion by porcine bronchial submucosal gland serous acinar cells. *Am J Physiol Lung Cell Mol Physiol* 2010: 298(2): 22.
6. Lee RJ, Foskett JK. cAMP-activated Ca<sup>2+</sup> signaling is required for CFTR-mediated serous cell fluid secretion in porcine and human airways. *J Clin Invest* 2010: 120(9): 3137-3148.
7. Widdicombe JH, Wine JJ. Airway Gland Structure and Function. *Physiol Rev* 2015: 95(4): 1241-1319.
8. Lee RJ, Foskett JK. Ca<sup>2+</sup> signaling and fluid secretion by secretory cells of the airway epithelium. *Cell Calcium* 2014: 55(6): 325-336.
9. Lee RJ, Foskett JK. Why mouse airway submucosal gland serous cells do not secrete fluid in response to cAMP stimulation. *J Biol Chem* 2012: 287(45): 38316-38326.
10. Lee RJ, Xiong G, Kofonow JM, Chen B, Lysenko A, Jiang P, Abraham V, Doghramji L, Adappa ND, Palmer JN, Kennedy DW, Beauchamp GK, Doulias P-T, Ischiropoulos H, Kreindler JL, Reed DR, Cohen NA. T2R38 taste receptor polymorphisms underlie susceptibility to upper respiratory infection. *J Clin Invest* 2012: 122(11): 4145-4159.
11. Lee RJ, Chen B, Doghramji L, Adappa ND, Palmer JN, Kennedy DW, Cohen NA. Vasoactive intestinal peptide regulates sinonasal mucociliary clearance and synergizes with histamine in stimulating sinonasal fluid secretion. *FASEB J* 2013: 27(12): 5094-5103.
12. Lee RJ, Kofonow JM, Rosen PL, Siebert AP, Chen B, Doghramji L, Xiong G, Adappa ND, Palmer JN, Kennedy DW, Kreindler JL, Margolskee RF, Cohen NA. Bitter and sweet taste receptors regulate human upper respiratory innate immunity. *J Clin Invest* 2014: 124(3): 1393-1405.
13. Lee RJ, Hariri BM, McMahon DB, Chen B, Doghramji L, Adappa ND, Palmer JN, Kennedy DW, Jiang P, Margolskee RF, Cohen NA. Bacterial d-amino acids suppress sinonasal innate immunity through sweet taste receptors in solitary chemosensory cells. *Sci Signal* 2017: 10(495).
14. McMahon DB, Workman AD, Kohanski MA, Carey RM, Freund JR, Hariri BM, Chen B, Doghramji LJ, Adappa ND, Palmer JN, Kennedy DW, Lee RJ. Protease-activated receptor 2 activates airway apical membrane chloride permeability and increases ciliary beating. *FASEB J* 2018: 32(1): 155-167.
15. Yan CH, Hahn S, McMahon D, Bonislawski D, Kennedy DW, Adappa ND, Palmer JN, Jiang P, Lee RJ, Cohen NA. Nitric oxide production is stimulated by bitter taste receptors ubiquitously expressed in the sinonasal cavity. *Am J Rhinol Allergy* 2017: 31(2): 85-92.

16. Lee RJ, Workman AD, Carey RM, Chen B, Rosen PL, Doghramji L, Adappa ND, Palmer JN, Kennedy DW, Cohen NA. Fungal Aflatoxins Reduce Respiratory Mucosal Ciliary Function. *Sci Rep* 2016; 6: 33221.
17. Zhao KQ, Cowan AT, Lee RJ, Goldstein N, Droguett K, Chen B, Zheng C, Villalon M, Palmer JN, Kreindler JL, Cohen NA. Molecular modulation of airway epithelial ciliary response to sneezing. *FASEB J* 2012; 26(8): 3178-3187.
18. Carey RM, Workman AD, Chen B, Adappa ND, Palmer JN, Kennedy DW, Lee RJ, Cohen NA. Staphylococcus aureus triggers nitric oxide production in human upper airway epithelium. *Int Forum Allergy Rhinol* 2015; 5(9): 808-813.
19. Hariri BM, McMahon DB, Chen B, Freund JR, Mansfield CJ, Doghramji LJ, Adappa ND, Palmer JN, Kennedy DW, Reed DR, Jiang P, Lee RJ. Flavones modulate respiratory epithelial innate immunity: anti-inflammatory effects and activation of the T2R14 receptor. *J Biol Chem* 2017; 292(20): 8484-8497.
20. Freund JR, Mansfield CJ, Doghramji LJ, Adappa ND, Palmer JN, Kennedy DW, Reed DR, Jiang P, Lee RJ. Activation of airway epithelial bitter taste receptors by Pseudomonas aeruginosa quinolones modulates calcium, cyclic-AMP, and nitric oxide signaling. *J Biol Chem* 2018; 293(25): 9824-9840.
21. Finkbeiner WE, Zlock LT, Mehdi I, Widdicombe JH. Cultures of human tracheal gland cells of mucous or serous phenotype. *In Vitro Cell Dev Biol Anim* 2010; 46(5): 450-456.
22. Fischer H, Illek B, Sachs L, Finkbeiner WE, Widdicombe JH. CFTR and calcium-activated chloride channels in primary cultures of human airway gland cells of serous or mucous phenotype. *Am J Physiol Lung Cell Mol Physiol* 2010; 299(4): L585-594.
23. Hariri BM, Payne SJ, Chen B, Mansfield C, Doghramji LJ, Adappa ND, Palmer JN, Kennedy DW, Niv MY, Lee RJ. In vitro effects of anthocyanidins on sinonasal epithelial nitric oxide production and bacterial physiology. *Am J Rhinol Allergy* 2016; 30(4): 261-268.
24. Tewson P, Westenberg M, Zhao Y, Campbell RE, Quinn AM, Hughes TE. Simultaneous detection of Ca<sup>2+</sup> and diacylglycerol signaling in living cells. *PLoS One* 2012; 7(8): e42791.
25. Edelstein A, Amodaj N, Hoover K, Vale R, Stuurman N. Computer control of microscopes using microManager. *Curr Protoc Mol Biol* 2010; Chapter 14: Unit14 20.
26. Schwarz H, Villiger PM, von Kempis J, Lotz M. Neuropeptide Y is an inducible gene in the human immune system. *J Neuroimmunol* 1994; 51(1): 53-61.
27. Schindelin J, Arganda-Carreras I, Frise E, Kaynig V, Longair M, Pietzsch T, Preibisch S, Rueden C, Saalfeld S, Schmid B, Tinevez JY, White DJ, Hartenstein V, Eliceiri K, Tomancak P, Cardona A. Fiji: an open-source platform for biological-image analysis. *Nat Methods* 2012; 9(7): 676-682.
28. Foskett JK. Optical Imaging of Ion Transport in Single Living Cells. *Comments Mol Cell Biophys* 1993; 8(3): 115-135.
29. Foskett JK. Optical Studies of Ion and Water Transport in Single Living Cells. In: Grinstein S, and Foskett, J. K., ed. *Noninvasive Techniques in Cell Biology*. Wiley-Liss, Inc., New York, 1990; pp. 237-272.
30. Foskett JK. Simultaneous Nomarski and fluorescence imaging during video microscopy of cells. *Am J Physiol* 1988; 255(4 Pt 1): C566-571.
31. Verkman AS, Sellers MC, Chao AC, Leung T, Ketcham R. Synthesis and characterization of improved chloride-sensitive fluorescent indicators for biological applications. *Anal Biochem* 1989; 178(2): 355-361.

32. Foskett JK, Melvin JE. Activation of salivary secretion: coupling of cell volume and  $[Ca^{2+}]_i$  in single cells. *Science* 1989; 244(4912): 1582-1585.
33. Foskett JK.  $[Ca^{2+}]_i$  modulation of  $Cl^-$  content controls cell volume in single salivary acinar cells during fluid secretion. *Am J Physiol* 1990; 259(6 Pt 1): C998-1004.
34. Roos A, Boron WF. Intracellular pH. *Physiol Rev* 1981; 61(2): 296-434.
35. Weintraub WH, Machen TE. pH regulation in hepatoma cells: roles for Na-H exchange,  $Cl^-HCO_3^-$  exchange, and Na- $HCO_3^-$  cotransport. *Am J Physiol* 1989; 257(3 Pt 1): G317-327.
36. Boron WF. Regulation of intracellular pH. *Adv Physiol Educ* 2004; 28(1-4): 160-179.
37. Renner EL, Lake JR, Persico M, Scharschmidt BF. Na<sup>+</sup>-H<sup>+</sup> exchange activity in rat hepatocytes: role in regulation of intracellular pH. *Am J Physiol* 1989; 256(1 Pt 1): G44-52.
38. Kreindler JL, Bertrand CA, Lee RJ, Karasic T, Aujla S, Pilewski JM, Frizzell RA, Kolls JK. Interleukin-17A induces bicarbonate secretion in normal human bronchial epithelial cells. *Am J Physiol Lung Cell Mol Physiol* 2009; 296(2): L257-266.
39. Irokawa T, Krouse ME, Joo NS, Wu JV, Wine JJ. A "virtual gland" method for quantifying epithelial fluid secretion. *Am J Physiol Lung Cell Mol Physiol* 2004; 287(4): L784-793.
40. Hariri BM, McMahon DB, Chen B, Adappa ND, Palmer JN, Kennedy DW, Lee RJ. Plant flavones enhance antimicrobial activity of respiratory epithelial cell secretions against *Pseudomonas aeruginosa*. *PLoS One* 2017; 12(9): e0185203.
41. Alakomi HL, Skytta E, Saarela M, Mattila-Sandholm T, Latva-Kala K, Helander IM. Lactic acid permeabilizes gram-negative bacteria by disrupting the outer membrane. *Appl Environ Microbiol* 2000; 66(5): 2001-2005.
42. Johnson L, Mulcahy H, Kanevets U, Shi Y, Lewenza S. Surface-localized spermidine protects the *Pseudomonas aeruginosa* outer membrane from antibiotic treatment and oxidative stress. *J Bacteriol* 2012; 194(4): 813-826.
43. Wang J, Chou S, Xu L, Zhu X, Dong N, Shan A, Chen Z. High specific selectivity and Membrane-Active Mechanism of the synthetic centrosymmetric alpha-helical peptides with Gly-Gly pairs. *Sci Rep* 2015; 5: 15963.
44. Lv Y, Wang J, Gao H, Wang Z, Dong N, Ma Q, Shan A. Antimicrobial properties and membrane-active mechanism of a potential alpha-helical antimicrobial derived from cathelicidin PMAP-36. *PLoS One* 2014; 9(1): e86364.
45. Zhang Y, Reenstra WW, Chidekel A. Antibacterial activity of apical surface fluid from the human airway cell line Calu-3: pharmacologic alteration by corticosteroids and beta(2)-agonists. *Am J Respir Cell Mol Biol* 2001; 25(2): 196-202.
46. Widdicombe JH. Regulation of the depth and composition of airway surface liquid. *J Anat* 2002; 201(4): 313-318.
47. Seiler F, Hellberg J, Lepper PM, Kamyschnikow A, Herr C, Bischoff M, Langer F, Schafers HJ, Lammert F, Menger MD, Bals R, Beisswenger C. FOXO Transcription Factors Regulate Innate Immune Mechanisms in Respiratory Epithelial Cells. *Journal of Immunology* 2013; 190(4): 1603-1613.
48. Lund VJ, Mackay IS. Staging in rhinosinusitis. *Rhinology* 1993; 31(4): 183-184.

49. Lund VJ, Kennedy DW. Staging for rhinosinusitis. *Otolaryngol Head Neck Surg* 1997; 117(3 Pt 2): S35-40.
50. Quintanilla-Dieck L, Litvack JR, Mace JC, Smith TL. Comparison of disease-specific quality-of-life instruments in the assessment of chronic rhinosinusitis. *Int Forum Allergy Rhinol* 2012; 2(6): 437-443.
51. Ghandi M, Huang FW, Jane-Valbuena J, Kryukov GV, Lo CC, McDonald ER, 3rd, Barretina J, Gelfand ET, Bielski CM, Li H, Hu K, Andreev-Drakhlin AY, Kim J, Hess JM, Haas BJ, Aguet F, Weir BA, Rothberg MV, Paoletta BR, Lawrence MS, Akbani R, Lu Y, Tiv HL, Gokhale PC, de Weck A, Mansour AA, Oh C, Shih J, Hadi K, Rosen Y, Bistline J, Venkatesan K, Reddy A, Sonkin D, Liu M, Lehar J, Korn JM, Porter DA, Jones MD, Golji J, Caponigro G, Taylor JE, Dunning CM, Creech AL, Warren AC, McFarland JM, Zamanighomi M, Kauffmann A, Stransky N, Imielinski M, Maruvka YE, Cherniack AD, Tsherniak A, Vazquez F, Jaffe JD, Lane AA, Weinstock DM, Johannessen CM, Morrissey MP, Stegmeier F, Schlegel R, Hahn WC, Getz G, Mills GB, Boehm JS, Golub TR, Garraway LA, Sellers WR. Next-generation characterization of the Cancer Cell Line Encyclopedia. *Nature* 2019; 569(7757): 503-508.
52. Shaul YD, Yuan B, Thiru P, Nutter-Upham A, McCallum S, Lanzkron C, Bell GW, Sabatini DM. MERAV: a tool for comparing gene expression across human tissues and cell types. *Nucleic Acids Res* 2016; 44(D1): D560-566.
53. Robertson MA, Foskett JK. Na<sup>+</sup> transport pathways in secretory acinar cells: membrane cross talk mediated by [Cl<sup>-</sup>]<sub>i</sub>. *Am J Physiol* 1994; 267(1 Pt 1): C146-156.
54. Kreindler JL, Peters KW, Frizzell RA, Bridges RJ. Identification and membrane localization of electrogenic sodium bicarbonate cotransporters in Calu-3 cells. *Biochim Biophys Acta* 2006; 1762(7): 704-710.
55. Abdulnour-Nakhoul S, Nakhoul NL, Wheeler SA, Wang P, Swenson ER, Orlando RC. HCO<sub>3</sub><sup>-</sup> secretion in the esophageal submucosal glands. *Am J Physiol Gastrointest Liver Physiol* 2005; 288(4): G736-744.
56. Namkoong E, Shin YH, Bae JS, Choi S, Kim M, Kim N, Hwang SM, Park K. Role of Sodium Bicarbonate Cotransporters in Intracellular pH Regulation and Their Regulatory Mechanisms in Human Submandibular Glands. *PLoS One* 2015; 10(9): e0138368.
57. Hong JH, Park S, Shcheynikov N, Muallem S. Mechanism and synergism in epithelial fluid and electrolyte secretion. *Pflugers Arch* 2013.
58. Gresz V, Kwon TH, Vorum H, Zelles T, Kurtz I, Steward MC, Aalkjaer C, Nielsen S. Immunolocalization of electroneutral Na<sup>(+)</sup>-HCO cotransporters in human and rat salivary glands. *Am J Physiol Gastrointest Liver Physiol* 2002; 283(2): G473-480.
59. Genovese M, Borrelli A, Venturini A, Guidone D, Caci E, Viscido G, Gambardella G, di Bernardo D, Scudieri P, Galletta LJV. TRPV4 and purinergic receptor signalling pathways are separately linked in airway epithelia to CFTR and TMEM16A chloride channels. *J Physiol* 2019.
60. Bernardinelli E, Costa R, Nofziger C, Paulmichl M, Dossena S. Effect of Known Inhibitors of Ion Transport on Pendrin (SLC26A4) Activity in a Human Kidney Cell Line. *Cellular Physiology and Biochemistry* 2016; 38(5): 1984-1998.
61. Namkung W, Phuan PW, Verkman AS. TMEM16A inhibitors reveal TMEM16A as a minor component of calcium-activated chloride channel conductance in airway and intestinal epithelial cells. *J Biol Chem* 2011; 286(3): 2365-2374.
62. Jang Y, Oh U. Anoctamin 1 in secretory epithelia. *Cell Calcium* 2014; 55(6): 355-361.

63. Hartzell C, Putzier I, Arreola J. Calcium-activated chloride channels. *Annu Rev Physiol* 2005; 67: 719-758.
64. Chiang L, Karvar S, Hamm-Alvarez SF. Direct imaging of RAB27B-enriched secretory vesicle biogenesis in lacrimal acinar cells reveals origins on a nascent vesicle budding site. *PLoS One* 2012; 7(2): e31789.
65. Xu S, Edman M, Kothawala MS, Sun G, Chiang L, Mircheff A, Zhu L, Okamoto C, Hamm-Alvarez S. A Rab11a-enriched subapical membrane compartment regulates a cytoskeleton-dependent transcytotic pathway in secretory epithelial cells of the lacrimal gland. *J Cell Sci* 2011; 124(Pt 20): 3503-3514.
66. Hsueh PY, Edman MC, Sun G, Shi P, Xu S, Lin YA, Cui H, Hamm-Alvarez SF, MacKay JA. Tear-mediated delivery of nanoparticles through transcytosis of the lacrimal gland. *J Control Release* 2015; 208: 2-13.
67. Rogers DF. The airway goblet cell. *Int J Biochem Cell Biol* 2003; 35(1): 1-6.
68. Stewart CE, Torr EE, Mohd Jamili NH, Bosquillon C, Sayers I. Evaluation of differentiated human bronchial epithelial cell culture systems for asthma research. *J Allergy (Cairo)* 2012; 2012: 943982.
69. Kreda SM, Okada SF, van Heusden CA, O'Neal W, Gabriel S, Abdullah L, Davis CW, Boucher RC, Lazarowski ER. Coordinated release of nucleotides and mucin from human airway epithelial Calu-3 cells. *J Physiol* 2007; 584(Pt 1): 245-259.
70. Zhou J, Perelman JM, Kolosov VP, Zhou X. Neutrophil elastase induces MUC5AC secretion via protease-activated receptor 2. *Mol Cell Biochem* 2013; 377(1-2): 75-85.
71. Rose MC, Piazza FM, Chen YA, Alimam MZ, Bautista MV, Letwin N, Rajput B. Model systems for investigating mucin gene expression in airway diseases. *J Aerosol Med* 2000; 13(3): 245-261.
72. Shao MX, Ueki IF, Nadel JA. Tumor necrosis factor alpha-converting enzyme mediates MUC5AC mucin expression in cultured human airway epithelial cells. *Proc Natl Acad Sci U S A* 2003; 100(20): 11618-11623.
73. Sikder MA, Lee HJ, Mia MZ, Park SH, Ryu J, Kim JH, Min SY, Hong JH, Seok JH, Lee CJ. Inhibition of TNF-alpha-induced MUC5AC mucin gene expression and production by wogonin through the inactivation of NF-kappaB signaling in airway epithelial cells. *Phytother Res* 2014; 28(1): 62-68.
74. Kim JO, Sikder MA, Lee HJ, Rahman M, Kim JH, Chang GT, Lee CJ. Phorbol ester or epidermal growth-factor-induced MUC5AC mucin gene expression and production from airway epithelial cells are inhibited by apigenin and wogonin. *Phytother Res* 2012; 26(12): 1784-1788.
75. Sharma P, Dudus L, Nielsen PA, Clausen H, Yankaskas JR, Hollingsworth MA, Engelhardt JF. MUC5B and MUC7 are differentially expressed in mucous and serous cells of submucosal glands in human bronchial airways. *Am J Respir Cell Mol Biol* 1998; 19(1): 30-37.
76. Martinez-Anton A, Debolos C, Garrido M, Roca-Ferrer J, Barranco C, Alobid I, Xaubet A, Picado C, Mullol J. Mucin genes have different expression patterns in healthy and diseased upper airway mucosa. *Clin Exp Allergy* 2006; 36(4): 448-457.
77. Berger JT, Voynow JA, Peters KW, Rose MC. Respiratory carcinoma cell lines. MUC genes and glycoconjugates. *Am J Respir Cell Mol Biol* 1999; 20(3): 500-510.
78. Ito Y, Iwashita J, Kudoh A, Kuramata C, Murata J. MUC5B mucin production is upregulated by fibronectin and laminin in human lung epithelial cells via the integrin and ERK dependent pathway. *Biosci Biotechnol Biochem* 2015; 79(11): 1794-1801.

79. Woo HJ, Yoo WJ, Bae CH, Song SY, Kim YW, Park SY, Kim YD. Leptin up-regulates MUC5B expression in human airway epithelial cells via mitogen-activated protein kinase pathway. *Exp Lung Res* 2010; 36(5): 262-269.
80. Bae CH, Kim JW, Ye SB, Song SY, Kim YW, Park SY, Kim YD. AMPK induces MUC5B expression via p38 MAPK in NCI-H292 airway epithelial cells. *Biochem Biophys Res Commun* 2011; 409(4): 669-674.
81. Vogel DY, Glim JE, Stavenuiter AW, Breur M, Heijnen P, Amor S, Dijkstra CD, Beelen RH. Human macrophage polarization in vitro: maturation and activation methods compared. *Immunobiology* 2014; 219(9): 695-703.
82. Murray PJ. Macrophage Polarization. *Annu Rev Physiol* 2017; 79: 541-566.
83. Wheway J, Herzog H, Mackay F. NPY and receptors in immune and inflammatory diseases. *Curr Top Med Chem* 2007; 7(17): 1743-1752.
84. Singer K, Morris DL, Oatmen KE, Wang T, DelProposto J, Mergian T, Cho KW, Lumeng CN. Neuropeptide Y is produced by adipose tissue macrophages and regulates obesity-induced inflammation. *PLoS One* 2013; 8(3): e57929.
85. Rasiah KK, Kench JG, Gardiner-Garden M, Biankin AV, Golovsky D, Brenner PC, Kooner R, O'Neill G F, Turner JJ, Delprado W, Lee CS, Brown DA, Breit SN, Grygiel JJ, Horvath LG, Stricker PD, Sutherland RL, Henshall SM. Aberrant neuropeptide Y and macrophage inhibitory cytokine-1 expression are early events in prostate cancer development and are associated with poor prognosis. *Cancer Epidemiol Biomarkers Prev* 2006; 15(4): 711-716.
86. Bedoui S, von Horsten S, Gebhardt T. A role for neuropeptide Y (NPY) in phagocytosis: implications for innate and adaptive immunity. *Peptides* 2007; 28(2): 373-376.
87. Kaushik KS, Stolhandske J, Shindell O, Smyth HD, Gordon VD. Tobramycin and bicarbonate synergise to kill planktonic *Pseudomonas aeruginosa*, but antagonise to promote biofilm survival. *NPJ Biofilms Microbiomes* 2016; 2: 16006.
88. Massip-Copiz MM, Santa-Coloma TA. Extracellular pH and lung infections in cystic fibrosis. *Eur J Cell Biol* 2018.
89. Newbrun E, Hoover CI, Ryder MI. Bactericidal action of bicarbonate ion on selected periodontal pathogenic microorganisms. *J Periodontol* 1984; 55(11): 658-667.
90. Dorschner RA, Lopez-Garcia B, Peschel A, Kraus D, Morikawa K, Nizet V, Gallo RL. The mammalian ionic environment dictates microbial susceptibility to antimicrobial defense peptides. *FASEB J* 2006; 20(1): 35-42.
91. Dobay O, Laub K, Stercz B, Keri A, Balazs B, Tothpal A, Kardos S, Jaikumpun P, Ruksakiet K, Quinton PM, Zsembery A. Bicarbonate Inhibits Bacterial Growth and Biofilm Formation of Prevalent Cystic Fibrosis Pathogens. *Front Microbiol* 2018; 9: 2245.
92. Workman AD, Carey RM, Kohanski MA, Kennedy DW, Palmer JN, Adappa ND, Cohen NA. Relative susceptibility of airway organisms to antimicrobial effects of nitric oxide. *Int Forum Allergy Rhinol* 2017; 7(8): 770-776.
93. Singh PK, Jia HP, Wiles K, Hesselberth J, Liu L, Conway BA, Greenberg EP, Valore EV, Welsh MJ, Ganz T, Tack BF, McCray PB, Jr. Production of beta-defensins by human airway epithelia. *Proc Natl Acad Sci U S A* 1998; 95(25): 14961-14966.

94. Lee SH, Kim JE, Lim HH, Lee HM, Choi JO. Antimicrobial defensin peptides of the human nasal mucosa. *Ann Otol Rhinol Laryngol* 2002; 111(2): 135-141.
95. Regenhard P, Goethe R, Phi-van L. Involvement of PKA, PKC, and Ca<sup>2+</sup> in LPS-activated expression of the chicken lysozyme gene. *J Leukoc Biol* 2001; 69(4): 651-658.
96. Lefevre P, Melnik S, Wilson N, Riggs AD, Bonifer C. Developmentally regulated recruitment of transcription factors and chromatin modification activities to chicken lysozyme cis-regulatory elements in vivo. *Mol Cell Biol* 2003; 23(12): 4386-4400.
97. Dios ID. Inflammatory role of the acinar cells during acute pancreatitis. *World J Gastrointest Pharmacol Ther* 2010; 1(1): 15-20.
98. Yamakawa M, Weinstein R, Tsuji T, McBride J, Wong DT, Login GR. Age-related alterations in IL-1beta, TNF-alpha, and IL-6 concentrations in parotid acinar cells from BALB/c and non-obese diabetic mice. *J Histochem Cytochem* 2000; 48(8): 1033-1042.
99. Tanda N, Ohyama H, Yamakawa M, Ericsson M, Tsuji T, McBride J, Elovic A, Wong DT, Login GR. IL-1 beta and IL-6 in mouse parotid acinar cells: characterization of synthesis, storage, and release. *Am J Physiol* 1998; 274(1 Pt 1): G147-156.
100. Kempuraj D, Twait EC, Williard DE, Yuan Z, Meyerholz DK, Samuel I. The novel cytokine interleukin-33 activates acinar cell proinflammatory pathways and induces acute pancreatic inflammation in mice. *PLoS One* 2013; 8(2): e56866.
101. Zhu L, Lee PK, Lee WM, Zhao Y, Yu D, Chen Y. Rhinovirus-induced major airway mucin production involves a novel TLR3-EGFR-dependent pathway. *Am J Respir Cell Mol Biol* 2009; 40(5): 610-619.
102. Yamaya M, Sekizawa K, Suzuki T, Yamada N, Furukawa M, Ishizuka S, Nakayama K, Terajima M, Numazaki Y, Sasaki H. Infection of human respiratory submucosal glands with rhinovirus: effects on cytokine and ICAM-1 production. *Am J Physiol* 1999; 277(2): L362-371.
103. Murakami K, Tamada T, Nara M, Muramatsu S, Kikuchi T, Kanehira M, Maruyama Y, Ebina M, Nukiwa T. Toll-like receptor 4 potentiates Ca<sup>2+</sup>-dependent secretion of electrolytes from swine tracheal glands. *Am J Respir Cell Mol Biol* 2011; 45(5): 1101-1110.
104. Hauber HP, Tulic MK, Tsicopoulos A, Wallaert B, Olivenstein R, Daigneault P, Hamid Q. Toll-like receptors 4 and 2 expression in the bronchial mucosa of patients with cystic fibrosis. *Can Respir J* 2005; 12(1): 13-18.
105. Dimitrijevic M, Stanojevic S. The intriguing mission of neuropeptide Y in the immune system. *Amino Acids* 2013; 45(1): 41-53.
106. White SR, Martin LD, Stern R, Laxman B, Marroquin BA. Expression of IL-4/IL-13 receptors in differentiating human airway epithelial cells. *Am J Physiol Lung Cell Mol Physiol* 2010; 299(5): L681-693.
107. Hauk V, Calafat M, Larocca L, Fraccaroli L, Grasso E, Ramhorst R, Leiros CP. Vasoactive intestinal peptide/vasoactive intestinal peptide receptor relative expression in salivary glands as one endogenous modulator of acinar cell apoptosis in a murine model of Sjogren's syndrome. *Clin Exp Immunol* 2011; 166(3): 309-316.
108. Vanesa H, Mario C, Esteban G, Laura F, Daniel P, Rosanna R, Claudia PL. Neuroimmune aspects of Sjogren's syndrome: role of VIP/VPAC system in immune and salivary gland epithelial cell function. *Curr Pharm Des* 2014; 20(29): 4760-4765.

109. Calafat M, Larocca L, Roca V, Hauk V, Pregi N, Nesse A, Perez Leiros C. Vasoactive intestinal peptide inhibits TNF-alpha-induced apoptotic events in acinar cells from nonobese diabetic mice submandibular glands. *Arthritis Res Ther* 2009; 11(2): R53.
110. Li C, Zhu F, Wu B, Wang Y. Vasoactive Intestinal Peptide Protects Salivary Glands against Structural Injury and Secretory Dysfunction via IL-17A and AQP5 Regulation in a Model of Sjogren Syndrome. *Neuroimmunomodulation* 2017; 24(6): 300-309.
111. Chandrasekharan B, Nezami BG, Srinivasan S. Emerging neuropeptide targets in inflammation: NPY and VIP. *Am J Physiol Gastrointest Liver Physiol* 2013; 304(11): G949-957.
112. Roan F, Obata-Ninomiya K, Ziegler SF. Epithelial cell-derived cytokines: more than just signaling the alarm. *J Clin Invest* 2019; 129(4): 1441-1451.
113. Laan M, Prause O, Miyamoto M, Sjostrand M, Hytonen AM, Kaneko T, Lotvall J, Linden A. A role of GM-CSF in the accumulation of neutrophils in the airways caused by IL-17 and TNF-alpha. *Eur Respir J* 2003; 21(3): 387-393.
114. Ritz SA, Cundall MJ, Gajewska BU, Swirski FK, Wiley RE, Alvarez D, Coyle AJ, Stampfli MR, Jordana M. The lung cytokine microenvironment influences molecular events in the lymph nodes during Th1 and Th2 respiratory mucosal sensitization to antigen in vivo. *Clin Exp Immunol* 2004; 138(2): 213-220.
115. Levy H, Murphy A, Zou F, Gerard C, Klanderma B, Schuemann B, Lazarus R, Garcia KC, Celedon JC, Drumm M, Dahmer M, Quasney M, Schneck K, Reske M, Knowles MR, Pier GB, Lange C, Weiss ST. IL1B polymorphisms modulate cystic fibrosis lung disease. *Pediatr Pulmonol* 2009; 44(6): 580-593.
116. Erbek SS, Yurtcu E, Erbek S, Atac FB, Sahin FI, Cakmak O. Proinflammatory cytokine single nucleotide polymorphisms in nasal polyposis. *Arch Otolaryngol Head Neck Surg* 2007; 133(7): 705-709.
117. Herbert C, Do K, Chiu V, Garthwaite L, Chen Y, Young PM, Traini D, Kumar RK. Allergic environment enhances airway epithelial pro-inflammatory responses to rhinovirus infection. *Clin Sci (Lond)* 2017; 131(6): 499-509.
118. Boron WF, De Weer P. Intracellular pH transients in squid giant axons caused by CO<sub>2</sub>, NH<sub>3</sub>, and metabolic inhibitors. *J Gen Physiol* 1976; 67(1): 91-112.
119. Wang KY, Arima N, Higuchi S, Shimajiri S, Tanimoto A, Murata Y, Hamada T, Sasaguri Y. Switch of histamine receptor expression from H<sub>2</sub> to H<sub>1</sub> during differentiation of monocytes into macrophages. *FEBS Lett* 2000; 473(3): 345-348.
120. Ohno S, Shirai A, Ueda A, Igarashi T, Ishigatsubo Y, Tani K, Okubo T, Hikawa N, Kawakami T, Takenaka T. Increase in intracellular calcium induced by stimulating histamine H<sub>1</sub> receptors in macrophage-like P388D1 cells. *Biochem Biophys Res Commun* 1991; 181(3): 1156-1163.
121. Marone G, Gentile M, Petraroli A, De Rosa N, Triggiani M. Histamine-induced activation of human lung macrophages. *Int Arch Allergy Immunol* 2001; 124(1-3): 249-252.